Direct contact Measurement of The Dielectric Properties of Glass Ionomer Cements for MEMs Design

Jonathan James Boissonade

UNIVERSITY OF BIRMINGHAM

A thesis submitted to the

University of Birmingham

For the degree of

DOCTOR OF PHILOSOPHY

School of Metallurgy and Materials

College of Engineering and Physical Sciences

University of Birmingham U.K.

March 2013

Acknowledgements

I would like to acknowledge the key support, assistance and expertise that has been provided to me by my supervisors Dr Artemis Stamboulis and Dr Mike Ward. Without their help this research would not have been possible. In particular I would like to express my great thanks to Artemis for her undertaking this project which was merely concept at the start of this investigation.

I would also like to acknowledge the assistance of Dr David Cheneler, who has provided a great deal of support to me in the complex maths involved in the analysis of the raw data, which mostly fell outside my area of knowledge at the start of this investigation. His vital assistance in both areas pertaining to MEMs and Matlab was also invaluable.

I would also like to thank the University of Birmingham and the EPSRC for both giving me the opportunity and funding required to pursue this research.

I also owe a dept of gratitude and thanks to the various people who have provided support and allowed the continuation of my PhD through to the end. I would like to thank, Anne Cabezas who has always provided answers and support when required, Geoffrey Dolman for putting up with issues with COSHH documentation, Tracy Parks for her help with financial issues and purchase's and Donna Johnson for her assistance with access to the illusive impedance bridge.

Dedication

I would like to dedicate this thesis to my parents, Michael and Susan Boissonade without whose support I would never have completed this thesis.

Abstract

Although great care is taken by dentists in their choice of material for a dental restoration, based on both its mechanical properties and aesthetics, they are unable to check for defects within the restoration, such as those caused by the natural variations in hand mixing of a cement. , This can reduce the lifetime and mechanical stability of the restoration through such errors, (such as a miss mixing of the restorative). The possible development of an implantable sensor which could provide information as to the condition of the restoration could help to prevent failures of this nature. Changes in dielectric properties of dental cements could provide a method of monitoring the changes within the material.

In this investigation, a test assembly was developed based on previous work by Braden et al [1, 2]., which could be attached to an impedance bridge, to measure the dielectric properties of a number of different glass ionomer cements as they set using a simple design. Using the received dielectric properties of the glass ionomer cements, it would be possible to develop a micro-electro-mechanical sensor (MEMS) based on this design, which could be implanted into a dental restoration and interrogated remotely.

The ultimate aim of the investigation is to look into the possibility of developing a MEMS which could be integrated into a glass ionomer cement. This would monitor the setting of the cement to ascertain whether or not is possible to monitor the changes in the conditions of the material, and consequently evaluate the potential of

the sensor to provide a method of monitoring a biomaterial after implantation into a patient.

This investigation was aimed at measuring the changes in dielectric properties of glass ionomer cements during their setting reaction in order to observe if there is a correlation between the dielectric properties and the setting reaction. In this study, commercial glass ionomer cements were prepared and their setting process was monitored over a 24 hour period using FT-IR and direct contact impedance measurement. During the setting of the cements examined in this investigation the dielectric data collected from the co-planar assembly also showed a change in the recorded value for the impedance over the course of the setting of the cement, which when compared to FT-IR spectra over the same period, indicating the chemical changes within the cement, gives and indication as to the rate of setting of the GIC.

List of Figures

Chapter 1

Figure 1.1: The repeating unit of PAA……4

Figure 1.2: Chemical reaction of GIC powder with liquid……7

Figure 1.3: Representation of the poly(acrylic acid) unit changes during curing…….8

Figure 1.4: The setting reaction in a glass ionomer cement…….10

Figure 1.5: Ca^{2+} cross linking between the tooth substrate and PAA……..11

Figure 1.6: Resistivity of different cements as they set over time……..15

Figure 1.7: Relative permittivity over a 90min time scale of different cements curing ……16

Figure 1.8: Visual representation of a 'like permeation cell' (LPC), ……19

Figure 1.9: Electrical field distribution through a material using co-planar plates…..21

Figure 1.10: Capacitance measured in concrete vs the defect depth……23

Figure 1.11: Method of the production of a MEMs surface using surface etching of the material…..27

Chapter 2

Figure 2.1: Fuji IX Liquid and polymer components…..32

Figure 2.2: Manufacturer's depiction of ideal mixing conditions ……33

Figure 2.3: Test assembly used by Braden et al for the measurement of the curing of zinc-oxide eugenol cements……35

Figure 2.4: Design and dimensions of the Perspex test condenser assembly, including the dimensions of the key components…….37

Figure 2.5: Photograph of parallel plate assembly after construction……..……...39

Figure 2.6: Set-up of the test assembly in conjunction to the Impedance Analyzer and controlling unit…….……..……41

Figure 2.7: Insertion and compression of the Fuji IX sample in the test assembly……..…42

Figure 2.8: Top down view of sensing plates in a co-planar design…...…….……43

Figure 2.9: Side view of the plate arrangement with the water well……...…….44

Figure 2.10: Design of co-planar assembly……..…….……45

Figure 2.11: Construction of co-planar assembly, a) Base plate, b) Teflon mould, c) Water well, d) Addition of GIC, e) Compression, f) Addition of distilled water. ……..46

Figure 2.12: Completed co-planar assembly……..……48

Figure 2.13: Close up image of completed co-planar assembly……..…48

Figure 2.14: Co-planar assembly post addition of cement to mould……..……49

Figure 2.15: Co-planar assembly encased in grounded box to reduce interference from 50Hz frequency of mains power…….……..…….49

Figure 2.16: Set-up of the coplanar test assembly in conjunction to the Impedance Analyzer and controlling unit ……..……..…….51

Figure 2.17: Image of completed co-planar assembly (A) connected to Agilent Impedance bridge (B), and the grounded base (C)..…….……..52

Figure 2.18: Modifications to test assembly ……..……54

Figure 2.9: Close up of the modifications to the test assembly to allow for rapid changing of the assembly……..……..54

Chapter 3

Figure 3.1: Theoretical resistance at 5000Hz using 5V…….....……..58

Figure 3.2: Theoretical impedance at 5000Hz using 5V……..……59

Figure 3.3: Theoretical capacitance at 5000Hz using 5V.....……...……60

Figure 3.4: Impedance of Fuji IX measured over 24hr of setting reaction using planar test assembly…….……62

Figure 3.5: Equivalent Resistance and Equivalent reactance calculated from the measured impedance of Fuji IX over 24hrs of setting reaction using the planar test assembly……...……..63

Figure 3.6: Resistivity and Relative Permittivity calculated from the measured impedance of Fuji IX over 24hrs of setting reaction using the planar test assembly……64

Figure 3.7: Resistance and capacitance calculated from the measured Impedance of Fuji IX over 24hr of setting reaction using the planar test assembly……..……..64

Figure 3.8: Rapid change in Impedance measured using the planar test assembly

…….……65

Figure 3.9: Minor drop in Impedance measured using the planar test assembly

…….……...……..66

Figure 3.10: Rapid changes in Impedance over 1hr as sample dehydrates…….……....67

Figure 3.11: Effect of dehydration on averaged Impedance over 1hr ……..……67

Figure 3.12: Identified issue with planar design if miniaturised ……...…...…69

Figure 3.13: Averaged Impedance of Fuji IX over 24hrs taken from the co-planar assembly……...……..70

Figure 3.14: Averaged Impedance of Fuji IX over 60 mins taken from the co-planar assembly…….71

Figure 3.15: Equivalent Resistance and Equivalent reactance calculated from the measured Impedance of Fuji IX over 24hrs of setting reaction using the co-planar test assembly……..……..……..72

Figure 3.16: Resistivity and Relative Permittivity calculated from the measured Impedance of Fuji IX over 24hrs of setting reaction using the co-planar test assembly……..……..72

Figure 3.17: Resistance and Capacitance calculated from the measured impedance of Fuji IX over 24hr of setting reaction using the planar test assembly…….……73

Figure 3.18: Averaged Impedance of Chemfil over 24hrs taken from the co-planar assembly……...……..74

Figure 3.19: Averaged Impedance of Chemfil over 60 mins from mixing taken from the co-planar assembly……..……..……75

Figure 3.20: Equivalent Resistance and Equivalent reactance calculated from the measured Impedance of Chemfil over 24hrs of setting reaction using the co-planar test assembly……..……..……..76

Figure 3.21: Resistivity and Relative Permittivity calculated from the measured Impedance of Chemfil over 24hrs of setting reaction using the co-planar test assembly……..……..……..76

Figure 3.22: Resistance and Capacitance calculated from the measured Impedance of Chemfil over 24hr of setting reaction using the planar test assembly…….……77

Figure 3.23: Averaged Impedance of Ketac Molar over 24hrs from mixing taken from the co-planar assembly……..…..……..78

Figure 3.24: Averaged Impedance of Ketac Molar over 60 mins from mixing taken from the co-planar assembly……..…….79

Figure 3.25: Equivalent Resistance and Equivalent reactance calculated from the measured Impedance of Ketac Molar over 24hrs from mixing using the co-planar test assembly……..…….……..79

Figure 3.26: Resistivity and Relative Permittivity calculated from the measured Impedance of Ketac Molar measured over 24hrs from mixing using the co-planar test assembly……..…..80

Figure 3.27: Resistance and Capacitance calculated from the measured Impedance of Ketac Molar over 24hr from mixing using the planar test assembly……80

Figure 3.28: A comparison of the collected Impedance for Fuji IX, Chemfil Superior and Ketac Molar…….……..…….……81

Figure 3.29: Collected impedance for Fuji IX, Chemfil Superior and Ketac Fil Plus compared to each other over first hour.……..…….……..83

Figure 3.30: Discolouring of cement after prolonged contact with copper.....84

Figure 3.31: Oxidation of the co-planar test assembly copper plates……..……..85

Figure 3.32: Damage to co-planar test assembly caused by prolonged exposure to sample and storage media……..……....….85

Figure 3.33: Real time FT-IR spectra of Fuji IX (green) , Ketac Molar (red) and Chemfil Superior (blue).…….....……..87

Figure 3.34: Deconvoluted FT-IR spectra of Fuji IX, indicating key peaks observed. ……..……..……...88

Figure 3.35: Deconvoluted FT-IR spectra of Ketac Molar, indicating key peaks observed. ……..……..……91

Figure 3.36: Deconvoluted FT-IR spectra of Chemfil Superior, indicating key peaks observed. ……..……..……93

Figure 3.37: Deconvoluted FT-IR spectra of the polyacrylic acid liquid, indicating key peaks observed. ……..……..95

Figure 3.38: Real time FT-IR spectra for Fuji IX over the course of an hour: a) 0min, b) 5min, c) 10min, d) 15min, e) 30min, f) 45min, g) 60min……..……98

Figure 3.39: Real time FT-IR spectra for Fuji IX over the course of a 24hour period: a) 0min, b) 15min, c) 1hr, d) 3hrs, e) 6hrs, f) 12hrs, g) 24hrs……..……..…100

Figure 3.40: Real time FT-IR spectra for Ketac Fill Plus over the course of an hour: a) 0min, b) 5min, c) 10min, d) 15min, e) 30min, f) 45min, g) 60min……...103

Figure 3.41: Real time FT-IR spectra for Ketac Fill Plus over the course of an 24hour period: a) 0min, b) 15min, c) 1hr, d) 3hrs, e) 6hrs, f) 12hrs, g) 24hrs……..……...104

Figure 3.42: Real timeFT-IR spectra for Chemfil Superior over the course of an hour: a) 0min, b) 5min, c) 10min, d) 15min, e) 30min, f) 45min, g) 60min……..…108

Figure 3.43: Real timeFT-IR spectra for Chemfil Superior over the course of an hour: a) 0min, b) 15min, c) 1hr, d) 3hrs, e) 6hrs, f) 12hrs, g) 24hrs……..……109

Figure 3.44: Ratio change between the peaks for Ca-PAA (1552cm^{-1}) and PAA (1705cm^{-1}) representing the degree of polymerisation of the polymer, and the ratio change between representing the un-hydrolysed glass particles (945cm^{-1}) and the hydrolysed glass particles (1042-1046cm^{-1})……..……112

Figure 3.45: Comparison of both change in impedance and ratio of the intensity of peaks as given by FT-IR data, for Ca-PAA and PAA, over a 24 hour period within Fuji IX.....114

Figure 3.46: Lossy capacitor circuit of a capacitor in series with a resistor…….116

Chapter 5

Figure 5.1: Co-planar assembly connected to flat induction loop……..……121

Figure 5.2: Co-planar assembly connected to a raised spiral induction loop…...…121

List of Tables

Chapter 1

Table 1.1: Chemical analysis of different ionomer glass compositions ..……..…….6

Table 1.2: Various assessed bio-compatibilities of the different materials used in MEMs. ……..……..……28

Chapter 2

Table 2.1: Manufacturer's recommended mixing ratio's for Fuji IX, Ketac Fil Plus and Chemfil Superior……32

Chapter 3

Table 3.1: Description and assignment of FT-IR peaks identified in Fuji IX……..…….90

Table 3.2: Description and assignment of FT-IR peaks identified in Ketac Molar……92

Table 3.3: Description and assignment of FT-IR peaks identified in Chemfil Superior ……..……94

Table 3.4: Description and assignment of FT-IR peaks identified in polyacrylic acid liquid (PAA) ……..……96

Table 3.5: Description and assignment of FT-IR peaks identified in Fuji IX over 24hrs post mixing……..……101

Table 3.6: Description and assignment of FT-IR peaks identified in Ketac Molar over 24hrs post mixing…….....…..105

Table 3.7: Description and assignment of FT-IR peaks identified in Chemfil Superior over 24hrs post mixing……..…….....110

List of Abbreviations

GIC - Glass Ionomer Cement

PAA - Poly (acrylic acid)

FT-IR - Fourier Transform Infra-Red spectroscopy

MEMS - Micro-electro-mechanical system

LPC – 'Like Permeation Cell'

p/l – Powder/Liquid ratio

PCB – Printed Circuit Board

List of chemical abbreviations

Al_2O_3 - lumina (aluminium oxide)

Al^{3+} - Aluminium

Ba^{2+} - Barium

$CaCO_3$ - Calcium carbonate

CaF_2 - Calcium fluoride

CaO - Calcium oxide

COOH - Carboxylate anions

SiO_2-Al_2O_3-CaF_2 - Fluoride/fluorine Ffluoride glass

CaF_2 - Fluorite

H^+ - Hydron

OH Hydroxide ion

SiO_2-Al_2O_3-CaO - Oxide glass

PO_4^{3-} - Phosphorus

$(C_3H_4O_2)_n$ - Poly (acrylic acid)

SiO_2 - Silicon dioxide

Si^{4+} - Silicon

Na^+ - Sodium

NaF - Sodium fluoride

La^{3+} - Lanthanum

Table of Contents

Acknowledgements.....i

Dedication..... ..ii

Abstract..... iii

List of Figures.....v

List of Tables..... xii

List of Abbreviations..... xiv

List of Chemical Abbreviations and Charges……...xv

Table of Contents..... xvi

Chapter 1

1 Introduction & Literature Review……..……1

1.1 Introduction……..……1

1.2 Material Composition……4

1.3 Setting Reaction……7

1.4 Dielectric properties……12

1.5 Properties of Cements……24

1.6 Applications of Cements……..25

1.7 MEMs……..…...26

1.8 Fabrication of MEMs……...….27

1.9 Biocompatibility……28

1.10 Applications……...28

1.11 MEMs for Dental Applications……....30

Chapter 2

2 Materials and Methods……..31

2.1 Materials……..…….31

2.1.1 Preparation of Glass Ionomer Cements……..…32

2.1.2 Storage Material…….....33

2.2 Methods……...34

2.2.1 Development of Planar Test Assembly ……...34

2.2.2 Set-up of Planar Test Assembly to Impedance Bridge……..40

2.2.3 Impedance Measurement…….....41

2.2.4 Co-planar Assembly Development…….....42

2.2.5 Set-up of Co-planar Test Assembly to Impedance Bridge....50

2.2.6 Post construction Modification……..…….53

2.2.7 FT-IR of Glass Ionomer Cements…….....….55

2.2.8 Labview Program…….....……56

Chapter 3

3 Results and Discussion……..…….…….57

3.1 Theoretical Values based on Fuji II……..……..….57

3.2 Planar Test Assembly…….…….62

3.2.1 Assembly Testing…….....62

3.2.2 Planar design issues and Coplanar redesign……....68

3.3 Co-planar Test Assembly…….70

3.3.1 Fuji IX……..……70

3.3.2 Chemfil Superior…….....…74

3.3.3 Ketac Fil Plus…….....78

3.3.4 Comparison of Co-planar Impedance…….……81

3.3.5 Issues with Co-planar Assembly……...….83

3.4 FT-IR Results…….……87

3.4.1 FT-IR of Powder…….…….87

3.4.2 Deconvolution of Fuji IX……...….88

3.4.3 Deconvolution of Ketac Fil Plus...…….…….91

3.4.4 Deconvolution of Chemfil Superior..……..…….93

3.4.5 Deconvolution of PAA Polymer…….…..…….95

3.4.6 FT-IR of Fuji IX During curing……..97

3.4.7 FT-IR of Ketac Fil Plus During curing…….…..102

3.4.8 FT-IR of Chemfil Superior During curing……106

3.5 FT-IR in Comparison with Impedance……..…….……..111

Chapter 4

4 Conclusions…….……117

Chapter 5

5 Future work……..……119

References…….……124

Chapter 1

1 Introduction & Literature Review

1.1 Introduction

Glass ionomer cements have been used for over 40 years since they were developed in 1969 by Wilson et al [3], who were trying to develop the ideal artificial material for replacement tooth tissue. Glass ionomer composites have since found a particular use in dentistry as a lining, fissure sealant and as a filling material. They are extensively used in dentistry for a number of different reasons. Chiefly, they adhere to both untreated tooth enamel and dentine, through the ionic bonding of the Ca^{2+} ions within the dental tissue to the polymer chains within the cured cement. which means they require little mechanical fixation [3, 4].

The vision behind the development of a sensor which is capable of monitoring the condition of a dental cement once it has been implanted into a tooth, is one in which the data the sensor collects could be passed back to the patient who has received the restoration providing them information as to the condition of the cement. This information could be, for example, received by an electric toothbrush and an alert given if there was an issue with the restoration or its interface with the surrounding dental tissue, which could be relayed to the patient via an indicator light changing colour if the received data fell outside of the accepted range given for a correctly performing cement. Ideally a dentist could take a more sophisticated measurement,

informing them of what the issue with the cement was, such as formation of cracks or fissures. This would allow for the repair or replacement of the restoration prior to its total failure.

The ultimate goal would be the development of a Micro Electro Mechanical sensor for implantation. However the full development of this type of device requires a large amount of information and research. One area that needs to be investigated is the method of measurement used to interrogate the cement for its current condition. Presently the monitoring of dental restorations post implantation is limited to infrequent visits to a dentist. Though frequent visits would waste resources, the ability to monitor a restoration in the interim between visits would allow a dentist to ascertain if there was a problem and act accordingly, thereby helping reduce the chance that a restoration will fail. Where the cement is not mixed correctly, a non-homogeneous cement is formed, leading to a weaker restoration prone to failure owning to large occlusions within the structure caused by particle aggregations, with the restoration having a significantly lower compressive strength [5].

Equally a failure to mix the correct ratio of powder/liquid also greatly affects the restoration. A ratio with a larger quantity of liquid will have reduced porosities and a longer working time allowing for easier manipulation by the dentist, however this reduces the reinforcement provided by the glass particles and thus produces a weaker restoration [6].

The potential development of a sensor which is incorporated into the restoration and passively monitors its condition, providing additional information to the dentist or patient as to the condition of the restoration, could help to reduce the likelihood of failure and equally patient discomfort.

The same concept could also be applied to other medical procedures which make use of cements, providing potentially invaluable information as to their state, as presently there are only a limited number of methods of monitoring a biomaterial or medical implants post implantation. Conventional techniques for monitoring an implant site, such as visual inspection and probing of the surface, are difficult to use and a failure of or damage to an implant could cause serious harm to a patient. The sensors could also be used by doctors to monitor the patient's activity and allow for the development of patient specific treatment/physiotherapy regimes during the recovery process.

Changes in dielectric properties of dental cements could provide a method of monitoring the material. Work by Braden et al [1, 2, 7, 8], showed that during the setting reaction of glass ionomer cements the dielectric properties change, potentially providing the ability to monitor the setting reaction of the cement within the tooth. In theory it would also be possible to monitor other changes such as fractures and damage to the cement, as the dielectric properties will change as a result of such distortions [9]. Based on the observations of Braden et al [1, 2, 7, 8], it is known that glass ionomer cements behave dielectrically in a comparable way to capacitors, which is due to the glass particulates that form part of their structure.

The scope of this project is to investigate the potential interactions and responses of a dielectric monitoring Microelectromechanical sensor, implanted into Glass ionomer cement, to various conditions in order to assess the viability of Microelectromechanical sensors as a method of monitoring an implant in-vitro. The sensor will then be tested under controlled situations to examine its interactions with the cement and whether or not it is possible to monitor any changes in its structure using the dielectric sensor.

1.2 Material Composition

Glass ionomer cement is actually a composite material, consisting of glass particles imbedded in a gel-like matrix[10]. This polysalt matrix is the result of the reaction between an aqueous acid, like polyacrylic acid, and an ion-leachable glass powder of phosphorous particles [10]. The chemical composition of the glass ionomer cement is pivotal to both the setting of the cement and its resulting mechanical and chemical properties [11].

The polymer component of GIC's varies with a number of different polymer acids being used with Poly(acrylic acid) being the base of the GIC development. Poly(acrylic acid) (PAA) is a polymer with a repeating chain of $(C_3H_4O_2)_n$ which when mixed with the glass particles , acts as an acid, attacking the surface to produce free ions, which initiates the setting reaction [12]. The repeating unit of PAA is shown below in **figure 1.1**.

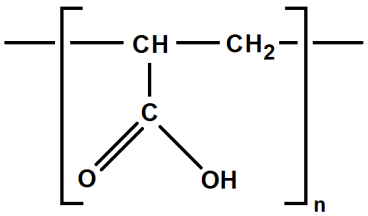

Figure 1.1: The repeating unit of PAA

The glass component of these systems milled glass particles of a basic composition of SiO_2-Al_2O_3-CaF_3. These particle act as both reservoirs for cross linking ions and as filler material in the system, and their composition varies depending on the specific system and requirements.

Within the glass component of GIC's the inorganic phosphorous particles provide a number of key functions to the material. The phosphorous provides a reservoir for the cross-linking ions which are leached on mixing with the PAA, and also provides a filler material within the resulting gel-sol matrix [12]. The phosphorous also aids in increasing the compressive strength over time, which is not observed in comparable cement systems, and improves the insolubility of the cement [12]. In phosphorous free glasses, the acid attacks the glass and hydrolyses the Si-O-AL bonds in the glass, causing the release of metal cations into the matrix, which then ironically crosslink the polyacrylic acid chains and produce an amorphous Silica gel (SiOH) surface coating [11]. However with phosphorous containing glasses, the phosphorous is first depleted before the hydrolysis of the Si-O-Al bonds [11].

In addition to this the specific composition of the glass dictates the number and types of cations and anions (e.g. Ca^{2+}, Al^{3+}, PO_4^{3-}, F^-), which are released from the glass

during the curing process, affect the degree of cross linking of the polymer chains [11]. Work by Stamboulis et al[11] showed the composition of a number of ionomer composites, five different glass (Fuji IX, Ketac Molar, G338, G2, and G2SR) ionomer cements were tested using ^{29}Si, ^{31}P, ^{27}Al and ^{19}F MAS-NMR, and x-ray florescence was used for the chemical analysis of the composition of the glasses [11]. The results of this study are shown in **table 1.1**.

Table 2
Chemical analysis of the commercial glasses: G2SR, G2, Ketac Molar, Fuji IX and G338 (values in at%)

Glass	Al	Si	P	Ca	O	F	Sr	La	Na
Fuji IX	0.129	0.115	0.017	0.000	0.547	0.126	0.056	0	0.010
G2	0.140	0.158	0.011	0.038	0.528	0.192	0.000	0	0.058
G338	0.131	0.098	0.030	0.041	0.536	0.143	0	0	0.055
G2SR	0.168	0.106	0.027	0.031	0.567	0.061	0.061	0	0.007
Molar	0.104	0.104	0.015	0.060	0.515	0.163	0	0.043	0.021

Table 1.1: Table showing the results of the chemical analysis of the different glasses, using XRF, with the amount of Al^{3+}, Si^{4+}, P^{3-}, Ca^{2+}, O^{2-}, F^{-}, Sr^{2+}, La^{3+} and Na^{+}, given in percent [11].

The primary cross linking ions vary depending on the cement, with all containing Al^{3+}, Si^{4+}, P^{3-}, and F^{-}. Fuji IX substitutes Ca^{2+} ions for Sr^{2+}, which is absent from G338 (Chemfil Superior) and Ketac Molar. These ions all form the primary crosslink's in the resulting gel-sol mixture. All the cements also contain Na^{+} and in Ketac Molar's case La^{3+} which act as compensators for excessive negative charges created in the system by the Al_{3}-Si_{4+} substitutions within the curing cement [13, 14]. Over time the Na^{+} ions also begin the process known as maturation, where they replace the hydrogen ions of the carboxyl groups, further cross linking the matrix [13, 14].

The presence of fluorine within a glass ionomer cement is one of its great strengths as a restorative as it is both essential for the formation of the crystalline apatite phase

and can be released into the surrounding tissues [15, 16]. Flourine is known to have a number of benifical properties in an oral environment, with its presence causing reduction in caries lesion formation and reducing enamel degradation [15, 16]. The fluorine content also affects the working and curing time of the cement, with its presence increasing both [15, 16]. Fluorine is also gradually released from a GIC over time, increasing the period over which its benefits can be experienced, and providing a replenishing surface coating while the fluorine is still present [15, 16]. Though fluorine contend does decrease over time, GICs have been shown to re-uptake fluorine in a fluorinated environment, which is then released as before [15, 16]. Given the beneficial nature of fluorine to the success of both the restoration and reduction of negative effects to the surrounding dental structure, there is a limit to the amount that can be included within the composition as at reduced fluorine levels the compressive strength of the cement increases, though increasing the concentration beyond the normal level, results in no significant effect on the compressive strength [15, 16].

1.3 Setting Reaction

Glass ionomer cements undergo setting when the fine glass component is reacts with aqueous poly(acrylic acid). The reaction of the glass ionomer cement to the PAA can be given by the equation below:

Base	+	Acid	⟶	Salt Hydrogel	+	Water
Glass Powder	+	Liquid (PAA or water)	⟶	Cement Matrix	+	H_20

Figure 1.2: Chemical reaction of GIC powder with liquid.

The setting reach of GICs is an acid-base reaction which is initiated when the PAA is mixed with the glass powder. The PAA is made up of repeating acrylic acid groups of (C3H4O2)n, as shown previously in **figure 1.1**. Once mixed the PAA acrylic anion ($COOH^-$) and hydron (H^+) dislocate and the hydrons (H^+) attack the surface of the glass particles releasing various metallic ions from the glass. These ions then crosslink with the PAA acrylic anions to form the gel matrix [12, 17]. The change in the PAA repeating acrylic group is shown in **figure 1.3** below.

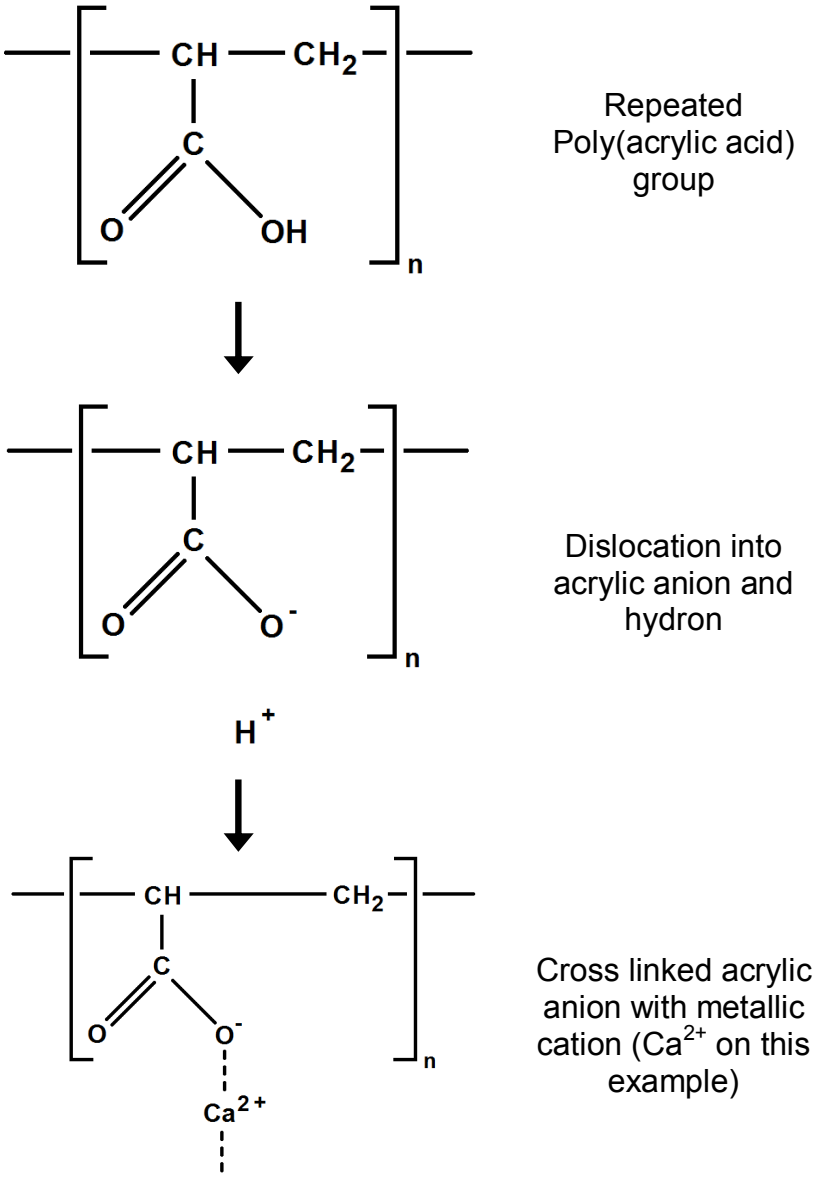

Figure 1.3: Representation of the poly(acrylic acid) unit changes during curing.

Where the glass is mixed with water rather than with PAA, such as with Chemfil, the PAA or other polymer is incorporated into the powder in a dehydrated form, and the addition of water initiates the curing. This can be represented by the equation below.

$$2(3CaO{\cdot}SiO_2) + 6H_2O \rightarrow 3CaP{\cdot}2SiO_2 \cdot 3H_20 + 3Ca(OH)_2$$

With either system, once mixed the hydrogen (H^+) ion's that are present in the liquid attack the surface of the glass particles, as shown in **figure 1.4, a)** and **b)**. This continuous hydrolysation of the glass causes the release of the various metallic ions and cations which are present in the glass, such as Fluorine (F^-) Phosphorous oxide (PO_4^{3-}), Aluminium (Al^{3+}) and Calcium (Ca^{2+}), into the PAA solution(**figure 1.4, b**). Initially the attack targets the Ca^{2+} rich areas followed by the Al^{3+} sites due to the high alkaline content [12, 17]. These ions then crosslink the PAA into a polysalt matrix, which encapsulates the glass particles as the matrix cures (**figure 1.4, c**) [12].

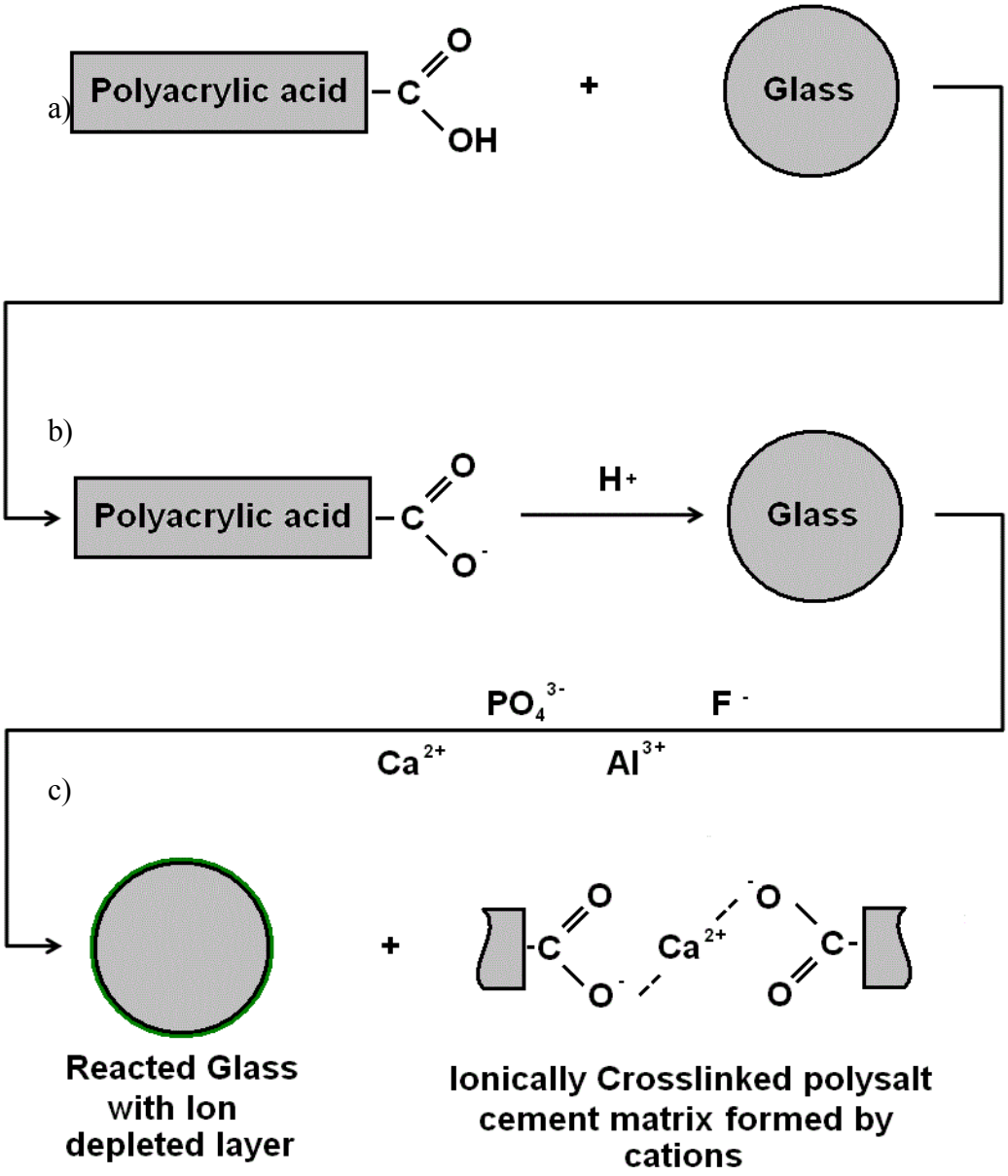

Figure 1.4: Setting reaction of glass ionomer cement.

In addition to the ions leached from the glass particles there is also an uptake of ions from the surrounding tissue such as with fluorine, and the PAA hydrolyse the surrounding dental tissue. This results in the availability of free Ca^{2+} bonding locations on the dental surfaces to which the PAA ionically crosslink's to, represented

in **figure 1.5**. This provides a greater mechanical fixation than could be provided through pure mechanical fixation.

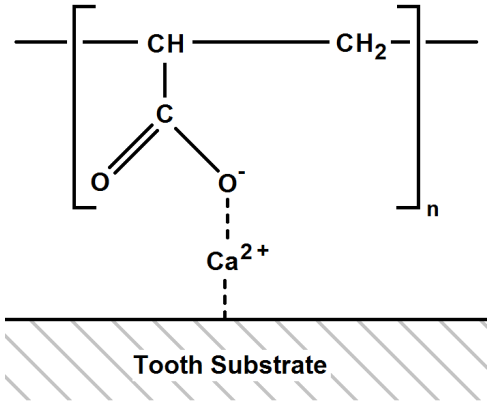

Figure 1.5: Ca^{2+} cross linking between the tooth substrate and PAA

Depending on the composition and setting mechanism of the cement, dental glass ionomer cements can be classified into two categories. Firstly there are conventional glass ionomer cements, which set by the standard acid–base reaction, and then there are resin-modified glass ionomer cements, which can be set by both the acid–base reaction and by photo-initiated polymerization [18]. In contrast to most other acrylic cements, e.g. PMMA, the acid – base curing reaction of regular glass ionomer cements does not generate a significant amount of heat, as does the low exothermic reaction with resin-modified ionomer cements, this low heat generation helps to reduce the heat damage to the surrounding tissue [4, 19]. In addition to not giving off a large amount of heat during the setting reaction, glass ionomer cements do not undergo significant shrinkage during the setting reaction, though resin-modified cements do contract slightly during setting [4, 19].

1.4 Dielectric properties

The relationship between voltage and current is known as Ohms law, which is given by the equation below:

$$I = \frac{V}{R}$$

Where current is proportional to voltage and inversely proportional to resistance. An increase in resistance would cause a decrease in current, in the same way that reducing the diameter of a water pipe would reduce the volume of water that could flow through said pipe [20].

Resistance and reactance are similar electrical properties of a material. Resistance is the resistance to a current passing through a material, and reactance is the resistance to a change in current within a material [20]. With a capacitor the ideal is to have a high reactance and no resistance, whereas an ideal resistor has a high resistance and no reactance. In a capacitor where there is a high resistance it is described as a Lossy-Capacitor, as it behaves as both a capacitor and a resistor [20].

As glass ionomer cements are used as both a cavity liner and as a filling agent to restore a cavity, they have to provide good thermal properties and thermal insulation to prevent changes in temperature affecting the internal structure of the tooth or causing discomfort to the patient [1]. In addition to thermal insulation, dental cement must function as an electrical insulator for the same reasons [1]. As a result of this the dielectric properties of dental cements are an interesting area of investigation. Apart from the electrical insulation properties, the study can also provide information

about the setting reaction within the cement, showing ionic availability within the curing cement and thus the progression of the cure through the cement [2].

The use of impedance measurement for the determining of materials properties is one that is both currently used in industrial settings to give details of the presence of faults and failures with portland cements [21, 22], and has also been used to investigate glass ionomer cements[1, 2, 7, 8, 22, 23].

In work by W.M. Tay and M. Braden [2], the setting reaction of glass ionomer cements was investigated by placing the setting cement between two copper plates and measuring their impedance. Four different commercial brands of glass ionomer cements (G-C Fuji Ionomer I, G-C Fuji Ionomer II at p/l ratios of 1.24 and 2.14, De Trey ASPA at p/l ratios of 1.00 and 2.19, De Trey CHEM bond) and a silicate for comparison (new filling porcelain) were mixed up and placed between copper plates connected to an impedance bridge, and the change in their dielectric properties over the first 90 minutes of their setting [2].

This investigation showed that the Fuji II glass ionomer cement, which is a resin modified cement, when in either of the two different powder/liquid ratio's, had an initially high resistivity which gradually rose as it set (**Figure 1.6**). This is in contrast to the polycarboxylates and silicates who showed a rapid increase in resistivity. Furthermore, variation in the ASPA's powder/liquid ratio had a greater effect on its resistivty compaired to the Fuji II, indicating a higher ionic content and lower molecular weight polymer reducing the resistivity [2]. The glass ionomer cements

also demonstrated a high relative permittivity, which reflects the high ionic content and polar nature of the material [2]. These values remain high, gradually decreasing, unlike the silicate which decreased quite rapidly (**Figure 1.7**).

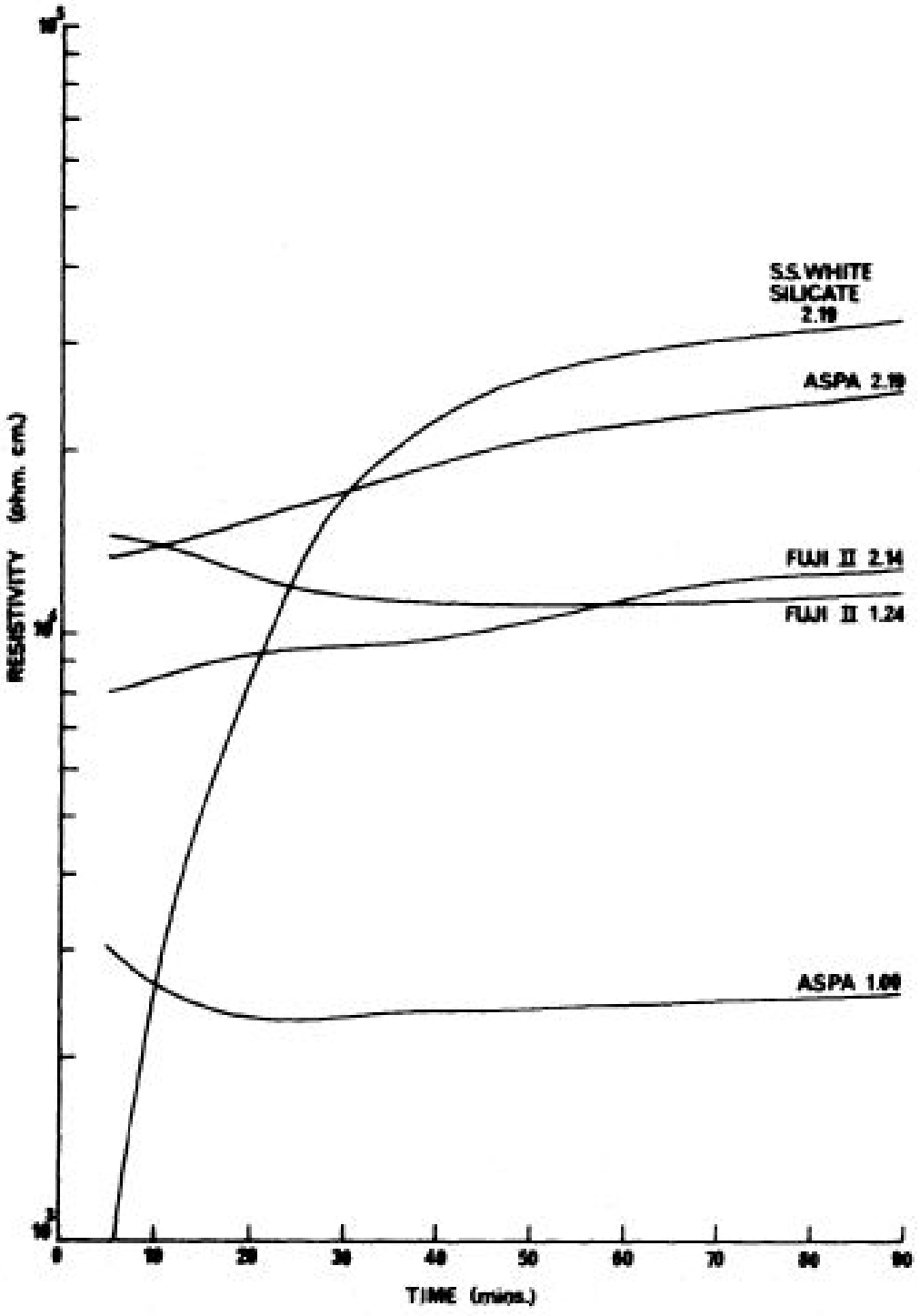

Fig. 1 – Plot of resistivity (log. scale) *vs.* time (linear scale) for silicate and glass ionomer cements. The numbers after the names of the cements indicate the powder-liquid ratios.

Figure 1.6: Resistivity of the different cements as they set over time [2].

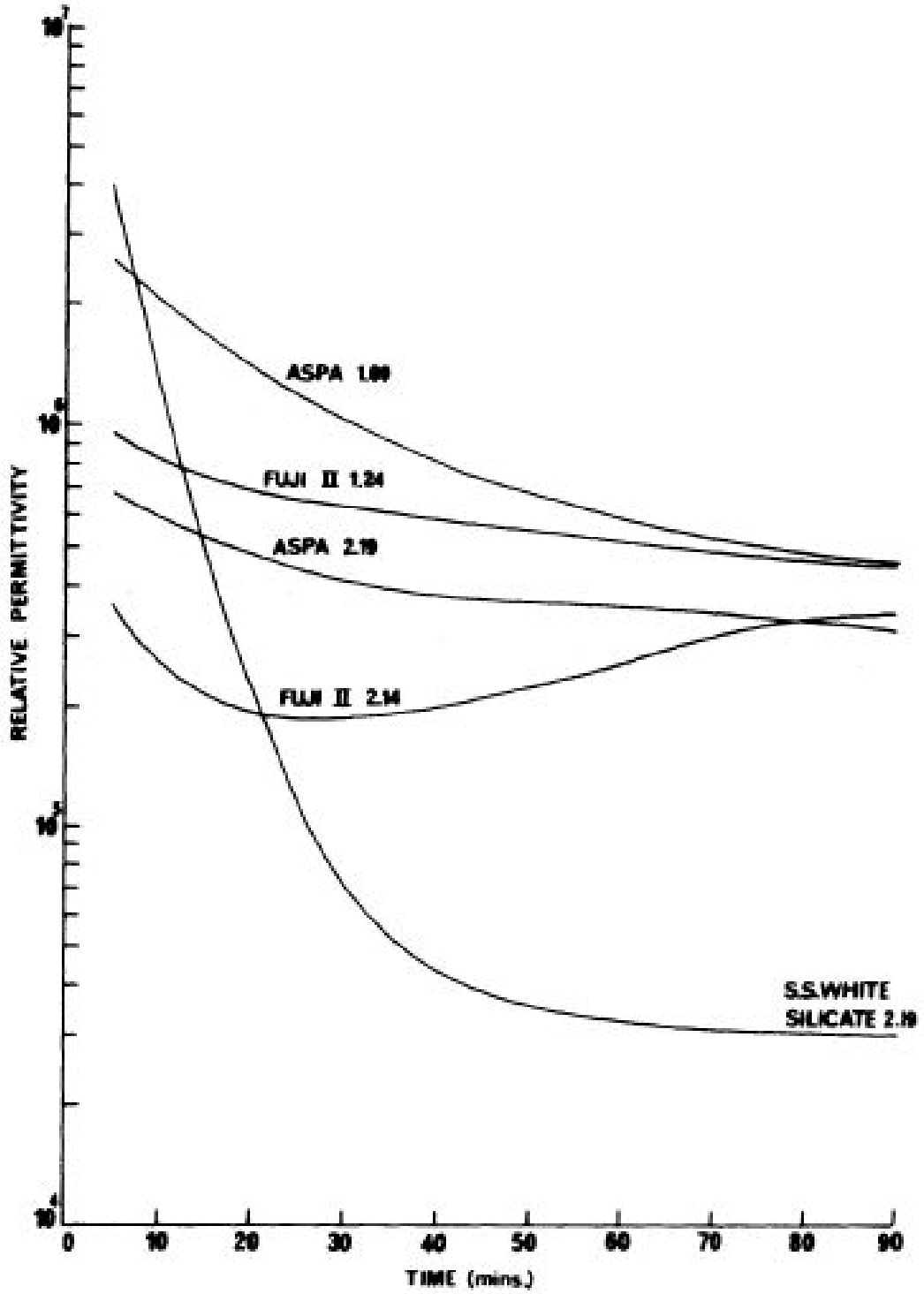

Fig. 2 – Plot of relative permittivity *vs.* time for silicate and glass ionomer cements.

Figure 1.7: Relative permittivity over a 90min time scale of different cements curing [2].

This change in dielectric properties of the GIC over time is due to the changes in the structure of the sample over time [2]. When mixed there is a release of charge carrying cations into the gel-sol matrix which are gradually removed from the matrix as they crosslink the polymer [11]. This reduces the availability of free ions within the cement increasing the resistivity of the cement, as shown in **figure 1.6**, and reducing the relative permiativity to electric current within the cement, **figure 1.7**. This avaiability of charge carriers is one of the key factors affecting the dielectric properties. The ions released are the primary charge carriers within the cement as the polymer component is not a significant charge carrier as like most polymers it does not have free electrons, and is crosslinking charged groups during the curing.

The prolonged conductivity of glass ionomer cements as shown here indicates that, if used in conjunction with metallic fillings, they may provide inadequate insulation against galvanic currents [2]. However, it also suggests that it may be possible to monitor the dielectric properties of the cement after setting as currents and ionic effects can still occur.

The internal curing mechanics and structural changes within a GIC, as with other restoratives, is difficult to monitor using conventional methods of chemical analysis such as FT-IR, in situ and alternative analysis techniques used. The monitoring of the impedance provides bulk measurements of physical properties, giving much greater detail to the internal chemical workings of the sample. The experiments conducted by D.C. Watts [24] demonstrated experimentally that in resin modified dental restorations the key influence to the changing impedance is that of the ionic

conductivity in a sample as it cures. He also demonstrated that as the setting reaction progressed the conductivity of the sample is reduced.

Currently the most used method of impedance measurements of dental restoratives is via a 'like permeation cell' (LPC), where the sample being interrogated is placed between two electrodes and a electrolyte of a known resistance, [23, 25]. The investigation by Cyril Villat et al [25] into the use of impedance spectroscopy for the monitoring of the curing of dental cements made use of a like permeation cell, with the cement to be monitored placed between the two electrolyte cells and was monitored over a prolonged period through storage of the whole assembly into a climate controlled chamber[25]. An example of this set up is detailed in **figure 1.8** [25].

A LPC like that detailed in **figure 1.8** has a number of advantages and disadvantages in impedance measurement. The use of a known electrolyte between the sample surface and the electrodes ensures that there is a constant connection for the current to pass, which is important as a good contact with the sample is key to gathering useable data and reducing noise caused by an interface between materials. The electrolyte also provides an easily controlled environment, with the electrolyte providing much needed moisture to the setting cement, and the temperature of whole assembly can be easily controlled. A disadvantage with an LPC is that it is very large and its design and use prevents the measurement of impedance in the initial stages of curing due to the time taken to set up. This means that vital information could be missed from the early reactions within a given sample.

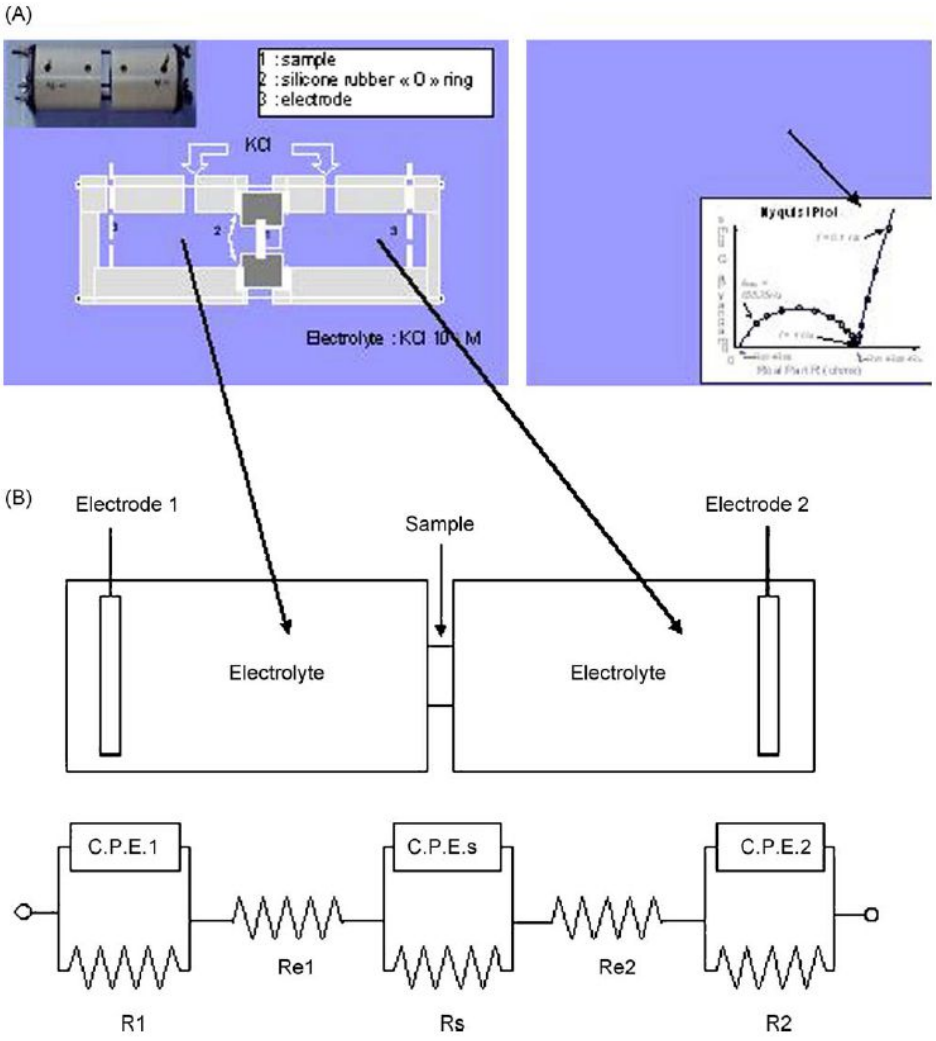

Fig. 1 – (A) Experimental setting [19] and (B) electrical equivalent circuit.

Figure 1.8: Visual representation of a 'like permeation cell' (LPC) [25].

In addition to these issues there is the possibility of exchange of ions between the electrolyte and the curing GIC. As the electrolyte will require free ions in-order to pass the current between electrode and sample, this adds ions to the GIC system which will interfere with the setting reaction, altering the curing time and the measured impedance within the sample. With a LPC the primary electrolyte used is potassium chloride (KCl). This posses a problem as Cl^- ions have a particular effect

on cement and concrete systems. The chlorine ions saturate the sample over time and decrease the resistivity of sample, affecting the resistance directly. The Cl^- also causes a localised decomposition of the cross linked polymer, releasing Ca^{2+}, OH^-, SO_4^{2-}, into the cement which then precipitate out of the system with the Cl^- ions [26].

The investigation showed that the dielectric properties of the studied cements changed with time; the impedance increase continued to for 28 days with a Portland cement and 5 days for the Glass Ionomer Cement, at which point the value ceases to change significantly [25].

Work undertaken by Nelly Pradelle-Plasse et al [23] investigated micro leakage by making use of the same LPC. In the investigation a like permeation cell was used to measure the resistance of dentin disks and thus the permeability and micro leaking that occurs through the movement of ions, molecules, bacteria and other fluids between the tooth and the restoration material [23]. This method allowed the preparation of a sample which can be aged and put through mechanical stress to induce damage within the structure before measuring the impedance again to see the effect [23].

The effect of porosities within the cement also has an effect on the impedance of the material. Pores within the structure could form wells for free ions, allowing for increase ionic permutation through the cement [22]. This porosity is linked in turn with the various ionic species that are present within the cement itself, specifically the free ions [22, 25]. This effect of the impedance and porosity linking ranges across

numerous types of materials, from concretes to portland cements [25]. When a current was applied to the sample of GIC its impedance was measured. The impedance of the cement can be used to calculate the dielectric properties of the cement [25].

With a co-planar design the electrical field strength decreases exponentially the further from the plates it travels. The electrical permittivity of the material in direct contact and in the immediate area to the electrodes playing a much greater role on the measured impedance than those further away (**figure 1.9**) [21].

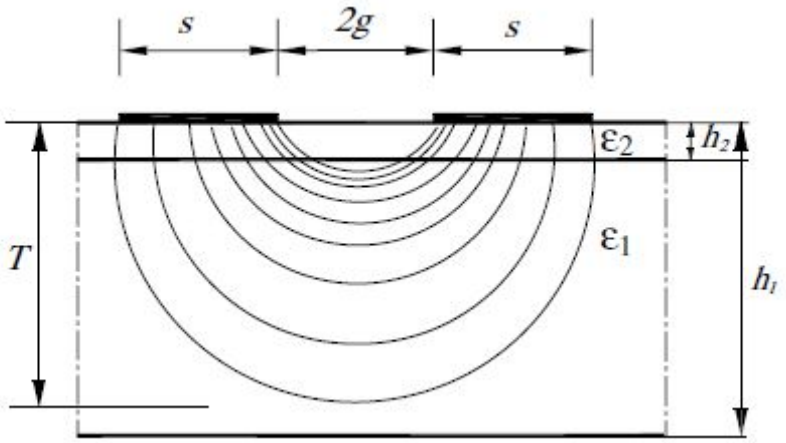

Figure 1.9: Electrical field distribution through a material using co-planar plates [21]

In this instance the electric field radiates out between the two plates, passing through the material at a decreasing intensity as the field radiates further out. Conformal mapping provides an approximate distance between the two conductive plates as the field extends further out [21]. The resulting capacitance between the two plates can be calculated using the following equation:

$$C = \varepsilon_0 \varepsilon_{\text{eff}} \frac{K(k_0')}{K(k_0)}$$

Where K is the complete elliptic integral of the first kind, ε_0 is the permittivity of free space and ε_{eff} is the effective dielectric constant of two layers [21], k_0 represents the modulus of the elliptic integral function and is given as:

$$k_0 = \frac{g}{s+g},$$
$$k_0' = \sqrt{1 - k_0^2}.$$

Where g is the distance between the plates and s the plate length [21].

Work by Amr A Nassr et al [21] used a co-planar capacitor set to show a change in dielectric properties of a concrete/glass-fiber composite into which defects of varying depths had been cast and water allowed to ingress. The results showed a change in the dielectric properties which was dependant on the change in depth, in this instance the change in the capacitance of the material was used (**figure 1.10**) [21].

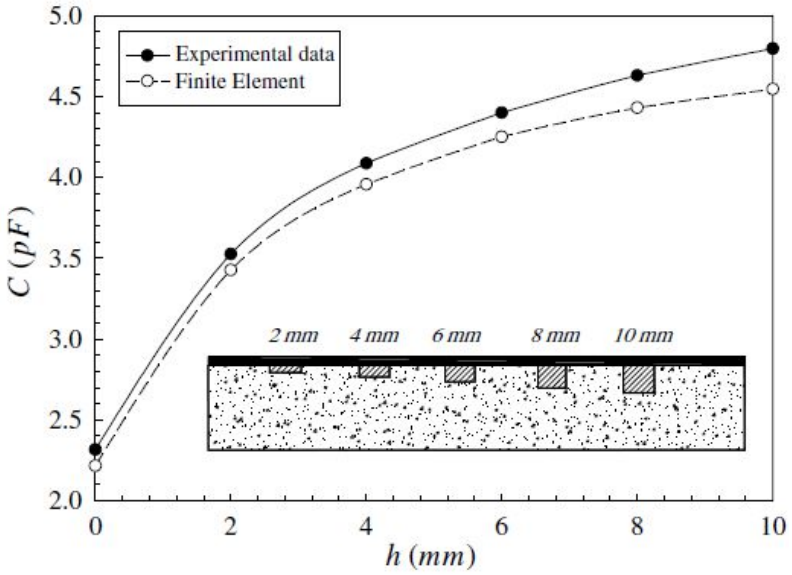

Figure 1.10: Capacitance measured in concrete vs the defect depth [21].

The change in the dielectric properties shown here is a result of a defect on the surface of the material, with a change for the presence of a small defect being markedly close to that of a deeper defect.

With a parallel plate capacitor a current is passed between two parallel conductors of a given area, through a material of a known thickness, and a uniform electric field is generated between the two conductors. The capacitance can then be measured through electrical contact. This forms an analytically simpler design than the co-planar capacitor set up [21], however conformal mapping can be used to give a approximation to the effect of arranging the capacitor plates in this fashion and thus allow the calculation of the impedance between the co-planar plates [21].

The objective of this investigation would be to see if it would be possible to use the same concept of direct contact measurement of dielectric properties of the glass

ionomer cement, whilst it cures post mixing, in a fashion similar to that used by Braden et al [1, 2, 7, 8]. The ability to use this particular design and method would provide a relatively simple design that could be utilised within a MEM's sensor, as opposed to the more complicated like permeation cell used to measure impedance currently.

1.5 Properties of Cements

The various properties of glass ionomer cements make them attractive as dental restoratives. When set, glass ionomer cements have an adequate load bearing capability for low to intermediate loading conditions within the body [4], making them quite suited for dental restorations. This limits their use in some applications as they do not have the ability to resist the required mechanical forces. Their ability to bond to both natural tissue such as bone and to metals also makes them desirable as a dental restorative [4], as this means that they do not rely solely on mechanical interactions to achieve fixation of the cement to the tooth or bone. The release of fluoride ions form the cement is thought to aid in resistance against dental caries (i.e. a cavity) [4], and as such an advantage in dental restorations. The bioactive nature of glass ionomer cements is another advantage, as glass ionomer cements exhibit an osteoconductive nature when in contact with bone. This is possibly due to the ion exchange between the glass ionomer cement and surrounding environment [4]. Since its introduction as a dental restorative material, a number of attempts have been made to improve its mechanical properties and as a result increase its potential applications to include direct filling [18].

Failures in the cementation procedure or mixing errors can result in debonding of the cement or secondary caries, which has been shown to be the major cause of failure of dental restorations [27].

1.6 Applications of Cements

There are a number of different applications in which glass ionomer cements are currently used. The major application of these cements is for dental restoration. In this field they are used as adhesives, as fissure sealants and as tooth filling materials [28], because of their ability to adhere to both untreated tooth enamel and dentine requiring little mechanical fixation unlike other restorative materials [3, 4]. The translucency of the cement also means that the glass ionomer is aesthetically pleasing as it closely resembles a tooth in coloration [28]. Cast gold crowns have also show an increased reliability and higher longevity when cemented into place using glass ionomer cements, when compared to dental amalgam or resin-based composite restorations [29].

Due to their success as dental cements, they have been further developed for other medical applications. The company Lonocem (ESPE GmBh and Co, seefeld Germany) developed the first medical grade glass ionomer cement for use in bone surgery [3], and they are now available both as a bone cement and as a pre-set cancellous bone substitute [28].

1.7 MEMs

Over the last 20 years there has been an increase in the amount of research into the development and application of both micro and nanotechnology, with research being focused on the fabrication of micro mechanisms and sensors [30]. As a result of this research into Microelectromechanical systems (MEMs) and nano-electro mechanical systems (NEMS) they are rapidly developing fields. There is a strong demand for MEMs devices for a number of different industrial and consumer products such as telecommunications and micro-electronics [31]. The significant advantages afforded by the cost reduction and miniaturization of equipment as a result of the use of micromachining technologies, which opens up the paths that allow for the integration of MEMs devices into high performance electronics [31].

The method of manufacture of complex MEMs is the same as the standard method of manufacturing an integrated circuit, which proves to be a significant advantage in their production as it relies on well developed and researched processes. Because integrated circuit production is based on the mass production of thousands of devices simultaneously the same methods can be applied to MEMs manufacture, thereby allowing batch fabrication [32]. The cost of the production of MEMs devices is also very low as very little material is required in their production, and they can be mass produced, lowering the cost further [32]. In addition to this the manufacture of the MEMs devices from a single starting material means that once produced MEMs devices show a greater reliability than a system which incorporates a large number of solder joins or wires, as less fabricated interconnections mean that there is less chance of a component failing, giving MEMs a reasonable reliability [32].

1.8 Fabrication of MEMs

The continued development of MEMs fabrication technology is an important issue, as there are a variety of manufacturing techniques which have been developed as a result of the diversity of applications for which the MEMs are developed. The surface micromachining technique, which is used to create MEMs, uses the sequential deposition of thin films onto Si wafers, the subsequent photo patterning of the film and then the etching of the films. This creates the microscopic mechanical elements and shapes on the substrate wafer [32]. This is illustrated by **figure 1.11** below, which shows the building up of a simple design on a silicon wafer, using the etching technique.

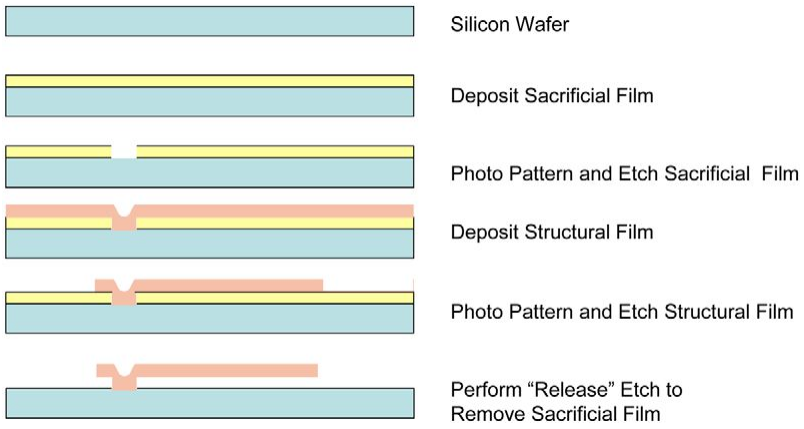

Figure 1.11: Method of the production of a MEMs surface using surface etching of the material [18].

This is the most suitable technique that could be used for the production of MEMs, though other techniques such as rapid prototyping deposition could be used.

1.9 Biocompatibility

In the case of the use of MEMs in a biological environment, a potentially serious issue is the biocompatibility of the MEMs. As with the various systems such as micro drug delivery systems, which would have to be implanted or simply placed under the skin, MEMs could elicit a negative response from the body [33]. **Figure 1.8** shows a list of different materials that could be used in the implantation of a MEMs system.

Table 2
Bio-compatibility materials for MEMS

Materials	Bio-compatibility	Characteristic	Application
PDDA	Good	Porous material	Reduce toxicity of nano particle
PDMS	Good	Ultra-thin active layer	Osmotic membrane (soft lithography)
SU-8 (PR)	Good	Thick-PR (high aspect ratio)	Microfluidic structure
PMMA	Good	Simply fabrication (hot embossing)	Microfluidic structure
ICPF	Very good	Difficult to fabrication (replica or modeling)	Sensor actuator
TiN alloy	Good	Shape memory effect	Actuator
Au	Good	Simply fabrication (low resistivity)	Electrode connection
Al_2O_3	Very good	Brittle	Microfluidic structure
Pt	Good	Simply fabrication (low resistivity)	Temperature sensor heater
Ti	Good	Simply fabrication	Heater

Table 1.2: Various assessed bio-compatibilities of the different materials used in MEMs [19].

1.10 Applications

MEMs have been used for a number of different applications ranging from the creation of high-performance projectors to relatively simple MEMs which are currently used in applications ranging from car air bags to sensors within electronic games. More complex devices have been designed for military applications [32]. MEMs development into the biomedical field is also moving forward, for example they are being investigated for use as micro machined tweezers for DNA handling [30].

One potential use for MEMs technology is in the medical field as drug delivery systems. When used on patients, drugs and chemicals function most effectively at a certain concentration, as concentrations bellow the optimum level may not be effective and concentrations that are too high can have toxic effects on tissues [33]. MEMs are attractive for use in this area, as they allow for the potential of micro-drug delivery systems. Such systems would be mainly used in patients who require continuous treatment due to chronic illness or disease, and example of which would be the release of insulin into the blood system of diabetic patients [33]. In another avenue, work by J.P.F. Spratley et al [34], showed the possibility of developing a inject able micro sensor, which could be deployed into the motor cortex of the brain, there for allow for the transmission of motor signals wirelessly from the brain to an external processor and potentially used to manoeuvre an electric wheelchair or control prosthetic devices [34].

The properties and size of MEMs means that they could potentially prove to be very useful in medical applications such as diagnostics or biomedical engineering. The potential to miniaturize diagnostic equipment from the lab down to the level where medical diagnosis could be moved from the laboratory to the bedside of a patient, potentially giving real-time results for tests, or more accurate monitoring of a patient's condition [32].

1.11 MEMs for Dental Applications

In addition to medical applications the properties of MEMs devices make them quite attractive for development within the dental field. The ability to monitor a dental restoration both during its setting and its condition once set, would help to provide dentists with up to date information about a restoration, potentially helping to prevent both failures in the restoration and allow for quick diagnosis of any problems; reducing both pain and inconvenience to a patient. One potential method of monitoring the glass ionomer cement could be through changes in dielectric properties of dental cement. Work by Braden et al [1, 2]. showed that during the setting reaction of glass ionomer cements the dielectric properties change quite significantly. For example, the resistivity of the Fuji II changed by approximately $5.6x10^3$ (**Figure 1.6**, [2]) during setting. This is quite a large change and it could be possible to develop a dielectric properties Microelectromechanical sensor which can monitor this change. It should also be possible to monitor other changes within the cement, such as fractures and damage to the cement, as the dielectric properties will change as a result of any change in the cement [9]. Damage in cement-based materials, for example concrete, has been shown to affect the dielectric properties of the material, with the damage producing an increase in the materials resistivity [9]. This property could be use to allow the monitoring of the cements condition once it has set.

Chapter 2

2 Materials and Methods

Throughout this investigation, the general terms cement and cements (in addition to GIC) will be used as a general term for glass ionomer cements.

2.1 Materials

It was decided that for this investigation the glass ionomer cements used were all commercially available. The GIC's used were Fuji IX (GC Corporation, Tokyo, Japan), Ketac Fil Plus Handmix (3MEspe, Neuss, Germany), and Chemfil Superior (DENTSPLY Limited, Konstanz, Germany).

Both Fuji IX and Ketac Fil Plus consist of a powder component of glass particles and a liquid component of aqueous polyacrylic acid. Fuji IX was designed to be used for class 1 or 2 restorations and Ketac Fil Plus for small class I, class III and V fillings [35, 36]. On the other hand, Chemfil Superior consists of a powder component that is an aluminium-sodium-calcium-fluoro-phosphoro-silicate glass in a ratio of 18:9:8:16:3:46, and Polyacrylic acid with a molecular weight of between 30000-45000 [37]. Unlike Fuji IX and Ketac Fil Plus, the liquid component is distilled water. This cement was designed for use in class I-III and V cavity restorations in both a temporary and semi-permanent situations [37].

Figure 2.1: Fuji IX Liquid and polymer components [38]

2.1.1 Preparation of Glass Ionomer Cements

Each of the cements used was a binary compound consisting of a solid powdered component, made up of glass particles, and a liquid component, nominally PAA or in some cases for example Chemfil Superior which makes use of glass particles with dehydrated PAA in the powder component and the addition of water initiates the curing. Each of the cements was prepared in accordance with the manufacturers instructions. The cements were hand-mixed at room temperature using a stainless steel spatula and a perspex mixing block, in accordance to the manufacturer's instructions, with the ratio of Polymer to liquid components shown in **Table 2.1** below.

Powder Component	Ratio	Liquid Component
Fuji IX glass	3.6:1	PAA
Ketac glass	3.2:1	PAA
Chemfil glass	7.4:1	Distilled Water

Table 2.1: Manufacturers recommended mixing ratio's for Fuji IX, Ketac Fil Plus and Chemfil Superior.

The manufacturers depiction of ideal mixing conditions in the case of Chemfil Superior cement is shown in **figure 2.2** below:

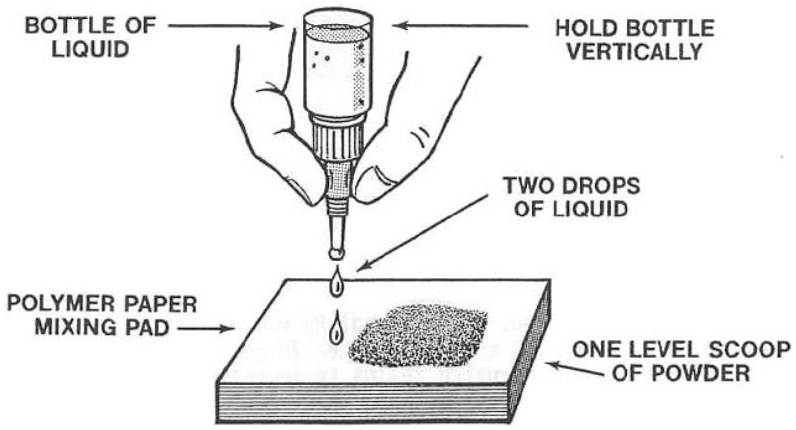

Figure 2.2: Manufacturers depiction of ideal mixing conditions [39]

Ideally a single level scoop of powder taken using the manufactures supplied scoop can be combined with two drops from the supplied bottle. However in practice this method is not particularly accurate and as a result a weighing balance was used to ensure that the ratios were maintained.

2.1.2 Storing samples of glass ionomer cements

Once prepared the GICs have to be stored in solution, ideally water, to ensure the cements remain suitably hydrated throughout their setting process and to prevent dehydration which would adversely affect their properties. Once prepared, the samples were stored under distilled water, which was distilled on site.

2.2 Methods

2.2.1 Development of Planar Test Assembly

Usually impedance in GICs is generally measured using a ‘’like permeation’ cell shown in detail in **figure 1.8** [25], where the sample is suspended between two known electrolytes containing known electrodes. A current is passed through the sample and the electrolyte giving the value for impedance. This design is quite large, and for the purposes of the miniaturisation of the design, a more direct method of measurement should be used to reduce the complexity. Given this design constraint, a sensor/test assembly set up was designed which is much simpler. The impedance of GIC is measured specifically because it is proportional to resistance and inversely proportional to resistance, capacitance and frequency, which accommodates for both resistive and capacitive behaviours of the setting cement.

Before the sensor could be designed, the electrical properties of the glass ionomer cements had to be ascertained, as the dielectric properties of Fuji IX had not been measured using a direct contact method at the inception of this investigation. The dielectric properties of Fuji IX were measured based on the experimental method used by M. Braden and R.L. Clarke [1]. The original design of test assembly used by Braden et al. is shown in **figure 2.3** [1].

What can be seen in **figure 2.3** [1] is that this design makes use of a polyethylene window which acts as a mould into which the GIC can be formed to give the controlled shape of the sample, with tin foil acting as the cathode surfaces and

connection to the measurement device. This control of sample size and demotions is critical in accurately measuring the impedance of the sample.

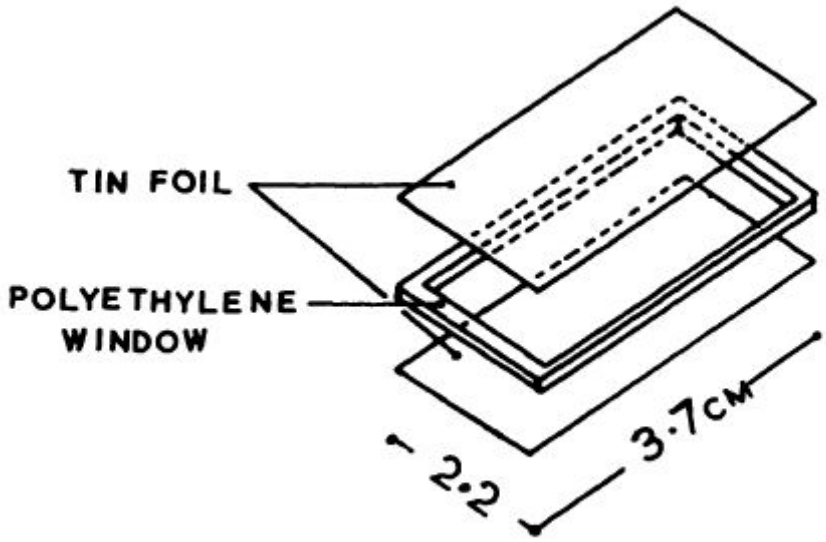

Figure 2.3: Test assembly used by Braden et al. for the measurement of the curing of zinc-oxide eugenol cements [1].

Due to the limited amounts of various GICs available and the need for a greater understanding of the general dielectric properties of the cement, a series of variations on the original design were made, using varying sizes of test assembly. These theoretical calculations were intended to show that it would be possible to change the dimensions of the assembly and still receive a measurable value. Based on the work of W.M. Tay and M. Braden's with glass ionomer cements [2], their original data for the curing of the two different Fuji II glass ionomer cement powder/liquid ratios were taken from the graphs of the resistivity and of the relative permittivity shown in **figures 1.6** and **1.7** [2].

The data from Braden et al.'s experiments was then used to establish the feasibility of a new design using the equations for both electrical resistance and impedance, detailed below:

$$R = \frac{L \times \rho}{A}$$

Using the calculation for resistance, where L is the thickness of sample, ρ the specific resistivity and A the area, all of which were provided in the data and the test assembly.

$$Z = \frac{R}{\sqrt{(1 + \omega^2 R^2 C^2)}}$$

Where R is resistance, ω the angular frequency and C the capacitance. The data was recalculated and the resistivity and relative permittivity were used to estimate the effect of varying the dimensions of the test assembly on the potential resistance, capacitance, impedance and phase values. These recalculated values are shown in the results, (**3.1** Theoretical Values based on Fuji II).

In order to reduce the amount of Fuji IX used, owing to the expense of using the amount of cement that Braden et al used, modifications were made to the design of the temporary capacitor used by M. Braden and R.L. Clarke [1]. **Figure 2.4** represents the finalised design for the planar test assembly:

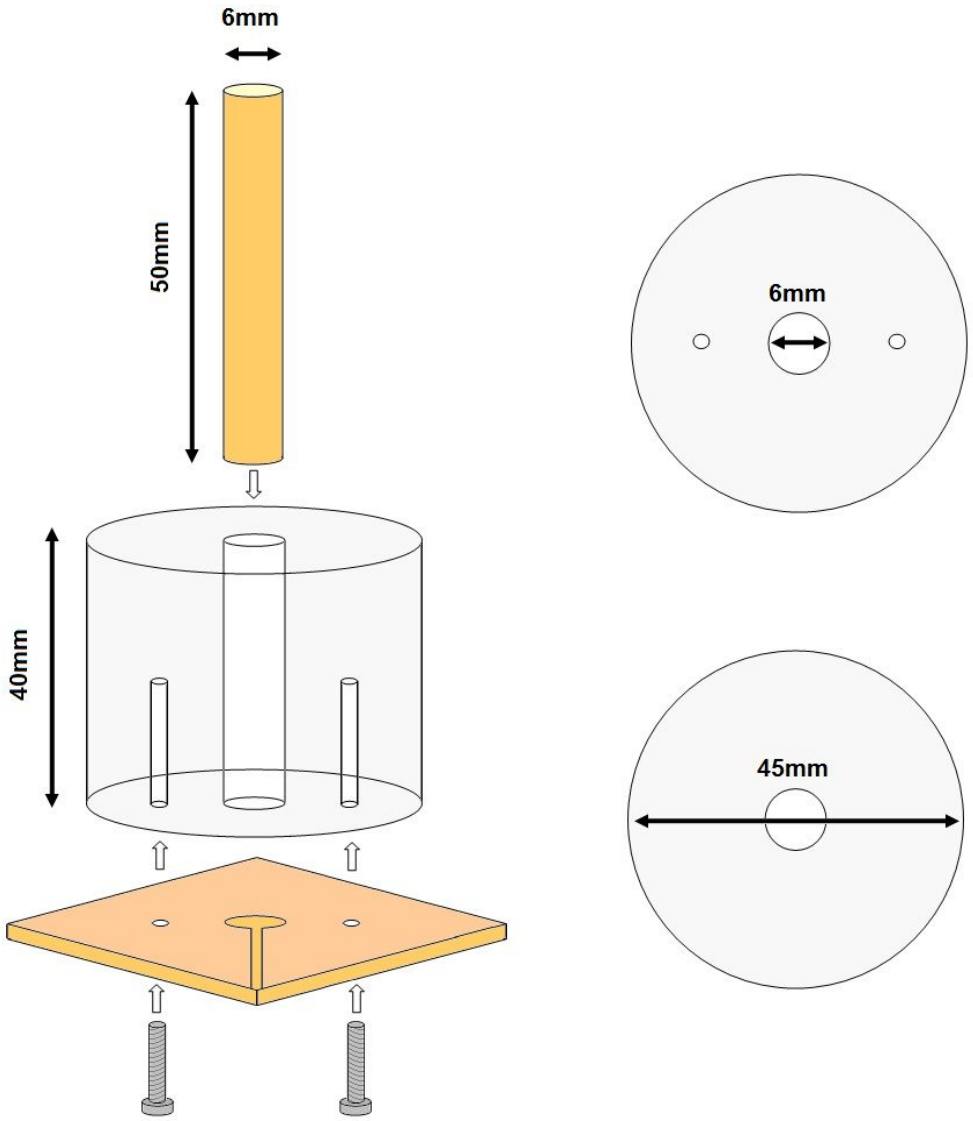

Figure 2.4: Design and dimensions of the perspex test condenser assembly, including the dimensions of the key components.

The change in this design was necessary for a number of reasons. As stated previously, the design used by Braden and Clarke [1, 2, 7], would not be suitable as it would not allow for the test assembly to be inserted into water to maintain the temperature. The size of the test assembly was also too large for the amount of material which was realistically available to be both tested upon and mixed. In order

to counter these two points, calculations were made using the values for resistivity and permittivity of Fuji II, given by W.M. Tay and M. Braden's work with glass ionomer cements [2] to give an indication as to whether it would be possible to measure the dielectric properties of the Fuji IX using a design similar to the one shown above.

In addition to the restrictive size issues, Braden's test assembly made use of a rectangular design. This gave rise to multiple corners, into which the cement must be formed before the impedance could be measured, giving rise to several drawbacks in this design. In order to accurately interpret the results collected, one of the key aspects of the design had to be its repeatability and control of the measurement start time. The addition of corners to the design provided a weak point in this, as it is significantly harder to quickly fill a sharp corner with the prepared cement and the time taken to do this accurately would affect the point at which the measurements start being collected. The simplest resolution to this issue was to make use of a cylindrical shape which eliminated the corners and allowed for the use of a rod/press design.

A perspex cylinder was drilled to a diameter of 6mm, which would act of the walls of the spacer, and into which a copper rod of 6mm in diameter with a length of 50mm, could descend. The decision to use a 6mm thick copper rod was based on the need to use the narrowest diameter rod which would not flex when force was placed onto it, as this rod would allow the sample to be forced onto an etched PCB (printed circuit board) base plate. This required the spacer's size to be extended to the 40mm

height, providing a solid guide to the rod as it descended and ensured that the two contact surfaces were parallel. The two surfaces of both the rod and the base plate can form the anode and cathode, similar to what was proposed by Braden and Clarke [1, 2]. The completed test assembly is shown in **figure 2.5.**

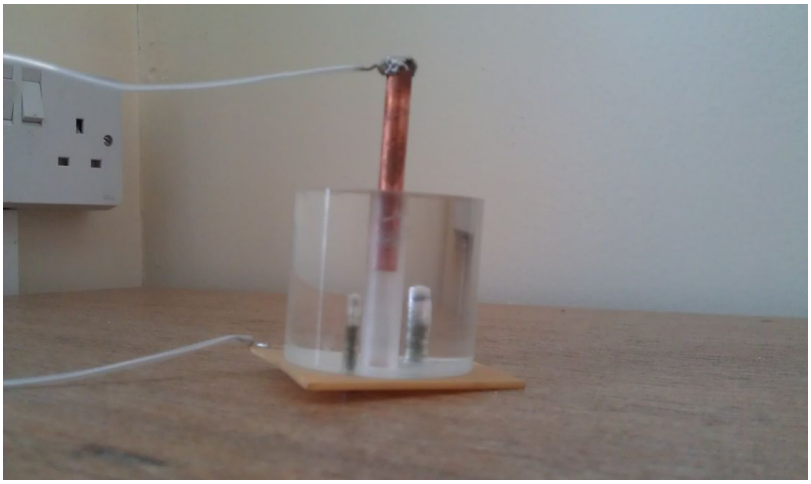

Figure 2.5: Photograph of parallel plate assembly after construction

The connection wires visible in **figure 2.5** are made of silver and were chosen due to their favourable electrical properties and good conductivity. These were soldered to the copper contacts of the base and rod as part of the finalisation of the assembly. The copper construction of the base and the rod presents an issue with the design, as though copper is a good conductor it is also a reactive metal. In the presence of the acid-base reaction and the water rich environment it is possible that the copper would oxidise releasing additional electrons and ions into the system, possibly accelerating or retarding the GIC curing at the interface between sample and cathode as the leached glass ions are neutralised. Though this presents an issue with the design, as the permutation of this effect will be low and the impedance is measured

across the bulk of the sample this should not have a significant effect on the data collected.

2.2.2 Set-up of Planar Test Assembly to Impedance Bridge

The above test assembly was connected to an Agilent 4294A Precision Impedance Bridge (Agilent Technologies, Inc, Santa Clara, CA, United States) which in turn was also connected to a computer. An impedance bridge is a specific device used to measure electrical impedance and capacitance through the passing of a sinusoidal voltage between two cathodes (with a sample between) and an internal resistor (of know resistance) and then measuring the voltage across both. The variance is then analysed and the impedance calculated and logged. The test assembly was connected via a silver wire, to reduce any errors in measurement from the wiring. With the assembly and bridge ready the sample could be prepared. This set-up is outlined further in **figure 2.6**.

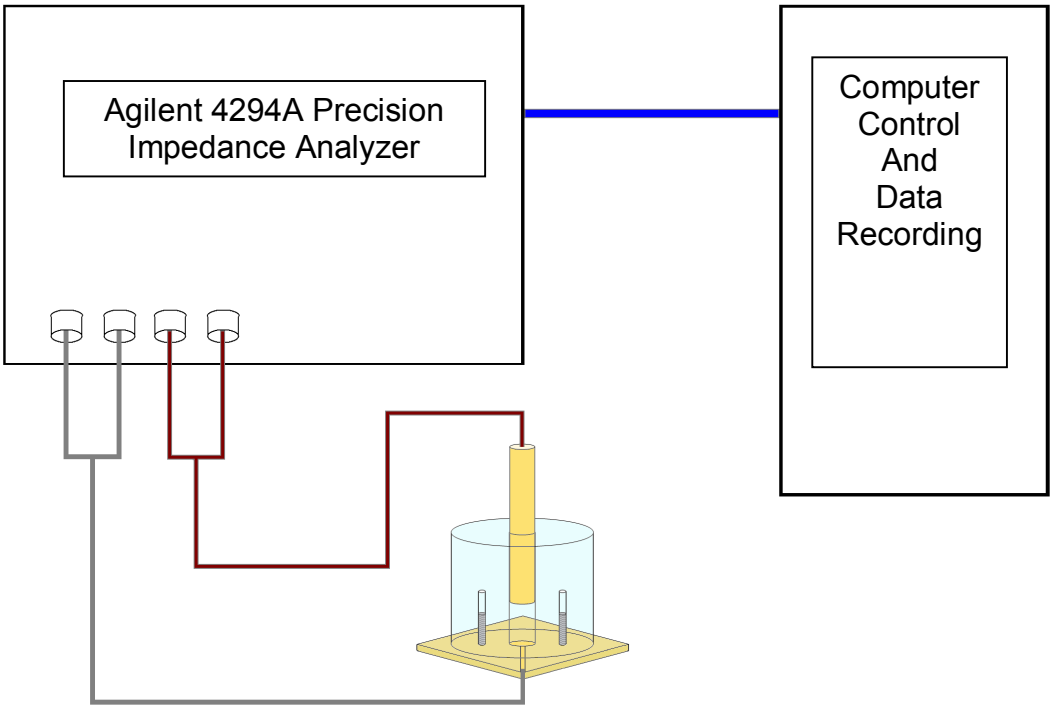

Figure 2.6: Set-up of the test assembly in conjunction to the Impedance Analyzer and controlling unit.

2.2.3 Impedance Measurement

Owing to a surplus of Fuji IX the initial results for this first iteration of the test assembly were only collected using Fuji IX. The sample of Fuji IX will be prepared according to the manufacturing specifications, at a powder to liquid ratio of 3.6/1, with an exact measurement of the powder and liquid components being made with an electric balance (Scout Pro SPU202, Ohaus Corporation, NJ USA) rather than the manufacturers single scoop to one droplet method. The Fuji IX paste was then inserted into the testing assembly, and using the copper rod as a plunger, forced to

the base of the perspex block (**figure 2.7**), whereupon the impedance bridge could began to measure its dielectric properties as the glass ionomer cement sets.

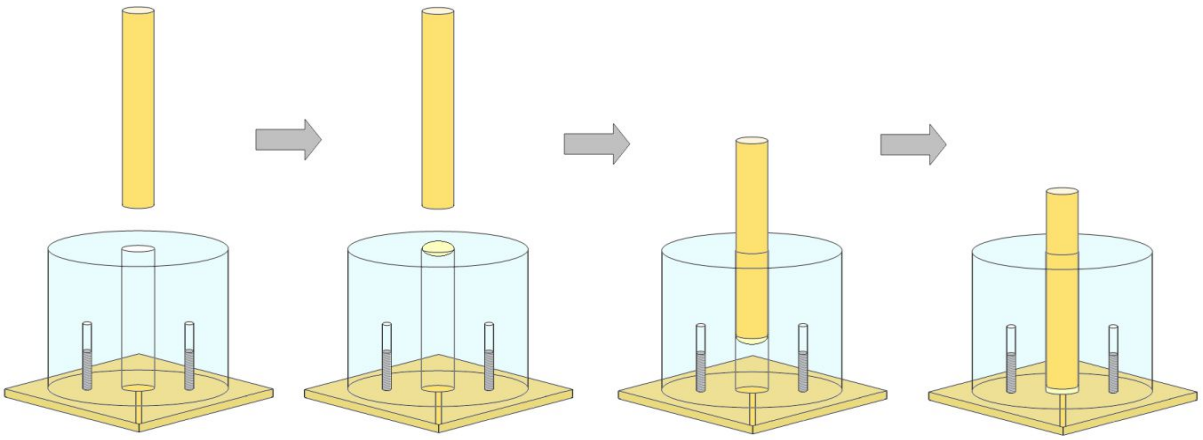

Figure 2.7: Insertion and compression of the Fuji IX sample in the test assembly.

The impedance bridge measured the dielectric properties of the setting cement over the course of 24hours, recording the impedance and the phase.

2.2.4 Co-planar Assembly Development

Though the planar test assembly provided a solid system which was easily used and repeatable, a number of failures in data collection and design issues were identified which needed to be addressed in order to ensure the results collected were accurate and to prevent future failures. During testing the samples were kept in a dry environment and had no access to additional fluids. Given that GICs are designed to cure in an aqueous environment this lack of hydration let to the dislocating of the sample from the connection surface and potentially altered the setting mechanics of the cement, leading to uncontrolled deviations in the results.

In addition to the dehydration there was an issue in the control of the sample thickness. Though exact quantities were thoroughly mixed as part of the preparation of a sample, during the formation of the bolus to be added to the assembly a certain amount of GIC was lost adhering to the mixing plate and spatula. This caused variation in the amount added to the assembly which in turn affected the sample thickness and thus the repeatability of the results. In order to ensure the experiment was repeatable and accurate and to provide an environment conducive to its setting mechanics changes had to be made to the design.

As a result of the issues, detailed further in the planar results section, discovered during the initial taking of results using the planar design of test assembly it became necessary to redesign the test assembly. The decision was made to move to a co-planer style of assembly, the design chosen is shown in **figure 2.8.**

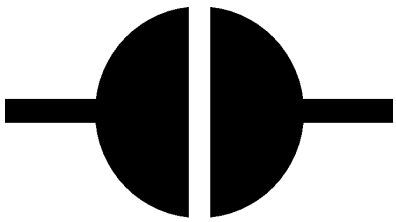

Figure 2.8: Top down view of sensing plates in coplanar design

This change in design also allows for the addition of a well for water allowing sample to be submerged under distilled water and thus prevent the dehydration of the samples as they set. This should eliminate the sudden drop in impedance which

occurs after the first hour of setting, and provide a more realistic curing environment. This new design is demonstrated in **figures 2.9** and **2.10**.

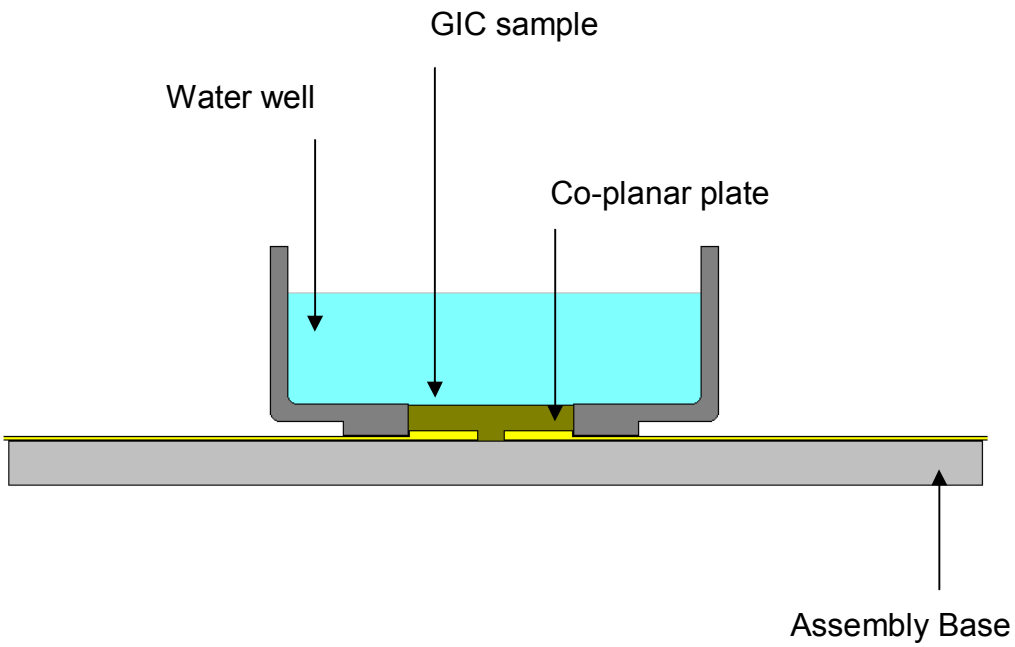

Figure 2.9: Side view of plate arrangement with water well

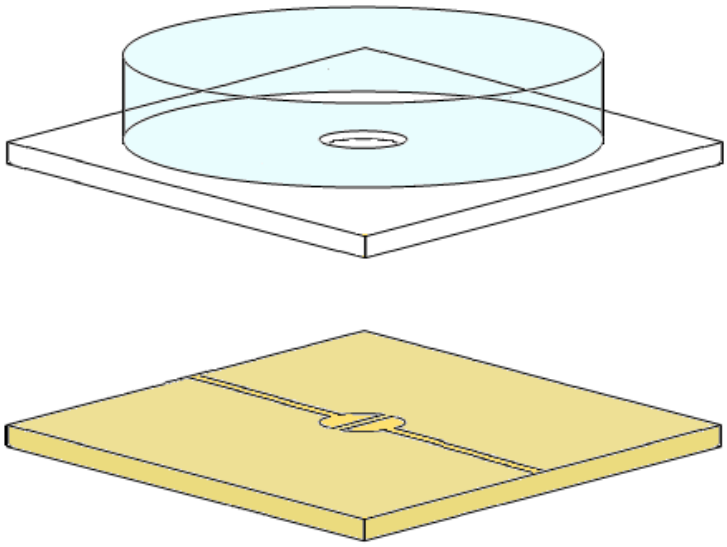

Figure 2.10: Design of co-planar assembly

The base of the assembly was formed out of two hemispherical copper contacts, of a diameter of 6mm, sitting parallel with each other. These could be connected to the wires leading to the impedance bridge via connecting copper strip runs from hemispheres to edge of the PCB board. The mould was formed out of a piece of Teflon 2mm thick, which was placed on top of the base plate with a central hole of a 6mm diameter aligned over the capacitor plates. The upper section of a plastic sample pot was bonded to the Teflon to act as the water reservoir wall. This provided the basic form for the co-planar test assembly, which could be rapidly constructed and maintained. The construction of the co-planar assembly is further detailed in **figure 2.11**.

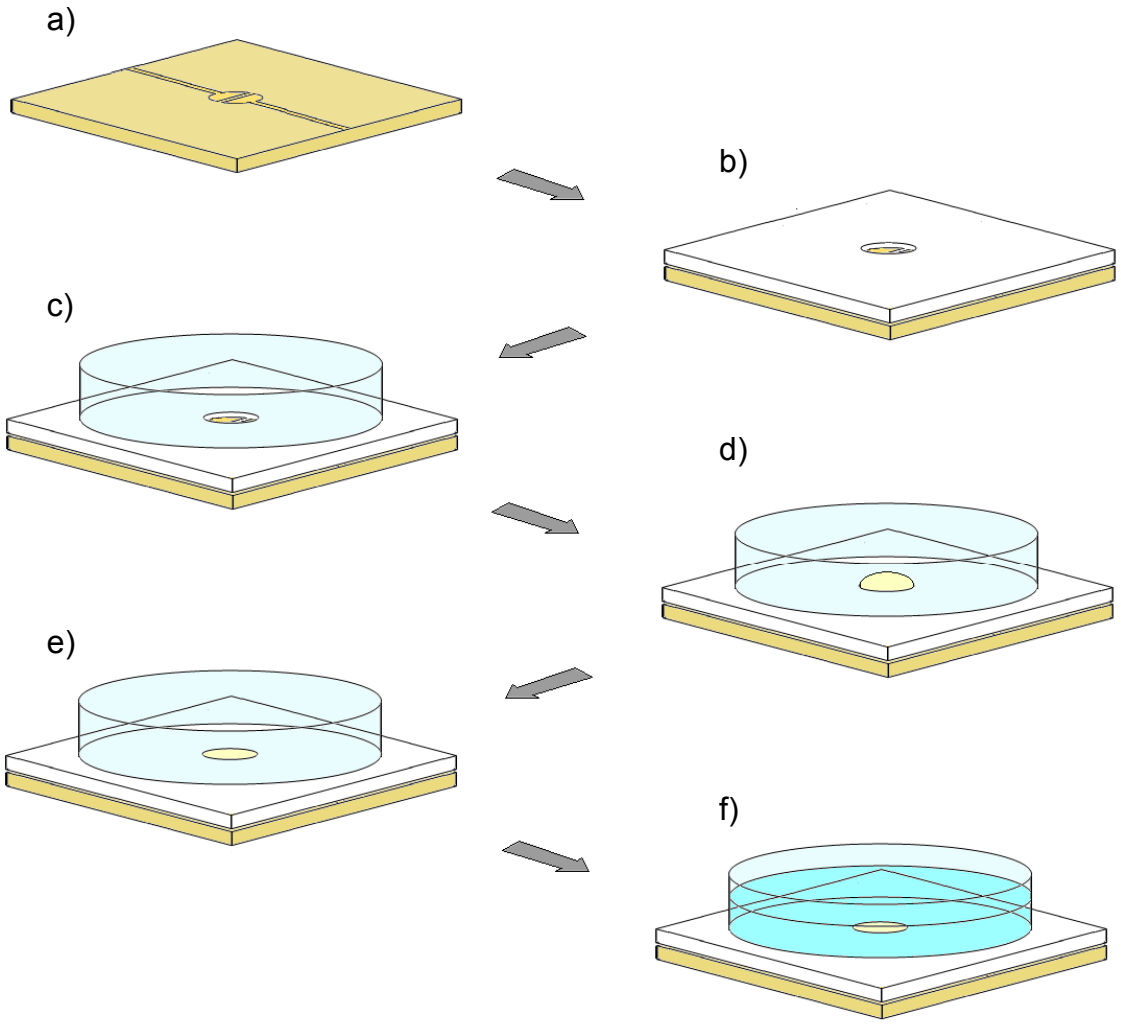

Figure 2.11: Construction and implementation of co-planar assembly, a) Base plate, b) Teflon mould, c) Water well, d) Addition of GIC, e) Compression, f) Addition of distilled water.

The initial steps outlined in **figure 2.11** detail the construction of a co-planar assembly, with the later stages detailing its use for data collection. First the PCD is etched to provide the hemispherical contacts and connection wires that are needed

to measure the sample (**figure 2.11**, a). Once this is complete the silver connection wire is soldered into place on the terminal ends of the etched board. A section of 2mm thick Teflon is then hand drilled with a 6mm hole which will form the basis of the mould. This Teflon is then carefully lined up over the contacts before it is cut to match the PCB's shape and adjusted to ensure a solid and clean contact with the base, with no obstructions or lifting away from its surface (**figure 2.11**, b). The Teflon was held in place with a combination of tape and bulldog clips, while the water well was affixed into position onto the Teflon using a bonding agent, before being left to cure prior to the assemblies use (**figure 2.11**, c).

When ready for use the assembly was placed in position within the grounding box (**Figures 2.12-2.15**) and connected to the impedance bridge, at which point the cement could be mixed and added. The cements were prepared in accordance with the manufacturer's instruction and then the resulting paste was formed into a bolus and added to the assembly within the mould (**figure 2.7**, d). Once within the mould a piece of transparency paper was used to cover the cement and allow the compression of the sample by hand into the mould (**figure 2.7**, e). This greatly reduced the formation of occlusions within the sample and allowed any excess cement being squeezed out of the edge to be cleared from the sample, ensuring that the samples were all of a uniform size. With the sample in place the water well could be flooder with distilled water (**figure 2.7**, f) and a constant force was applied to the cement via a non conductive spacer (formed from a modified specimen tube), which was compressed through weights placed onto the top of the metal housing to reduce the likelihood of dislocation.

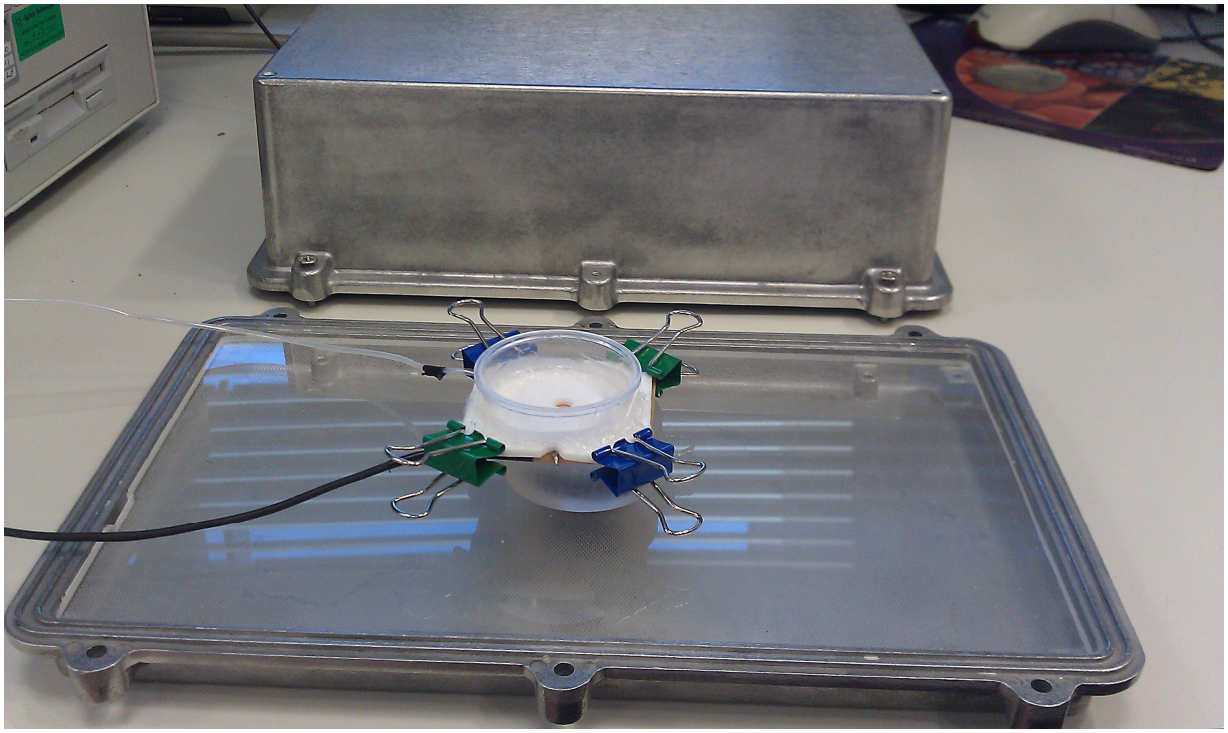

Figure 2.12: Completed co-planar assembly.

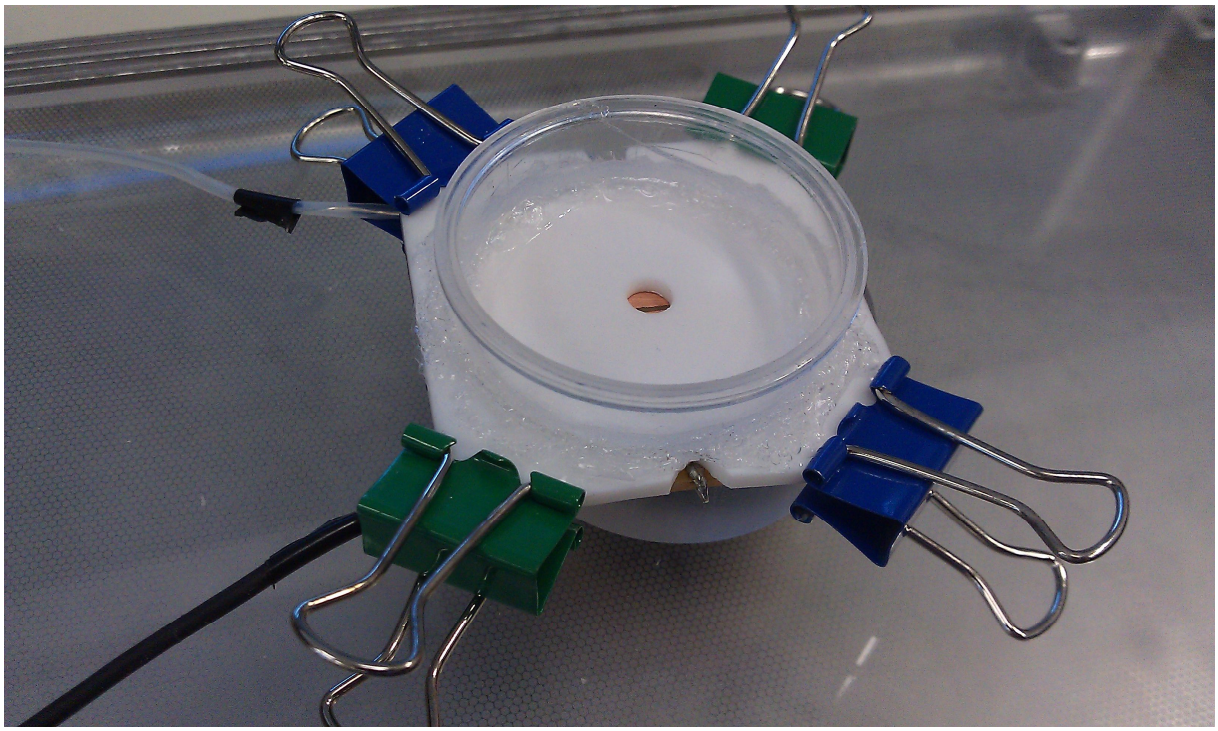

Figure 2.13: Close up image of completed co-planar assembly.

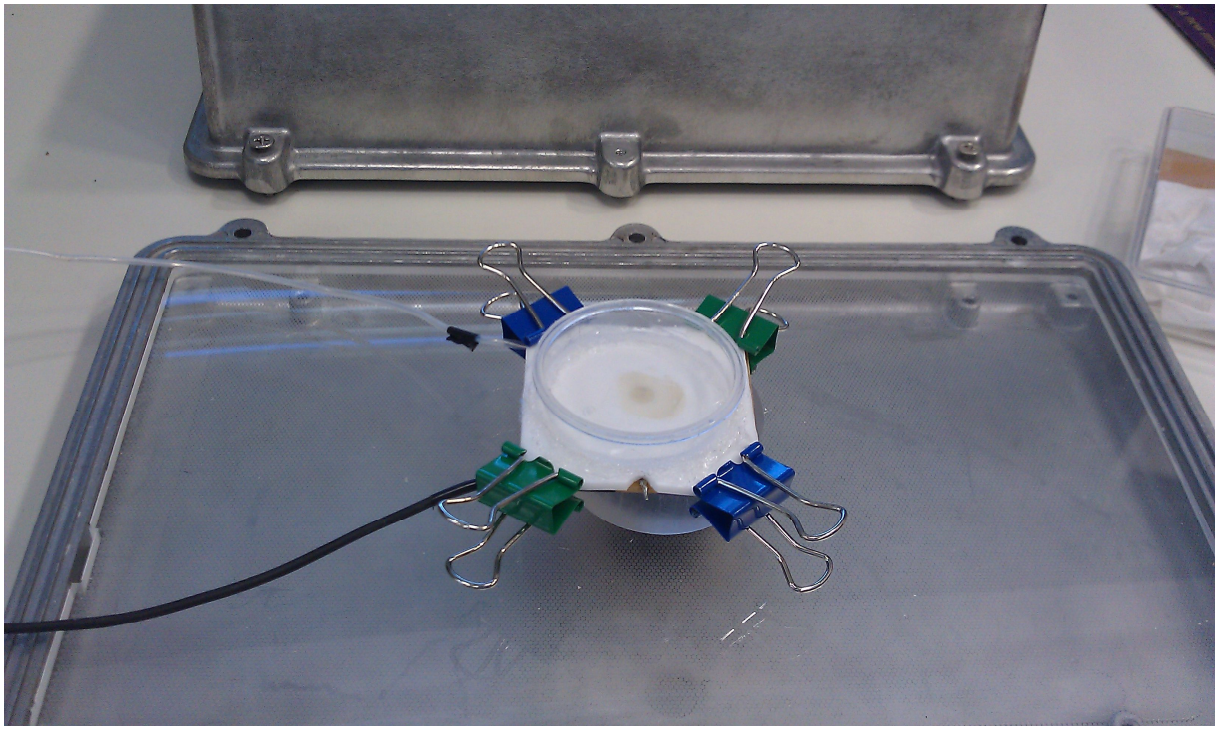

Figure 2.14: Co-planar assembly post addition of cement to mould.

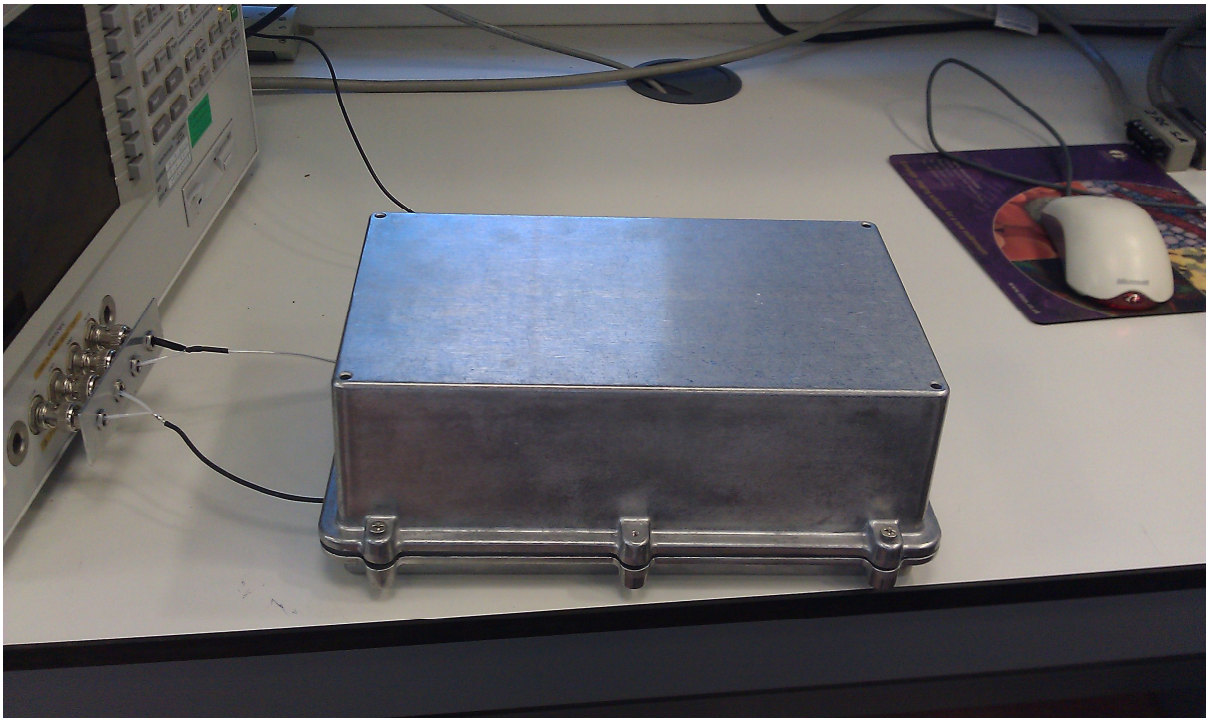

Figure 2.15: Co-planar assembly encased in grounded box to reduce interference from 50Hz frequency of mains power.

2.2.5 Set-up of Co-planar Test Assembly to Impedance Bridge

With the test assembly completed it was then connected to the Agilent 4294A Precision Impedance Bridge (Agilent Technologies, Inc, Santa Clara, CA, United States). The test assembly was connected via silver wire, to reduce any errors in measurement from the wiring. With the assembly and bridge ready the sample could be prepared. This set-up is outlined further in **figure 2.16** and **image 2.17**. The impedance was then recorded at a frequency of 1000Hz - 5000Hz at a voltage of 5v. These specific variables were chosen as the result of limitations with the impedance bridge and test assembly. Though the impedance bridge was capable of operating up to 50,000Hz, initial testing showed that the data collected showed an increase in noise over time possibly which would have negatively affected the quality of the data collected. Increasing the frequency would also have affected the dielectric properties of the cement, with an increase in frequency leading to a decrease in the impedance to electric current within the sample. It would also have compensated for any frequency specific interference such as those associated with –COOH or Na^+ hoping, additionally shifting between multiple frequencies would allow for a similar reduction of interference from any specific bond associated frequency.

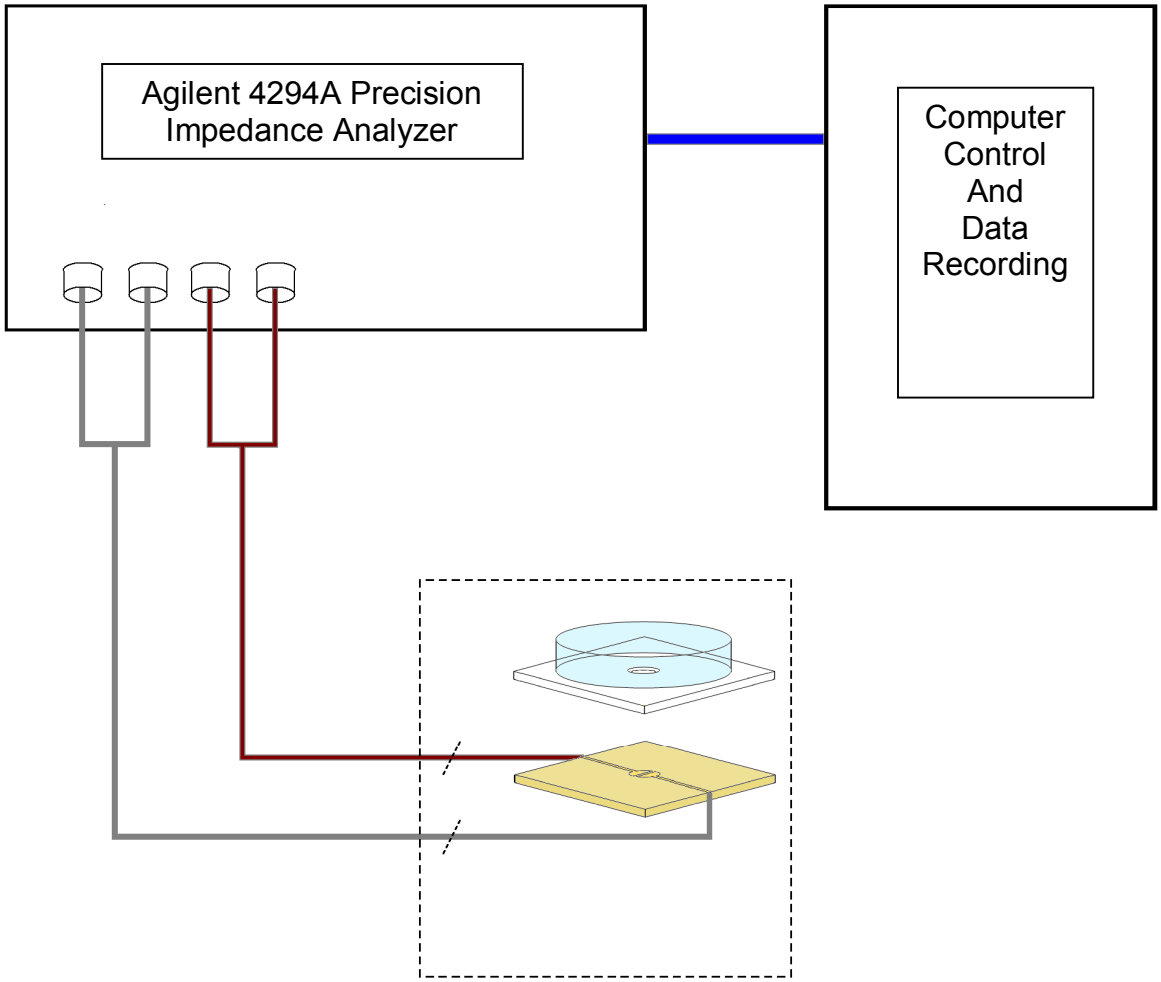

Figure 2.16: Set-up of the coplanar test assembly in conjunction to the Impedance Analyzer and controlling unit

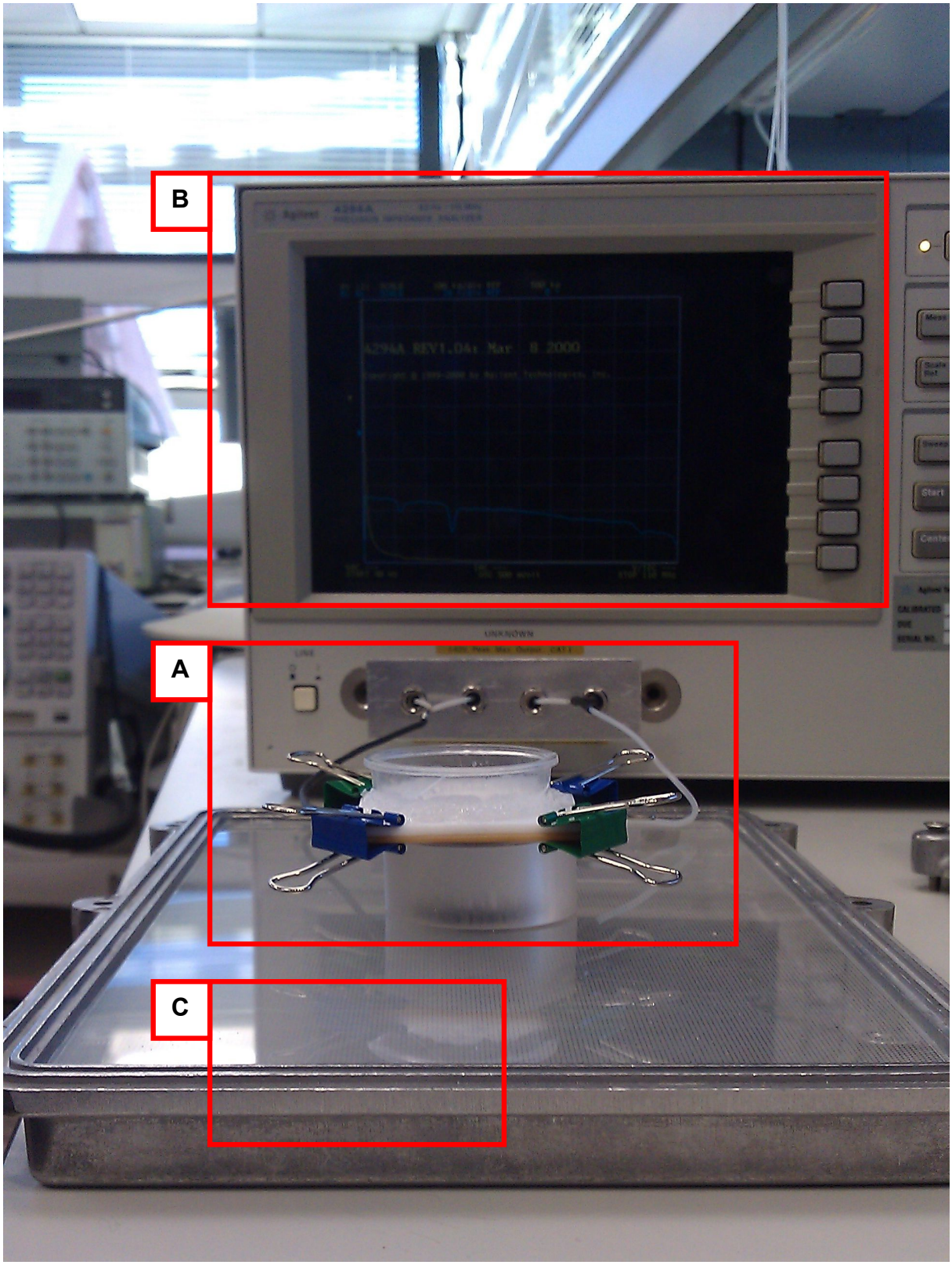

Figure 2.17: Image of completed co-planar assembly (A) connected to Agilent Impedance bridge (B), and the grounded base (C).

As you can see in **figure 2.16** the test assembly is connected to the impedance analyser in the same fashion as with the planar assembly with the only alteration being the change to the co-planar design. This connection of the co-planar assembly is shown in **figure 2.17**, in this image you can see the co-planar assembly (A) connected to the impedance bridge in the background (B). In order to reduce noise which could interfere with the collected data, the assembly is mounted on a disk of perspex and a perspex base plate, both of which are earthed directly to the impedance bridge via the metal enclosure, highlighted in **figure 2.17** (C).

2.2.6 Post construction Modification

After the implementation of the new co-planar design, despite improvements to the quality of the results the wear and tear of use resulted in the new design failing in a number of different ways. The adhesion of the water well to the Teflon spacer proved to be a weak point in the design and showed a tendency to fail during cleaning ready for its next use. The creation of a bulk of these spacers, with wells, allowed for rapid change over and the continuation of data collection whilst the used spacers were cleaned and maintained.

In addition to this the PCB base was shown to have a limited lifespan as repeated use, cleaning and corrosion (caused by periodic leaks of assembly) damaged the contact surface. In-order to prevent delays whilst repairs were made, the ability was added to rapidly add/remove a test assembly, through the use of a screw based

crimping system, detailed in **figure 2.18** and **2.19**. This allowed for several assemblies be built ready for use and added when required.

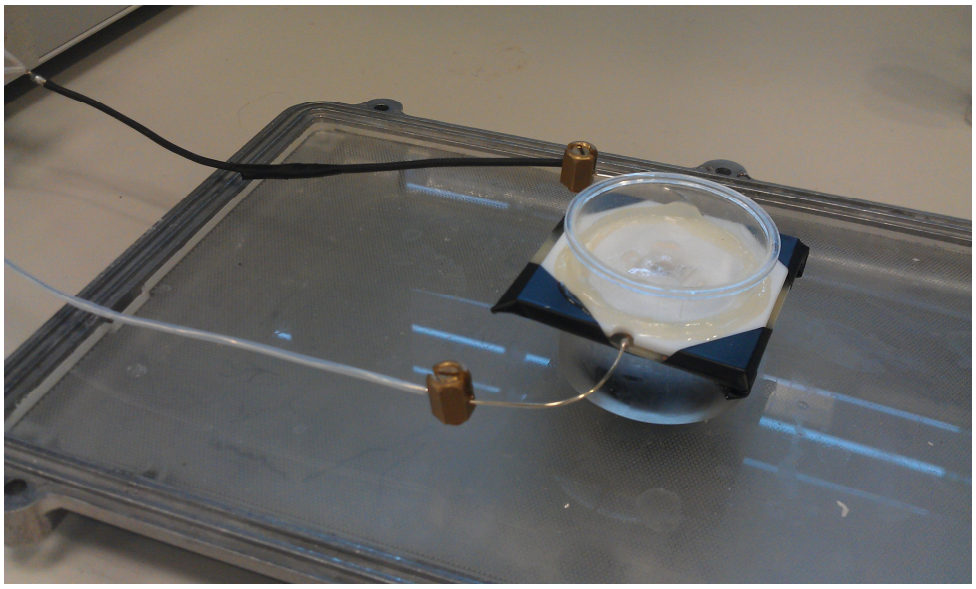

Figure 2.18: Modifications to test assembly

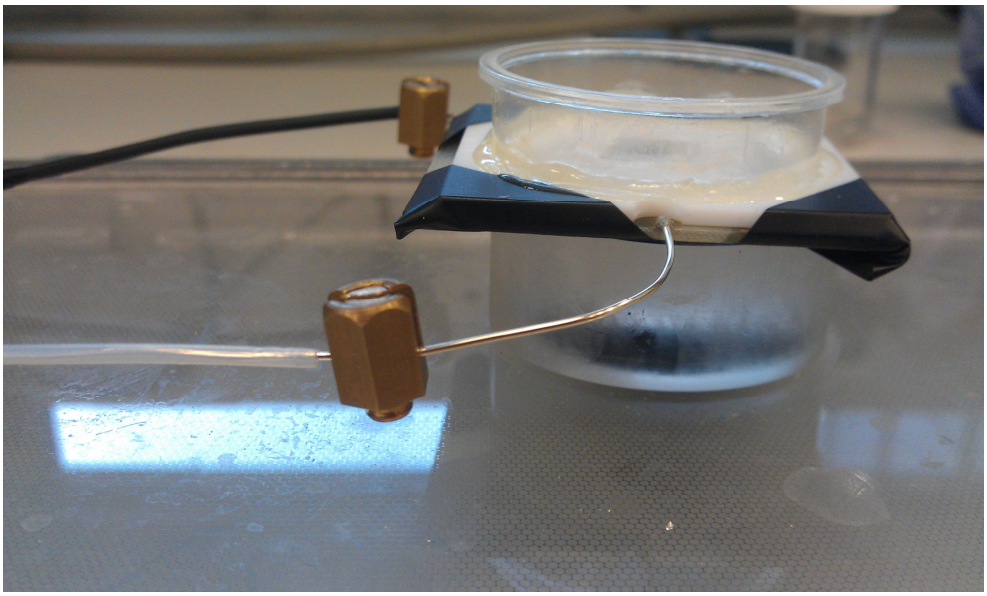

Figure 2.19: Close up of the modifications to the test assembly to allow for rapid changing of the assembly.

2.2.7 FT-IR of Glass Ionomer Cements

In order to monitor the changes in the cement as it sets the cement was monitored through the use of Fourier transform infrared (FT-IR) spectroscopy. Each particular bond within a sample under FT-IR interrogation has a specific IR wavelength associated with it which is the product of the vibration and stretching of the molecular bonds within the sample. The vibration and stretching energy levels of the bond correspond to the wavelength of light emitted or absorbed by the bond.

The FT-IR interrogation of the glass powders, PAA and GIC's, post mixing were performed using a Nicolet^{TM} FT-IR spectrometer (Nicolet^{TM} 8700, Thermo Electron Scientific Instruments LLC, Madison, USA), using a golden gate single reflection diamond Attenuated Total Reflectance attachment and Omnic software suite. The range of wavenumbers measured was 4000 – 700cm^{-1} with the number of scans being set to 64 and an optical resolution of 6.329cm^{-1}.

The samples were prepared in accordance with the manufacturers guidelines, at the suggested ratios and at room temperature. Once mixed the sample was placed on the diamond aperture of the golden gate bridge. The sample was then gently compressed with a volatiles cover. This compression of the sample ensured that there was a solid contact between the sample and the aperture, reducing noise and removing atmospheric affects. In-order to prevent the sample dehydrating once the scan is under way a rubber O-ring was then placed around the sample which was then flooded with distilled water before a cap was placed on top to prevent the

evaporation of the water. Once this was done the scan was then collected over the 24hrs.

2.2.8 Labview Program

In order to use the Agilent precision impedance bridge to full effect and obtain the most exact readings for the impedance and phase change of the glass ionomer cement as it sets, the control of the impedance bridge is done through a Labview program. This program controls the impedance bridge, which operates at 5000Hz and gives a reading every ten seconds for impedance and phase, for the 24 hour period.

Chapter 3

3 Results and Discussion

3.1 Theoretical Values based on Fuji II

The results calculated for the resistance, capacitance and impedance values for the new design of the impedance test assembly, based on the values of resistivity and of relative permittivity of Fuji II given in **figures 1.2** and **1.3** [2], are shown in the next few graphs. The theorised values of glass ionomer cements for the chosen design of test assembly are given here. These calculations were performed with an applied voltage amplitude of 5V at a frequency of 5000Hz. The radius the spacer was 3mm in line with the designs 6mm diameter, and the approximation for the sample thickness was 1mm. Using these values following values were calculated:

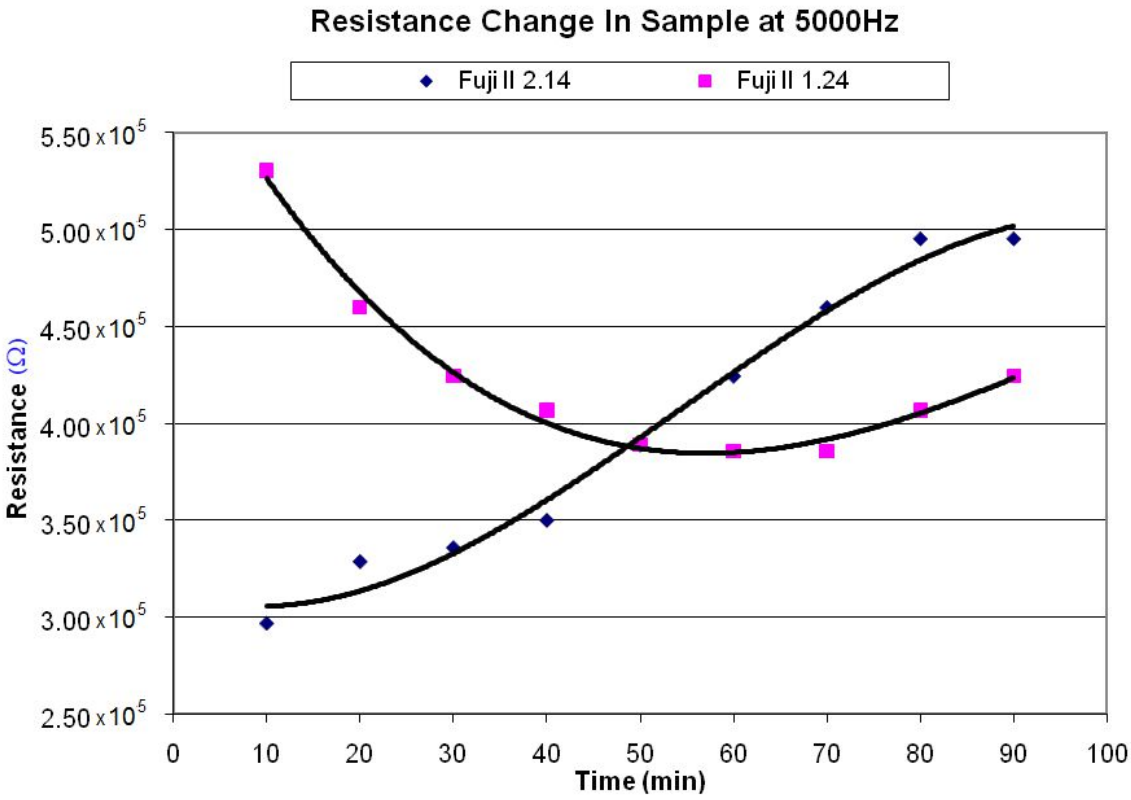

Figure 3.1: Theoretical resistance at 5000Hz using 5V.

The resistance here was calculated using:

$$R = \frac{L \times \rho}{A}$$

Where L is the thickness of sample, ρ the specific resistivity and A the area.

Looking at the calculated resistance change in Fuji II samples, shown in **figure 3.1**, what can be seen is that over time the resistance of the Fuji II 2.14 sample increases in a slight S curve, whereas the Fuji II 1.24 samples resistance initially decreases before rising towards the later end of the 2hrs. This variation is due to the ratio change between the samples, with the Fuji II 2.14 sample curing quicker at the larger

volume of glass provides access to a greater number of ions to crosslink the PAA, increasing the cure speed. The Fuji II 1.24 sample will continue to attack the glass particles until it is neutralised by the resulting released ions. This means that there is an initial period of high ionic content where the free ions will freely conduct current through the GIC before the ions become cross linked. This behaviour can be seen again in **figure 3.2.**

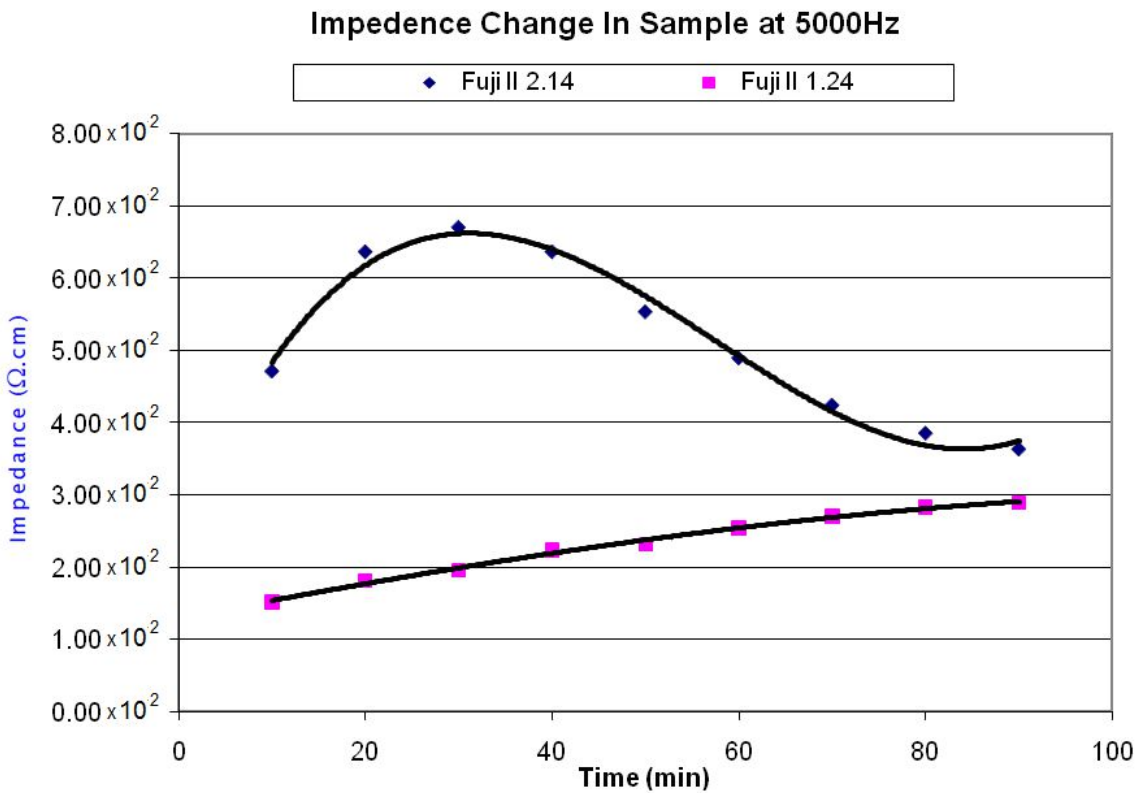

Figure 3.2: Theoretical impedance at 5000Hz using 5V over 90 minutes.

The impedance was calculated using:

$$Z = \frac{R}{\sqrt{(1+\omega^2 R^2 C^2)}}$$

Where R is resistance, ω the angular frequency and C the capacitance.

Here the impedance of the Fuji II 2.14 increases initially and then falls off, where as the Fuji II 1.24 shows a gradual increase. The gradual increase shown in Fuji II 1.24 is an expected, based on the curing behaviour of the cement, with the large volume of ions which are slowly removed as charge carriers by the curing reaction providing little resistance to the flow of current or the change in current. This is in contract that of Fuji II 2.14 where the impedance increases to start and then falls off, which is indicative of the rapid changes in ionic availability to start, and then the gradual curing of the cement. The difference between **figure 3.1** and **figure 3.2** is due to the different behaviour of the samples, where Fuji II 2.14 behaves as a lossy-capacitor providing both capacitive and resistive behaviours, and Fuji II1.24 behaving more as a resistor.

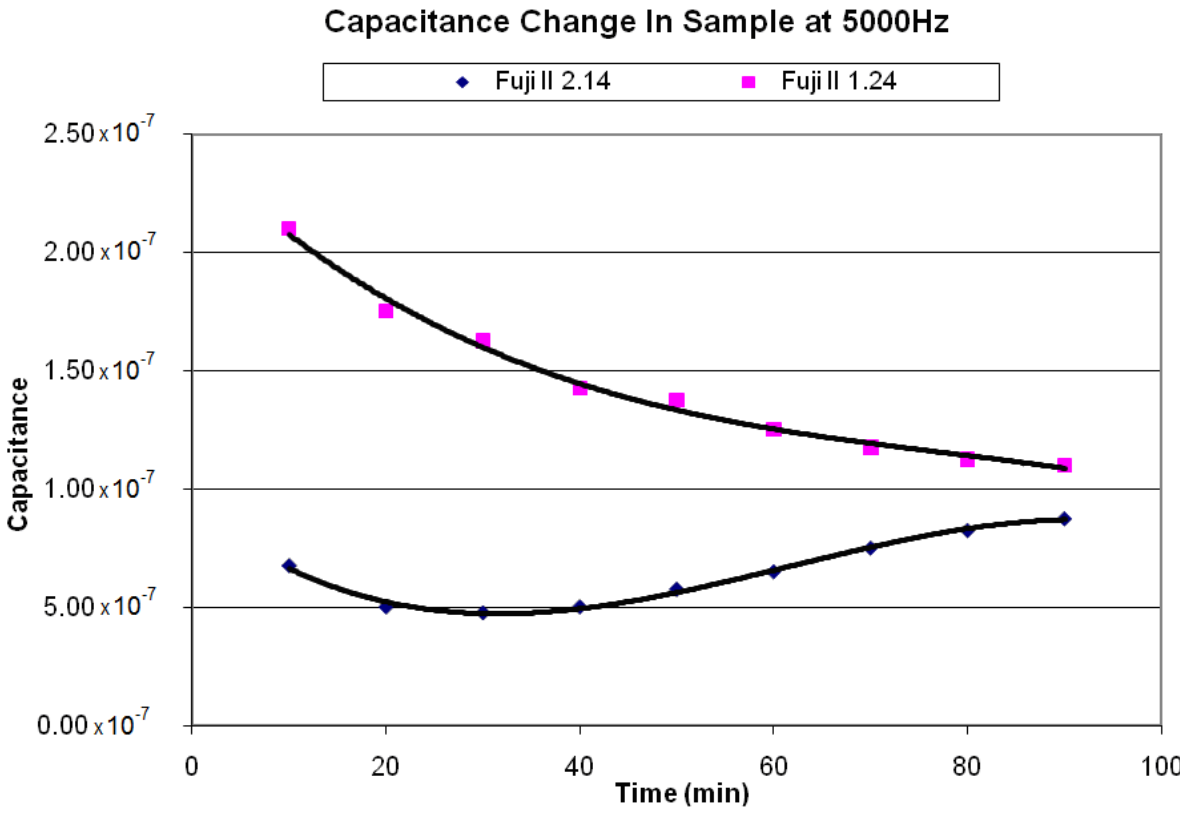

Figure 3.3: Theoretical capacitance at 5000Hz using 5V.

The capacitance was calculated using:

$$C = \frac{(\varepsilon_o \varepsilon_r A)}{d}$$

Where ε_o is the absolute permittivity, ε_r the relative permittivity, A the Area and d the distance between the plates.

Based on the data for resistivity and relative permittivity of Fuji II given in **figures 1.6** and **1.7** [2], the calculated results for the resistance, capacitance, impedance, current and phase of the Fuji II as it sets within the chosen test assembly design indicated that it should be possible to measure the change in the dielectric properties of a setting glass ionomer cement. The variation in the values of resistance and current were both sufficiently large that theoretically the change could be monitored using a dielectric monitoring MEMs sensor. The change indicated here also suggests that the change in the design would also maintain the ability to functionally measure the change in the impedance.

However these reults only provide an indication, as Fuji IX and the other GIC's chosen have a different composition and they do not take into acount the fact that the setting of Fuji II, and the other glass ionomer cements normally occurs in an aqueous environment, which would be difficult to replicate using the impedance bridge, due to the conductive nature of water.

Based on these results calculated for the dielectric properties of the Fuji II, it should be possible to measure the dielectric properties of Fuji IX using an impedance bridge and this assembly design. The calculated values, given above in **figures 3.1, 3.2** and

3.3 indicate that the values of impedance are measureable using the proposed design. Based on this the design was constructed and finalised. The results which are then collected can also be used to help to create a design for the MEMs sensor which will be used in the further experimentation.

3.2 Planar Test Assembly

The following results are those collected from the planar test assembly and the issues that were encountered in the testing of the test assembly.

3.2.1 Assembly Testing

The impedance of Fuji IX over a 24hour period was collected multiple times and the resulting impedance values averaged out to produce the graph shown in **figure 3.4**.

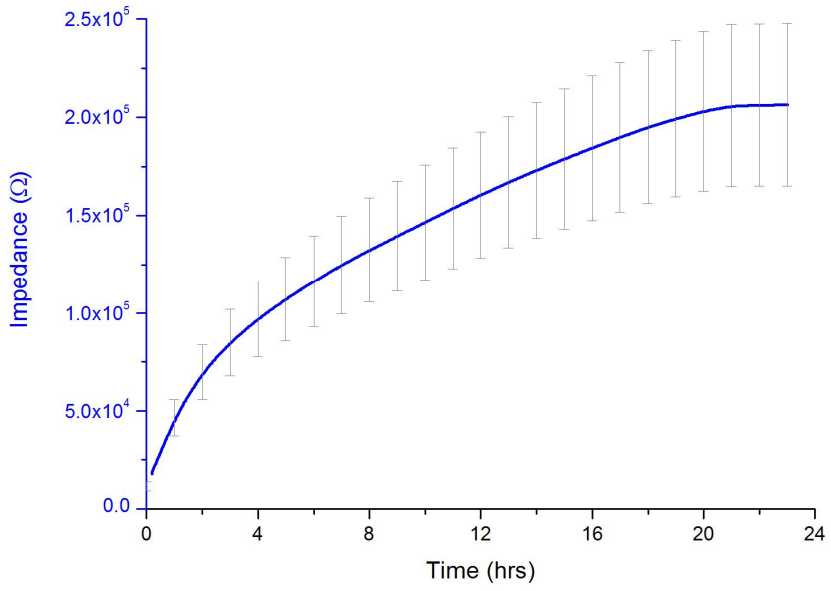

Figure 3.4: Impedance of Fuji IX measured over 24hrs of setting reaction using planar test assembly

The measured impedance shown in **figure 3.4** shows a rise from an impedance value of $2x10^4$ Ω to $2x10^5$ Ω, this represents a significant rise in the impedance and could possibly be a sufficiently large rise as to be detectable if scaled down to a small size test assembly.

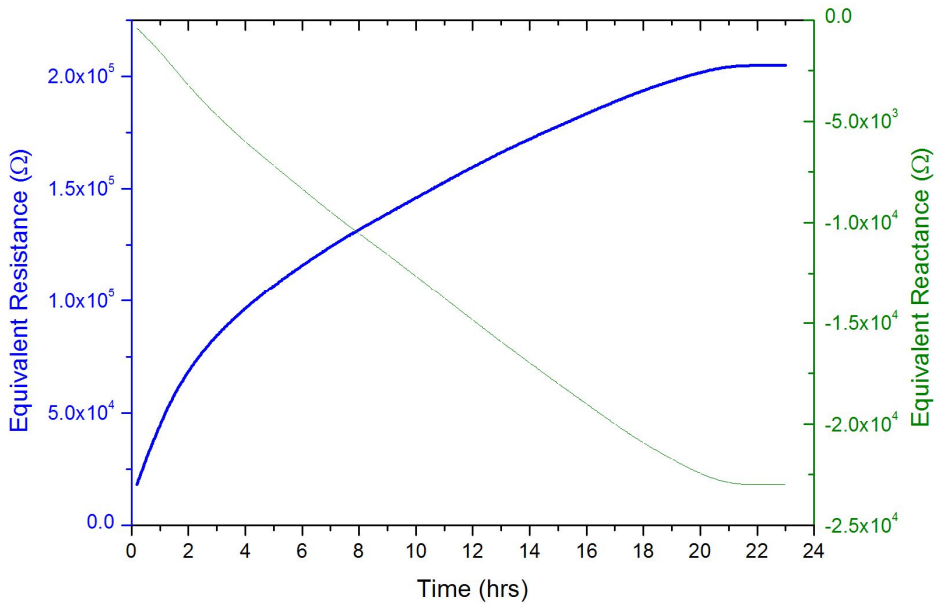

Figure 3.5: Equivalent resistance and equivalent reactance calculated from measured impedance of Fuji IX measured over 24hr of setting reaction using planar test assembly.

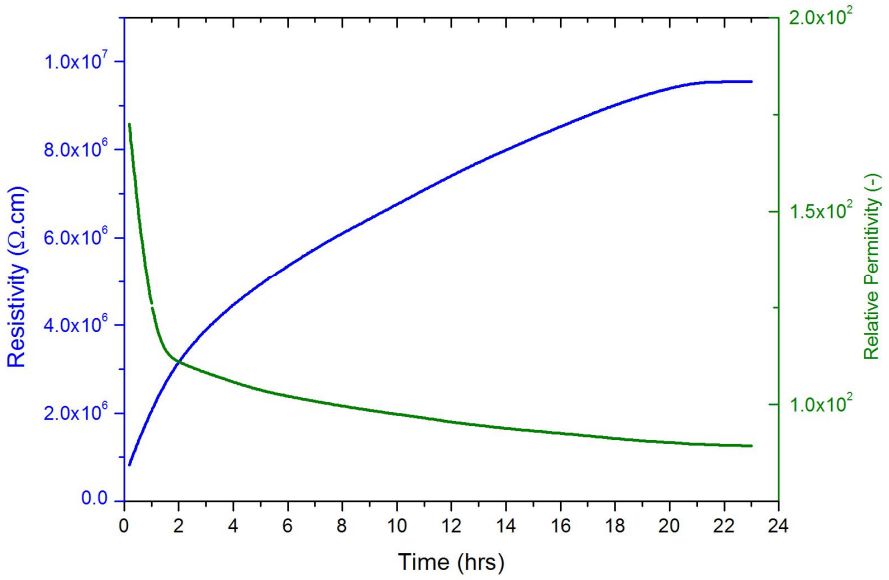

Figure 3.6: Resistivity and relative permittivity calculated from measured impedance of Fuji IX measured over 24hr of setting reaction using planar test assembly.

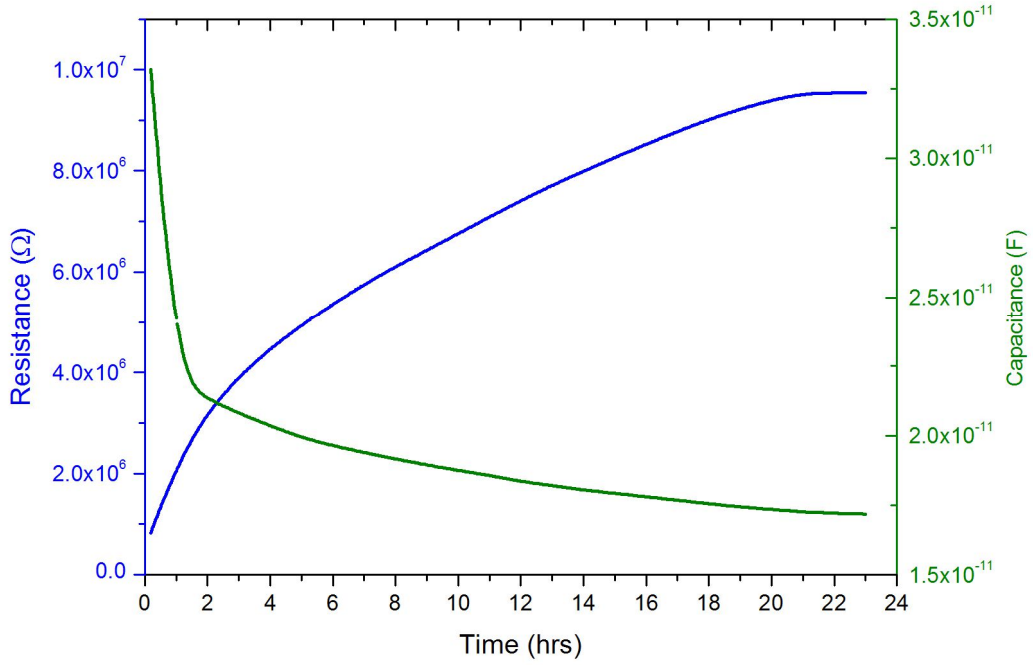

Figure 3.7: Resistance and capacitance calculated from measured impedance of Fuji IX measured over 24hr of setting reaction using planar test assembly

Despite the apparent success of the design in gathering the impedance of the cement, there were a number of issues with the results which indicate issues with the design. After the first hour of measurement all of the collected results showed a sudden change in the measured impedance, dropping rapidly. This particular effect can be seen in both its most extreme case in **figure 3.8** and at a much more minor level in **figure 3.9**.

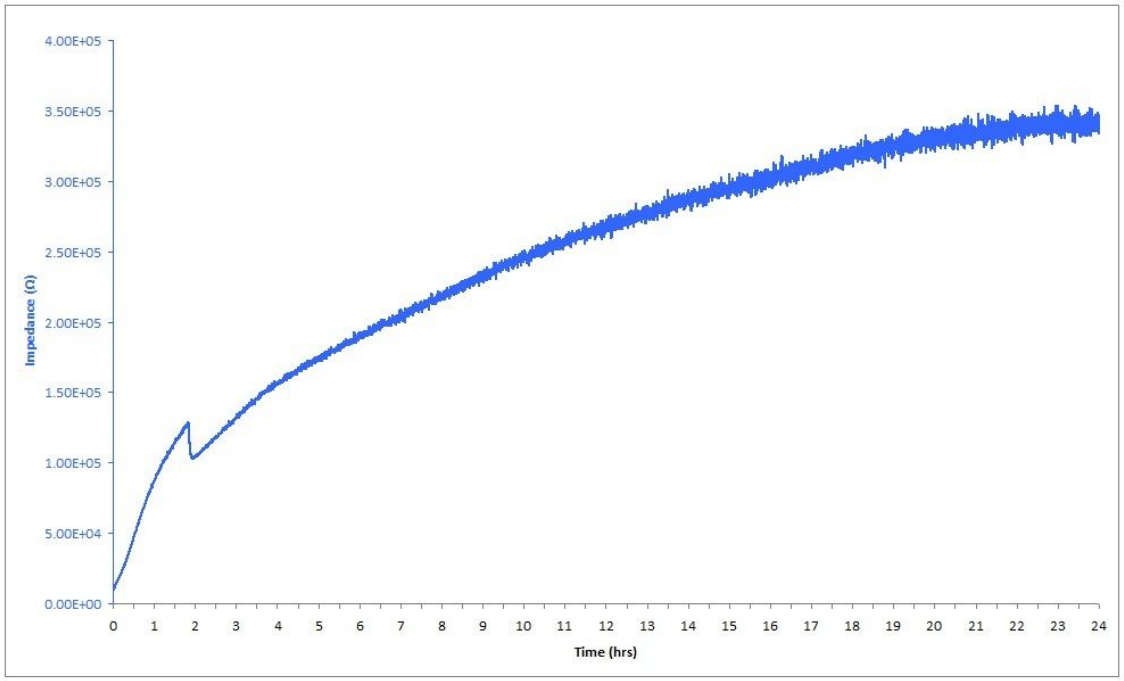

Figure 3.8: Rapid change in impedance measured using planar test assembly

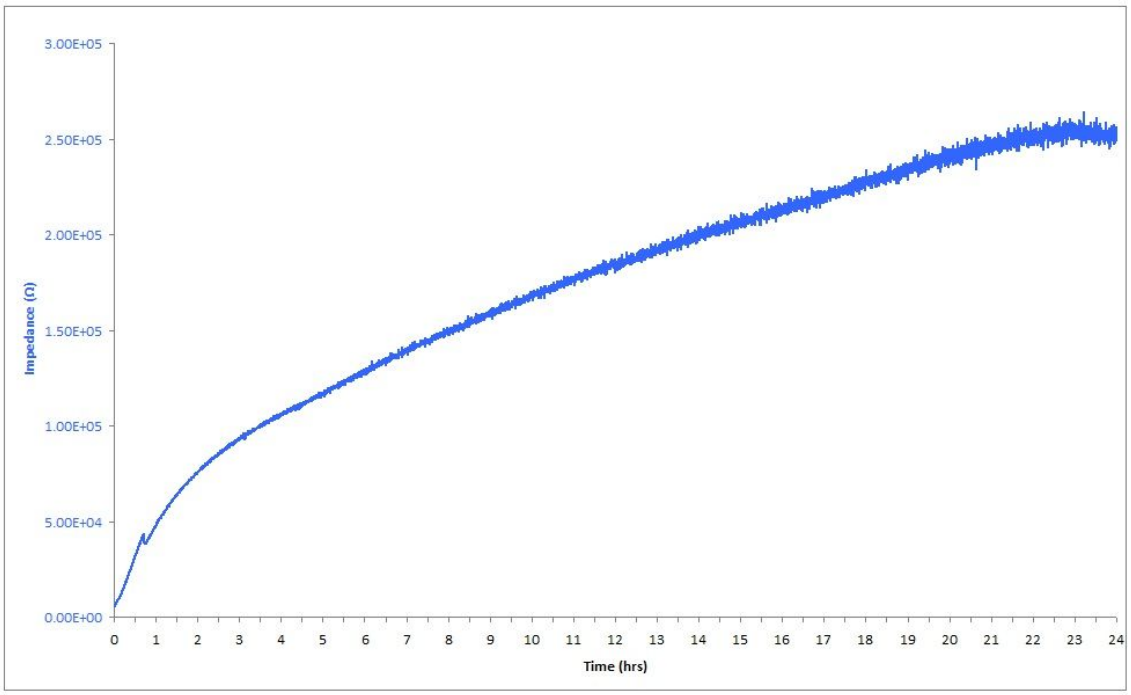

Figure 3.9: Minor drop in impedance measured using planar test assembly

This dramatic change in recorded impedance is unlikely to be down to a change in the samples setting chemistry but rather either a mechanical failure in the samples connectivity to the test assembly or possibly due to an environmental effect.

As GICs are designed to cure in the aqueous environment of a patients mouth it is likely that the dry environment of the planar test assembly caused the samples to dehydrate completely. The sample data shown in **figures 3.10** and **3.11** was recorded from 3 samples where the cement was clearly dislocated from either of the copper cathode surfaces. On inspection the samples were found to be dry and had cured normally however had pulled away from the cathodes as they had contracted.

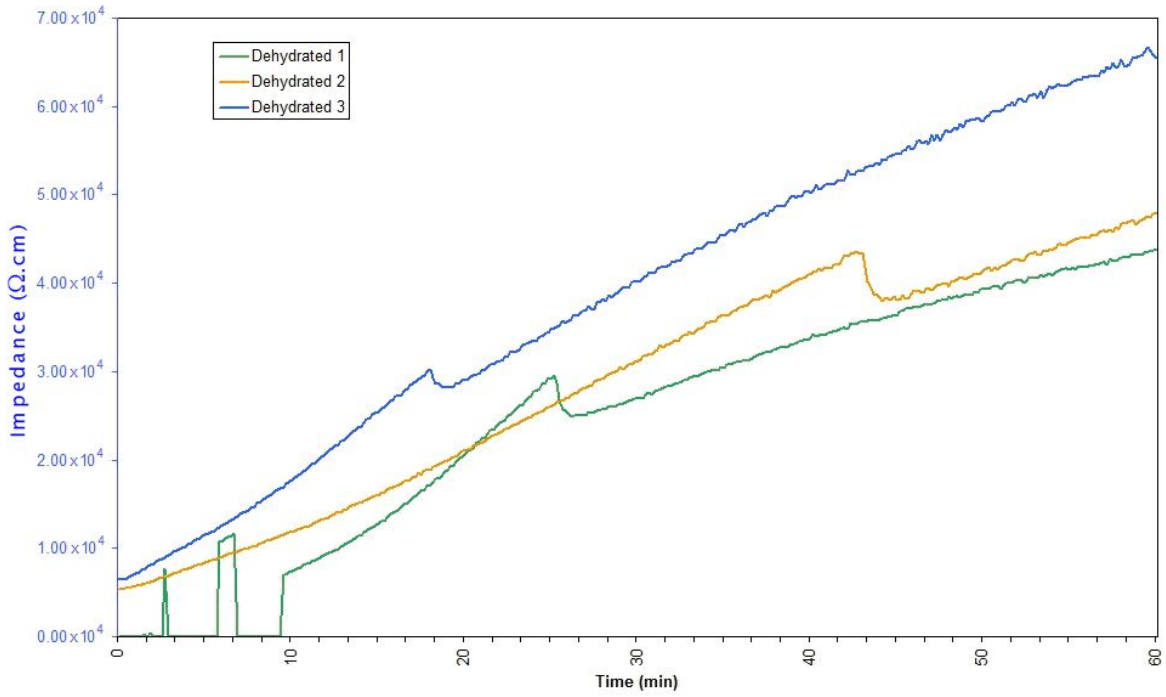

Figure 3.10: Rapid changes in impedance over 1hr as sample dehydrates.

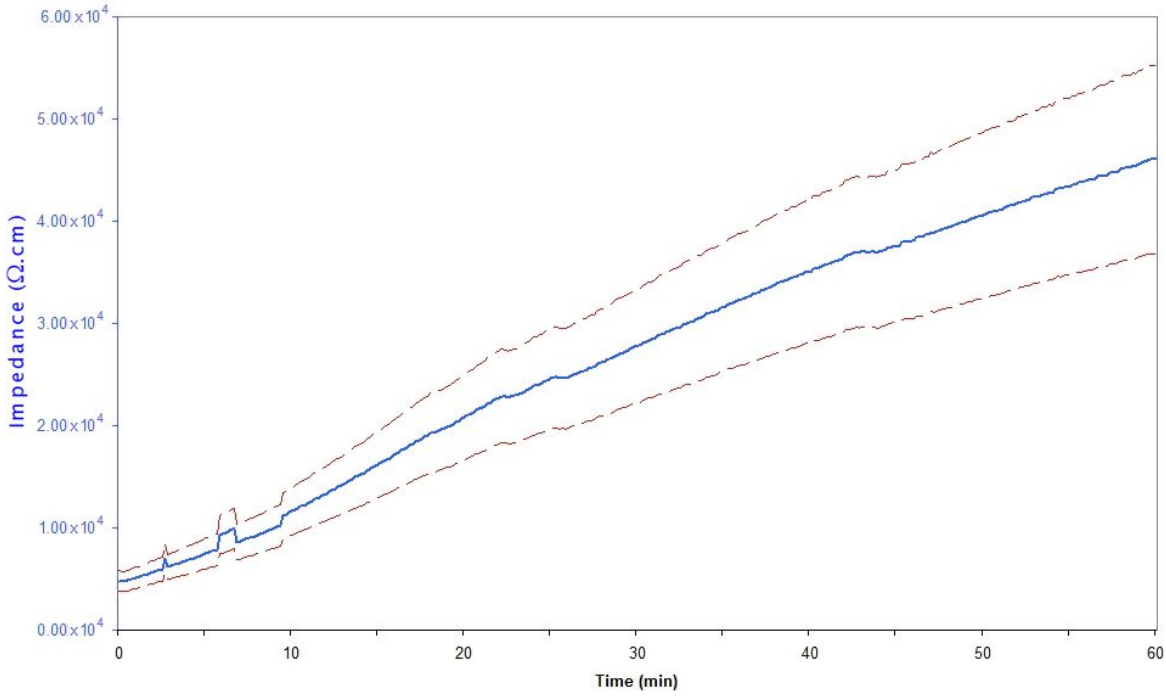

Figure 3.11: Effect of dehydration on averaged impedance over 1hr.

3.2.2 Planar design issues and Coplanar redesign

As previously stated there were a number of issues with this method; the dry environment was not ideal as indicated by the dip in results indicated in **figures 3.9** and **3.10**. This change in the results was most likely the result of the dehydration of the sample. As Fuji IX, as with all GIC's is designed to set in an aqueous environment of the mouth, the lack of water would have a negative effect on the setting reaction and is the most likely source of this error in the collected result. This is possibly very significant as the impedance could have risen to a much higher level had the cement been allowed to cure in a more natural fashion. To counter this, the test assembly would have to be redesigned to allow for the addition of a source of water to reduce and ideally eliminate the effect of dehydration on the measured impedance.

The lack of control in the thickness in the sample also posed an issue, though the samples were all mixed with the same volume of glass and liquid component the amount of resultant glass ionomer in the mixed form that was actually inserted into the assembly varied slightly. This resulted in a deviation of approximately 0.2mm from the ideal 2mm distance between the plates.

Another potential issue is with the design of the test assembly itself. The construction of a MEMs system with parallel plate should not prove an issue however an issue would arise as the result of the necessity for the cement to fully permeate between the plates, which would be difficult given the viscosity of the cement and the size of the spacing between the capacitor plates. A further issue with this is the potential

damage that could be caused to the assembly when the sensor was implanted. Any deviation form the manufactured design would result in an erroneous result and render any data collect unusable (**figure 3.12**).

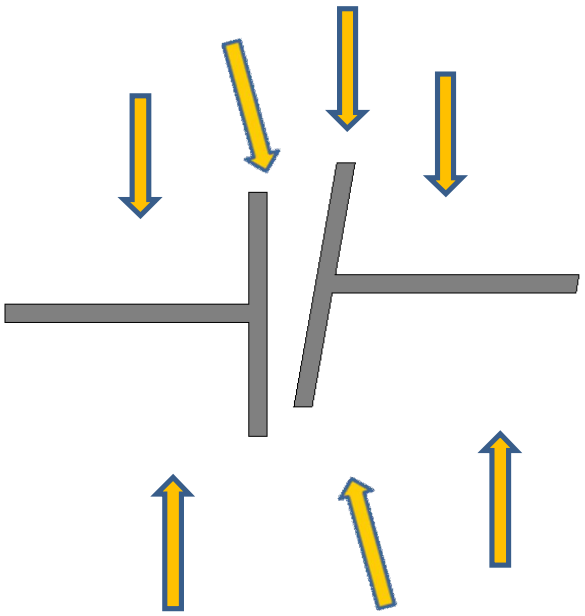

Figure 3.12: Identified issue with planar design when miniaturized

Based on these issues the decision was made to move to a co-planar design of test assembly. In this design the plates would be aligned next to each other on the same plane and the impedance measured across the cement as the current arcs between plates through the cement.

3.3 Co-planar Test Assembly

The following results were collected using the co-planar test assembly, and the collected value for impedance and calculated values for the additional dielectric properties of each of the GIC tested over the 24hrs of data collection.

3.3.1 Fuji IX

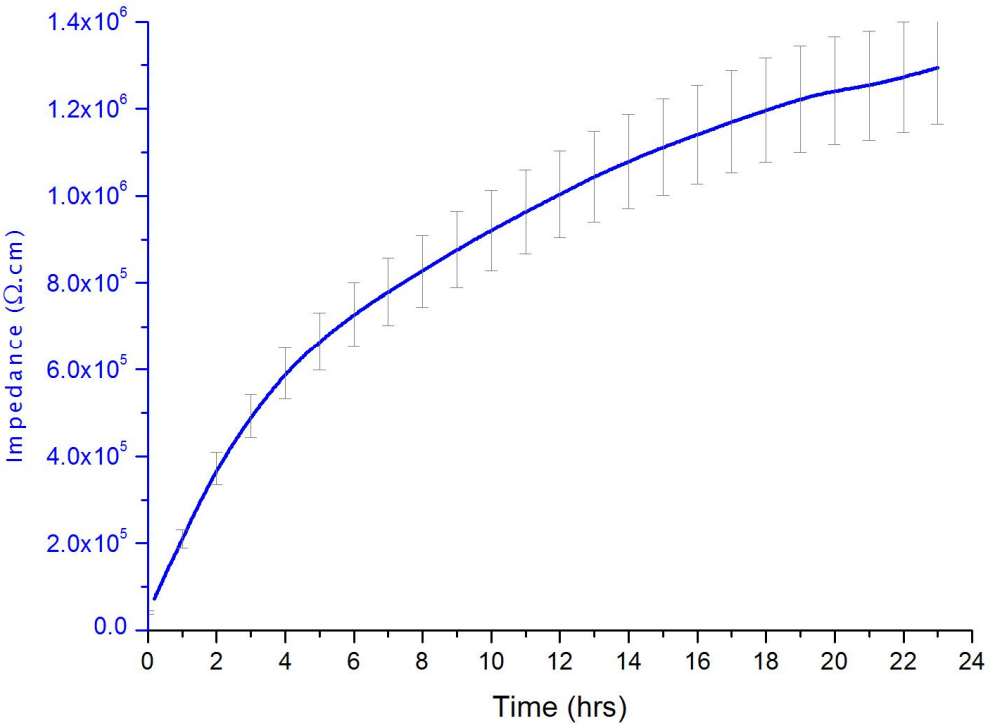

Figure 3.13: Averaged Impedance of Fuji IX measured over 24hrs taken from co-planar assembly.

The impedance for Fuji IX shown in **figure 3.13** changed markedly over the 24hrs that the impedance was recorded, and much like that recorded with the planar test assembly, started at a values around $2.75x10^4\Omega.cm$, however unlike with the planar

assembly the measured value of impedance did not level out at $2x10^5\Omega.cm$ but rather continued to up to $1.2x10^6\Omega.cm$. This difference in the value of impedance recorded indicates that the addition of a water well positively affected the setting of the cement, reducing the effect of dehydration on the setting cement. It also highlights the errors resultant in using the simpler test assembly. The change in impedance over the first hour of testing, shown in **figure 3.14**, also reflects this positive effect of the water well in that stability of the collected results, particularly when compared to **figure 3.11** for the same data using the planar assembly.

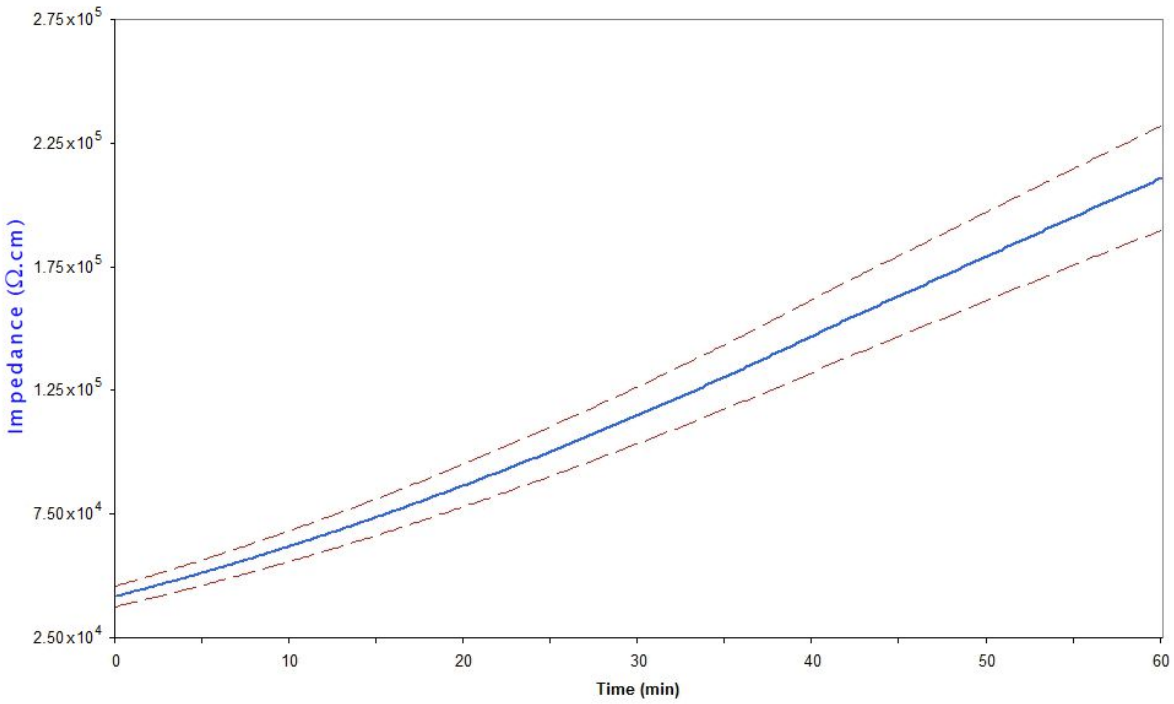

Figure 3.14: Averaged Impedance of Fuji IX over 60 mins taken from the co-planar assembly.

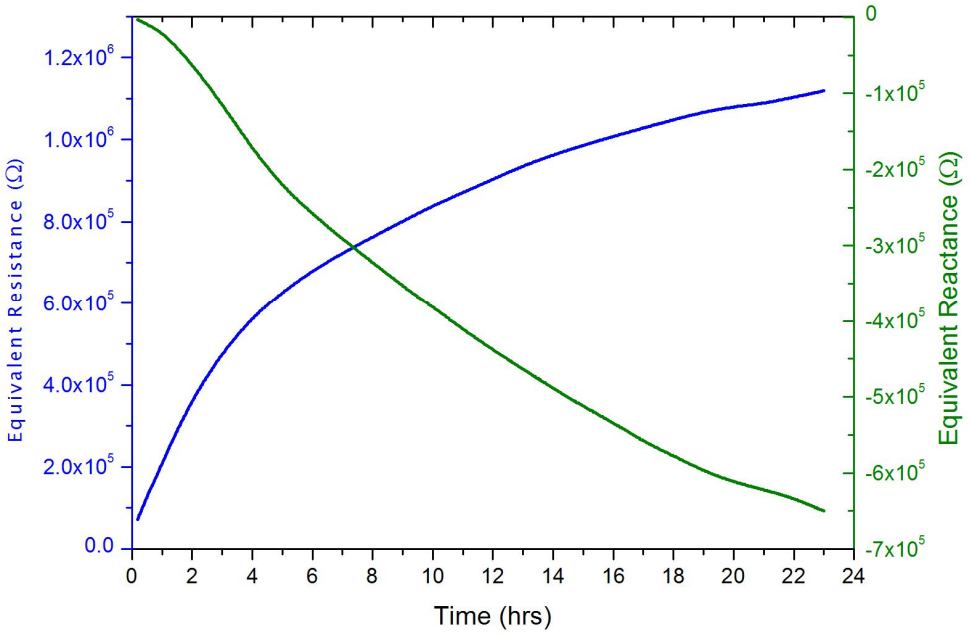

Figure 3.15: Equivalent resistance and equivalent reactance calculated from measured impedance of Fuji IX measured over 24hrs of setting reaction using co-planar test assembly.

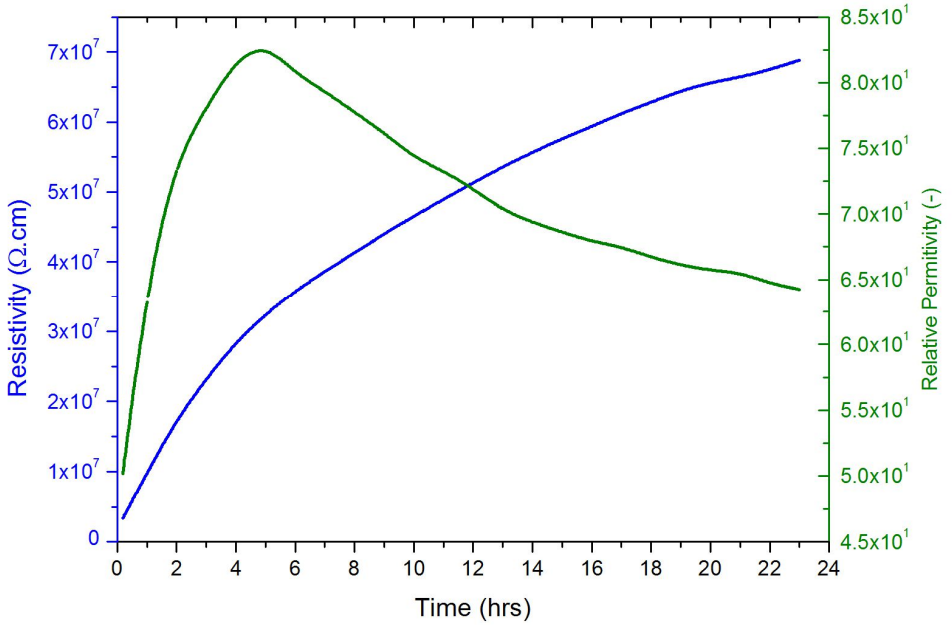

Figure 3.16: Resistivity and relative permittivity calculated from measured impedance of Fuji IX measured over 24hrs of setting reaction using co-planar test assembly.

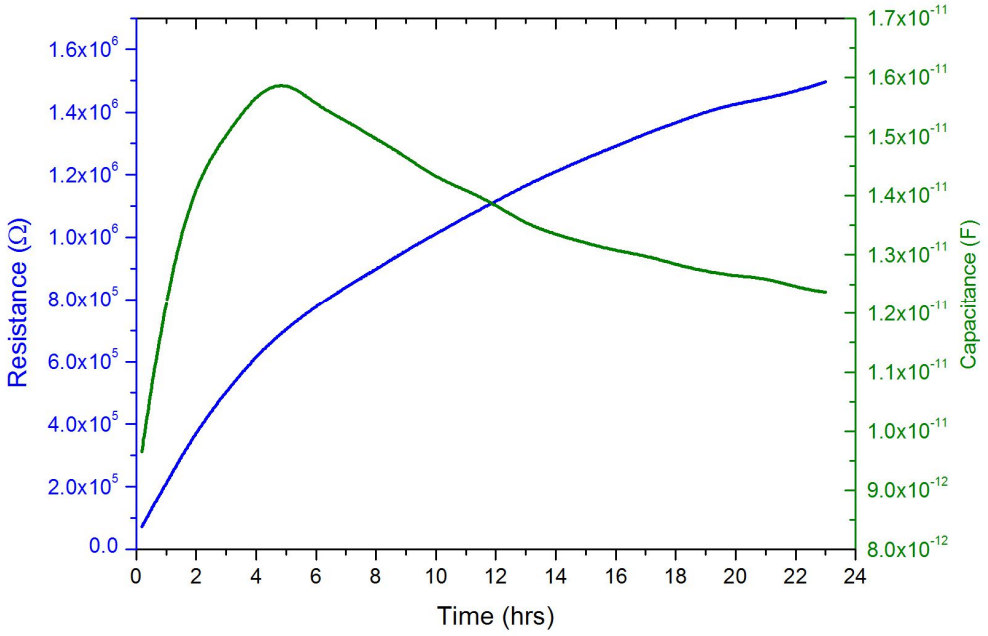

Figure 3.17: Resistance and capacitance calculated from measured impedance of Fuji IX measured over 24hr of setting reaction using planar test assembly.

Looking at the relative permittivity (**figure 3.16**) and capacitance (**figure 3.17**) changes that occurs over the course of the curing of the Fuji IX show a different pattern compared to that of the other dielectric properties. As the cement cures the impedance and resistivity of the cement increase as the availability of free ions in the system decreases with curing [25]. During the acid base reaction of the powder and the liquid components of the GIC there is a release of cations (Na^{+}, Ca^{2+}, Sr^{2+} and Al^{3+}) leached from the glass particles, which gradually crosslink the polymer as the gel-sol mixture cures [25]. However this increase in availability of cations in the initial phase of the setting reaction results in an increase in the permittivity of the material, as more charge carriers are available. Once the available cations have all been leached from the glass their availability will decrease, which will cause a decrease in

the relative permittivity within the sample. This means that the point of change in the relative permittivity and capacitance is indicative of a change in the phase of the setting reaction of the Fuji IX, where its electrical properties move from that of a simple capacitor in the initial phase, over the first 4hours as shown in **figures 3.16** and **3.17**, to that of a lossy capacitor in the latter stage of the setting reaction.

3.3.2 Chemfil Superior

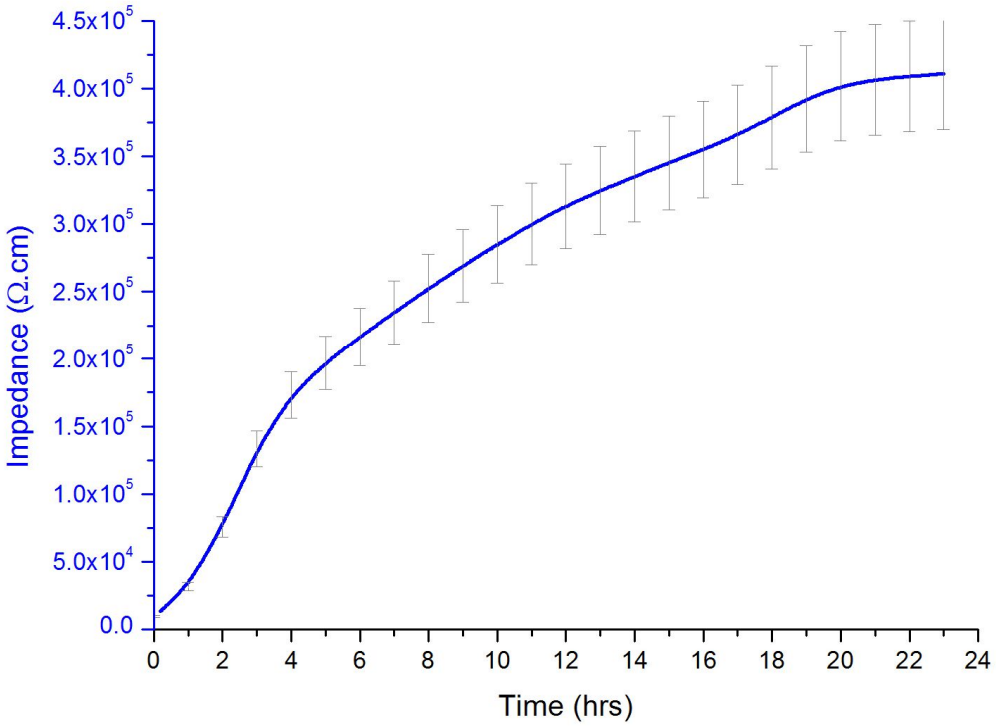

Figure 3.18: Averaged Impedance of Chemfil Superior measured over 24hrs taken from co-planar assembly

The impedance for Chemfil shown in **figure 3.18** also changed over the 24hrs that the impedance was recorded, starting at a value of $9x10^3\Omega.cm$, continuing to up to a value of $4x10^6\Omega.cm$. This change in impedance is much like that of the Fuji IX over the same period, and though it is an order lower, it does also increase by more than an order of magnitude. The impedance change of the first hour of the setting (**figure 3.19**) also increases at a rapid rate much like that demonstrated with Fuji IX.

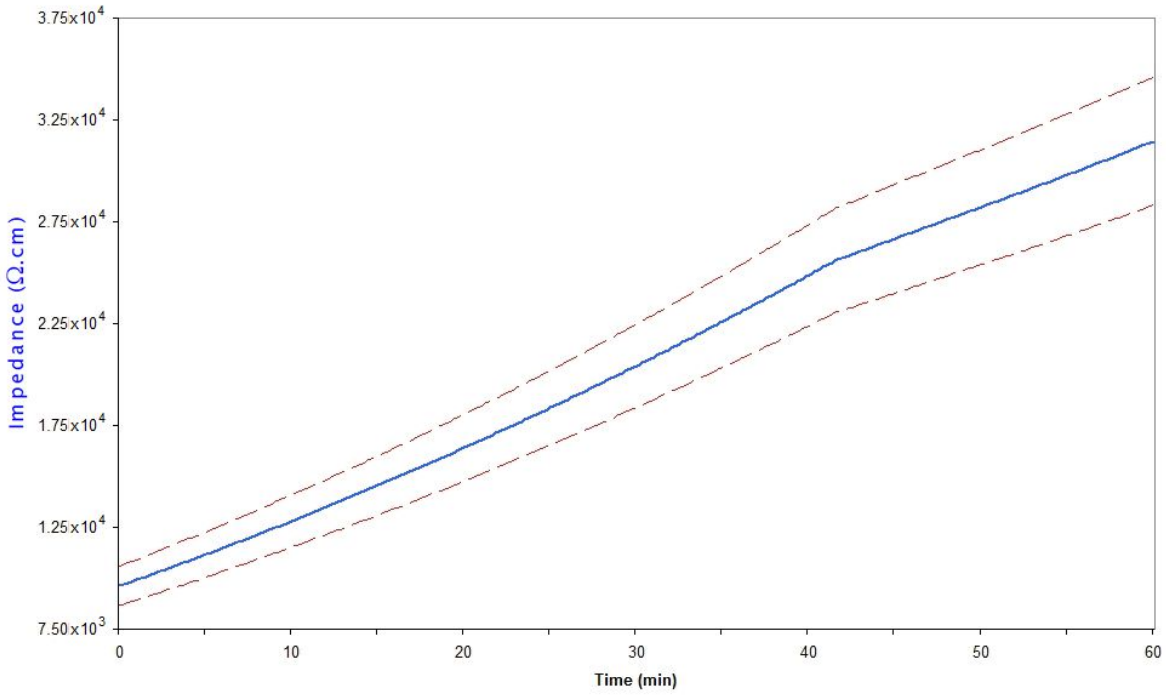

Figure 3.19: Averaged Impedance of Chemfil Superior measured over first hour taken from co-planar assembly

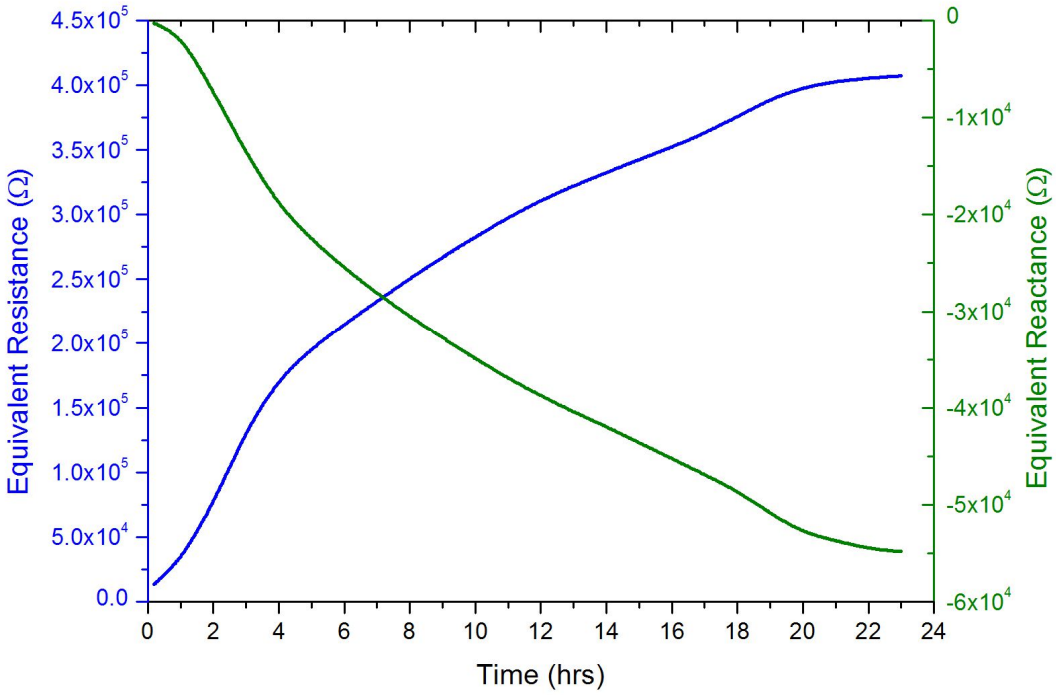

Figure 3.20: Equivalent resistance and equivalent reactance calculated from measured impedance of Chemfil Superior measured over 24hrs of setting reaction using co-planar test assembly

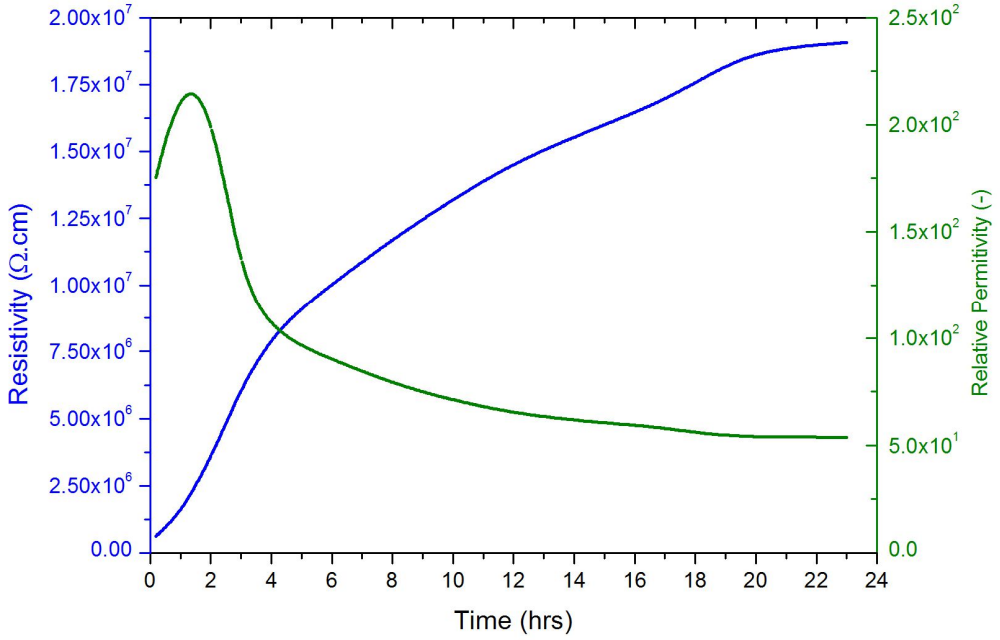

Figure 3.21: Resistivity and relative permittivity calculated from measured impedance of Chemfil Superior measured over 24hrs of setting reaction using co-planar test assembly

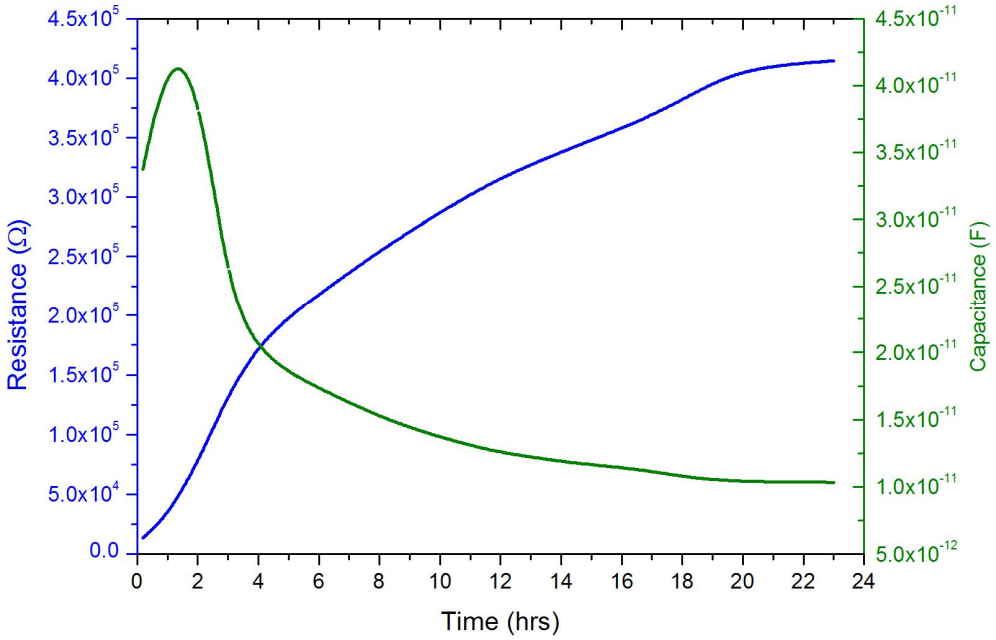

Figure 3.22: Resistance and capacitance calculated from measured impedance of Chemfil Superior measured over 24hr of setting reaction using planar test

The curing of the cement progresses in much the same way with the impedance, resistance and resistivity of the cement increasing as the free ions in the system decrease [25]. As with Fuji IX the relative permittivity (**figure 3.21**) and capacitance (**figure 3.22**) of Chemfil Superior also changes in the same fashion. Here as with the Fuji IX the relative permittivity and capacitance initially increases as the cations are leached and then decreases as their availability decreases due to the cross linking of the gel-sol matrix. This is indicative of a change in the phase of the material at around 2hrs, moving from that of a simple capacitor in the initial phase, over the first hour to that of a lossy capacitor in the latter stage of the setting reaction. The measured value for impedance also has a slight s curve to its nature with is another sign of the lossy capacitor nature of the cement.

3.3.3 Ketac Fil Plus

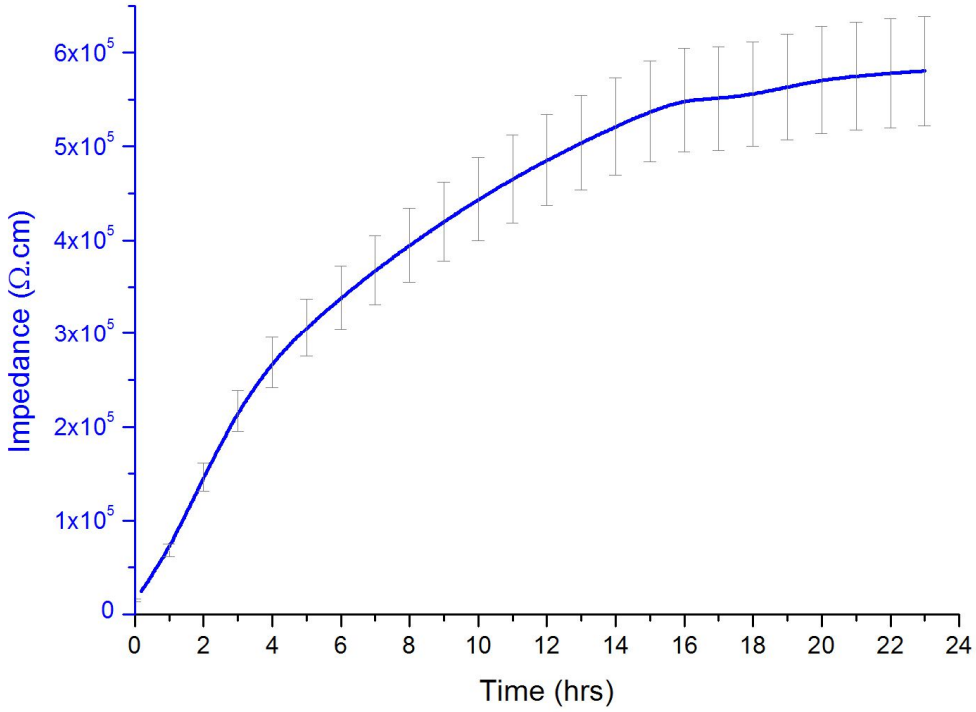

Figure 3.23: Averaged Impedance of Ketac Fil Plus measured over 24hrs taken from co-planar assembly

The impedance for Ketac shown in **figure 3.23** from a starting at a value of $1.5x10^4\Omega.cm$, continuing to up to a value of $5.5x10^5\Omega.cm$ at the end of the 24hr period of measurement. The change in impedance change much like that of the Fuji IX and Chemfil, and the change in the first hour of the setting (**figure 3.26**) also increases at a rapid rate much like that demonstrated with the other GIC's tested.

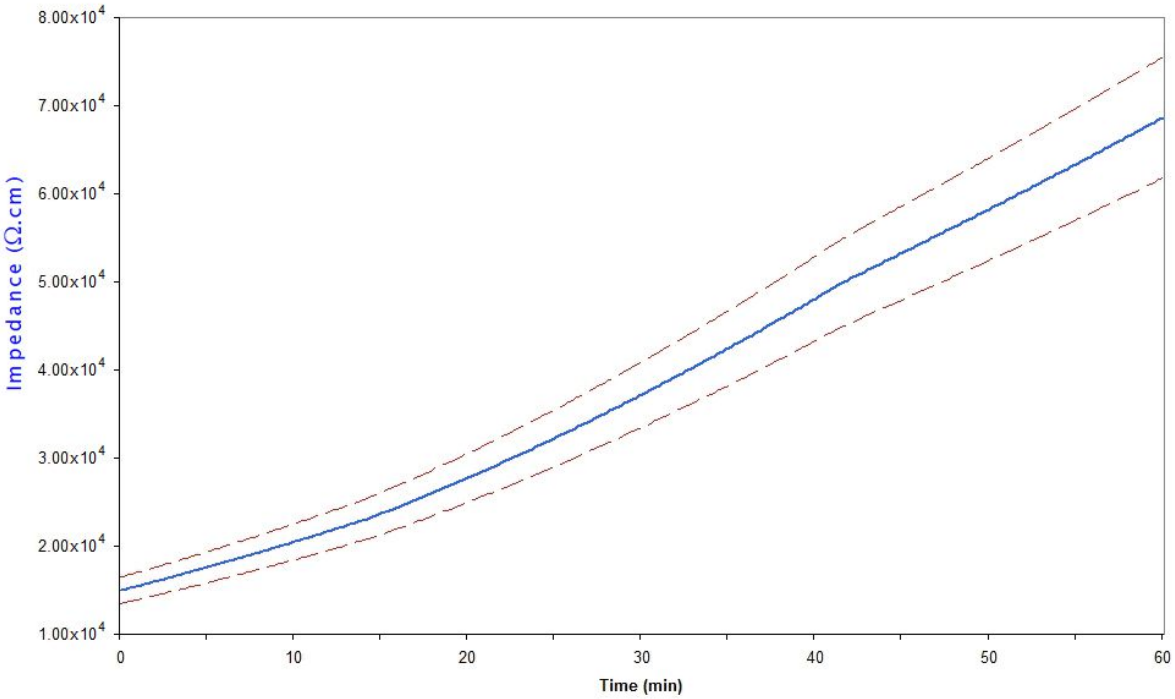

Figure 3.24: Averaged Impedance of Ketac Fil Plus measured over first hour taken from co-planar assembly

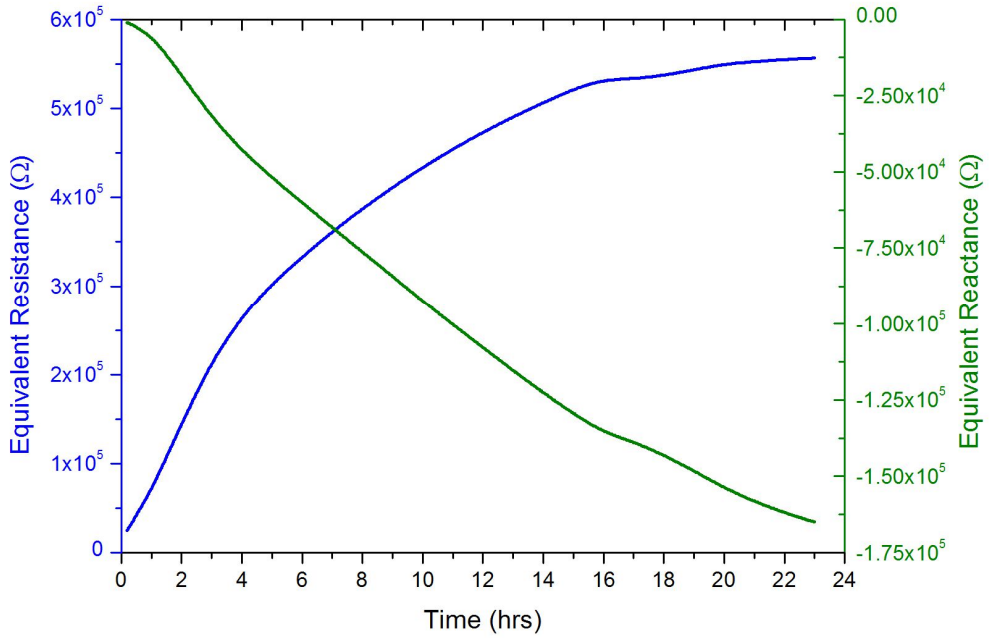

Figure 3.25: Equivalent resistance and equivalent reactance calculated from measured impedance of Ketac Fil Plus measured over 24hrs of setting reaction using co-planar test assembly

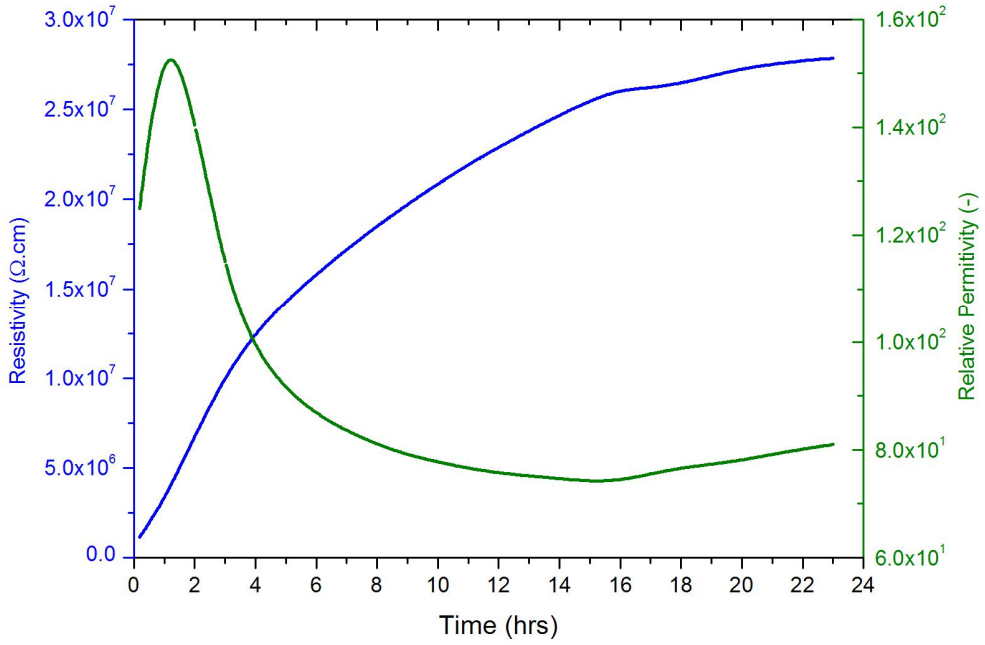

Figure 3.26: Resistivity and relative permittivity calculated from measured impedance of Ketac Fil Plus measured over 24hrs of setting reaction using co-planar test assembly

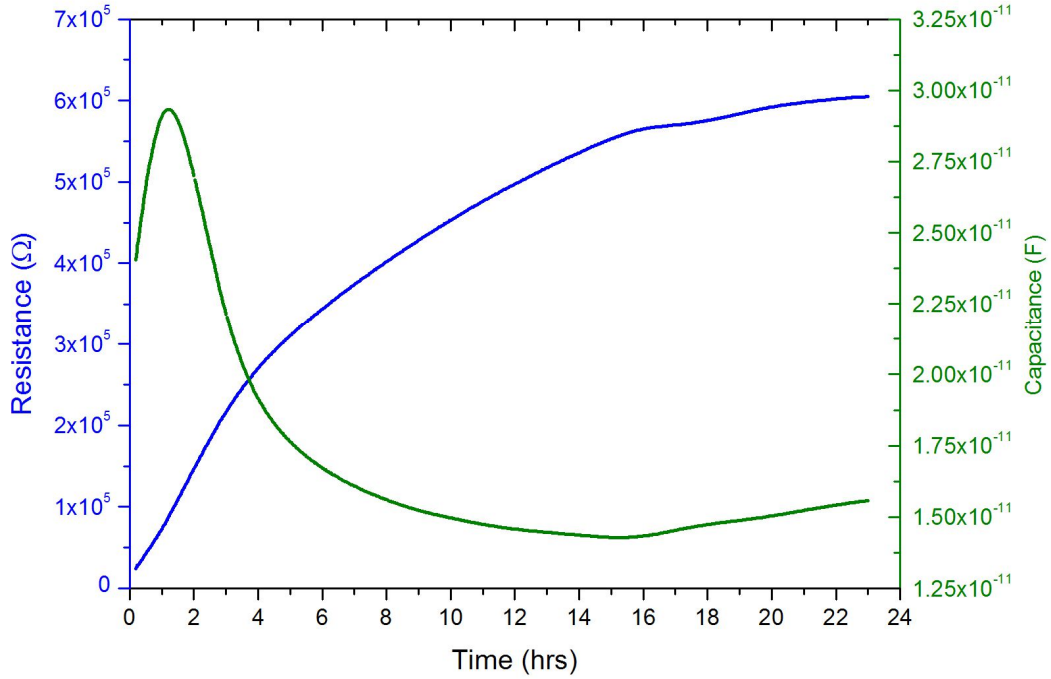

Figure 3.27: Resistance and capacitance calculated from measured impedance of Ketac Fil Plus measured over 24hr of setting reaction using planar test assembly

Once again the impedance, resistance and resistivity of the cement increased as was the case with the other measured GIC's. The relative permittivity (**figure 3.26**) and capacitance (**figure 3.27**) of Ketac also changed in the same fashion at around 2hrs which is similar to that of Chemfil Superior. The change in the relative permittivity and capacitance once again indicate of a change in the phase of the material, with the setting Ketac having the same possible profile as that of a lossy capacitor, as discussed in 3.4.9, like that of Fuji IX and Chemfil Superior.

3.3.4 Comparison of Co-planar Impedance

Over the 24hr period of the setting of the cements there was an increase in the impedance in all samples (**figures 3.28** and **3.29**).

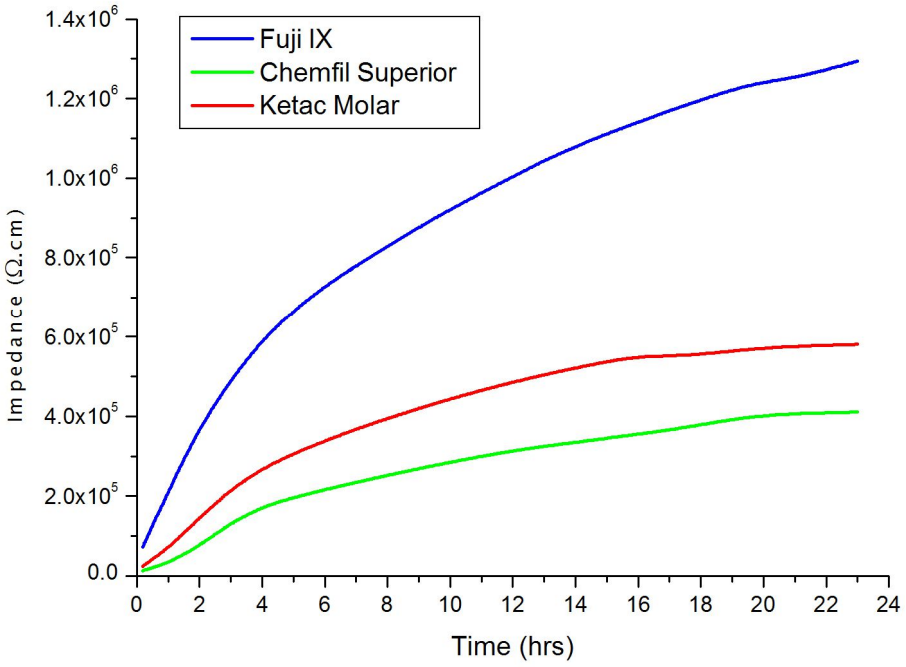

Figure 3.28: Collected impedance for Fuji IX, Chemfil Superior and Ketac Fil Plus compared to each other over 24hrs.

In **figure 3.28** the impedance of all three of the tested GICs is shown for the first 24hrs. Over this time the impedance of all three cements increases as time progresses, with the rate of change decreasing as time progresses, though clearly continuing beyond the recorded data. This behaviour is expected given the known and designed nature of GIC setting reactions, with the cement setting rapidly initially and continuing to cure beyond this initial setting time.

Though there is a similarity in the rate of change in impedance between the cements, what can also be seen in **figure 3.29** is that Chemfil Superior and Ketac Molar both have markedly lower impedance compared to that of Fuji IX. This variance in the impedance could be caused by a number of factors however it is important to not that the composition of both Chemfil Superior and Ketac Molar is very similar, they both contain a nearly identical chemical make-up, whereas Fuji IX has a different chemical structure. Chemfil Superior and Ketac Molar both contain 0.041 and 0.060 (respectively) of Ca^{2+}, within their composition, however Ca^{2+} is absent from Fuji XI, replaced with 0.056 of Sr^{2+} [24]. This variance in chemical make-up is a likely cause for the variance in impedance, and identifies the need to consider the chemical structure of the cements themselves in designing any sensor as this will have a dramatic effect on any results collected.

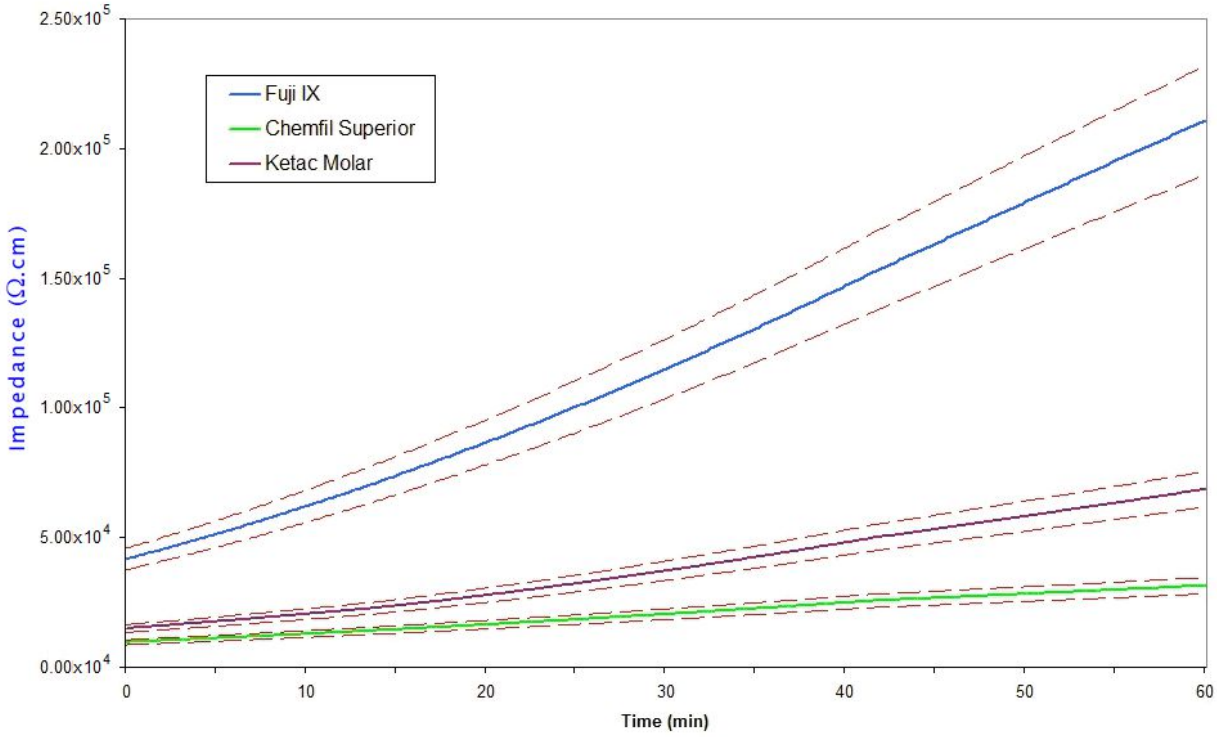

Figure 3.29: Collected impedance for Fuji IX, Chemfil Superior and Ketac Fil Plus compared to each other over first hour.

3.3.5 Issues with Co-planar Assembly

Despite the improvements in the test assembly design which eliminated the errors which occurred as a result of the dehydration in the cement, the new design had a number of new issues which affected the ease of results collection. During operation of the impedance bridge at least a third of results collected were not suitable as a source of data as the cement pulled away from the copper contact plates as the cement cured. As the cement was not designed to adhere to the copper this was expected and the addition of a modified specimen tube acting as a spacer which allowed a small weight to be added to the top of the metal insulation box to help prevent this occurring.

There was also an issue with prolonged exposure of the cements to the copper contact plates, with the cement becoming stained by copper (**figure 3.30**) and the corrosion of the surface of the assembly plates **figures 3.31** and **3.32**. This staining occurred to varying levels and could have had an effect on the measured values of impedance. However though this was a noted effect of the exposure the staining of the cements was not present on visual inspections throughout the measurement bar the final few hours of measurement. Further more there was no coloration between spurious measurements and the presence of staining.

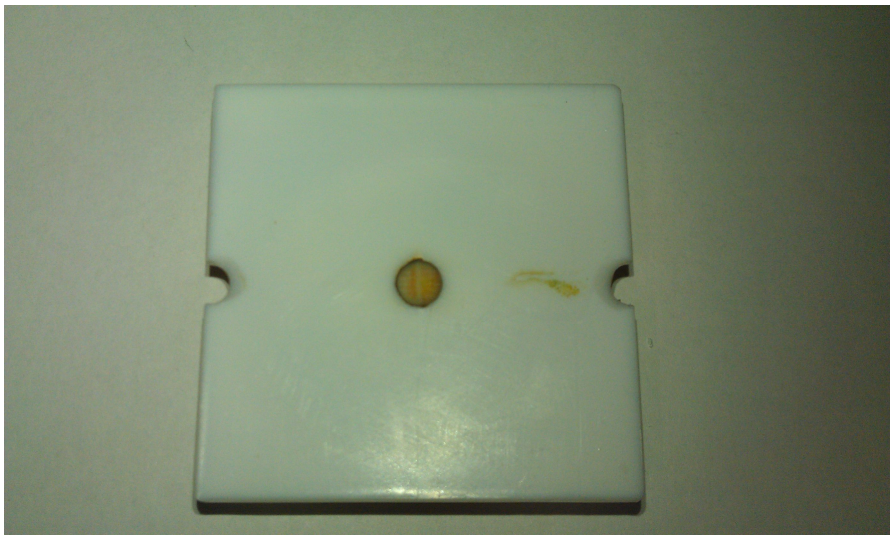

Figure 3.30: Discolouring of cement after prolonged contact with copper

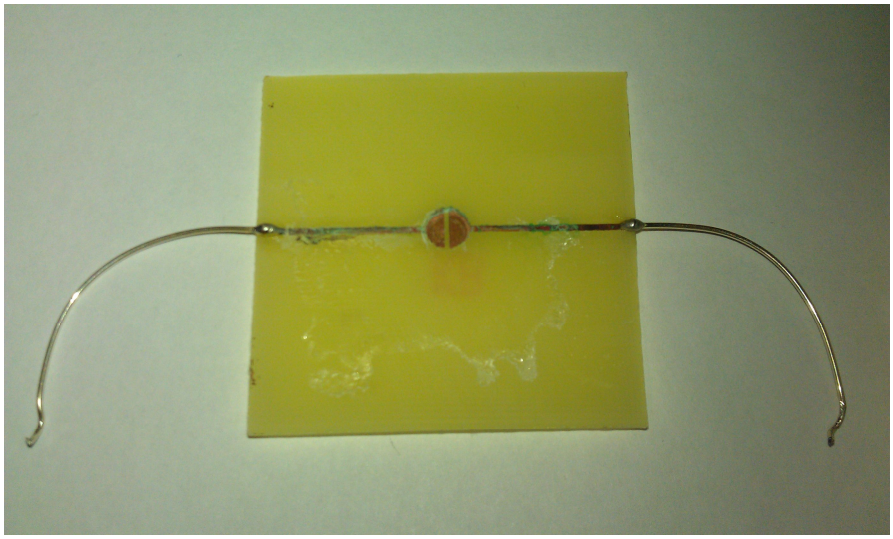

Figure 3.31: Oxidation of the co-planar test assembly copper plates

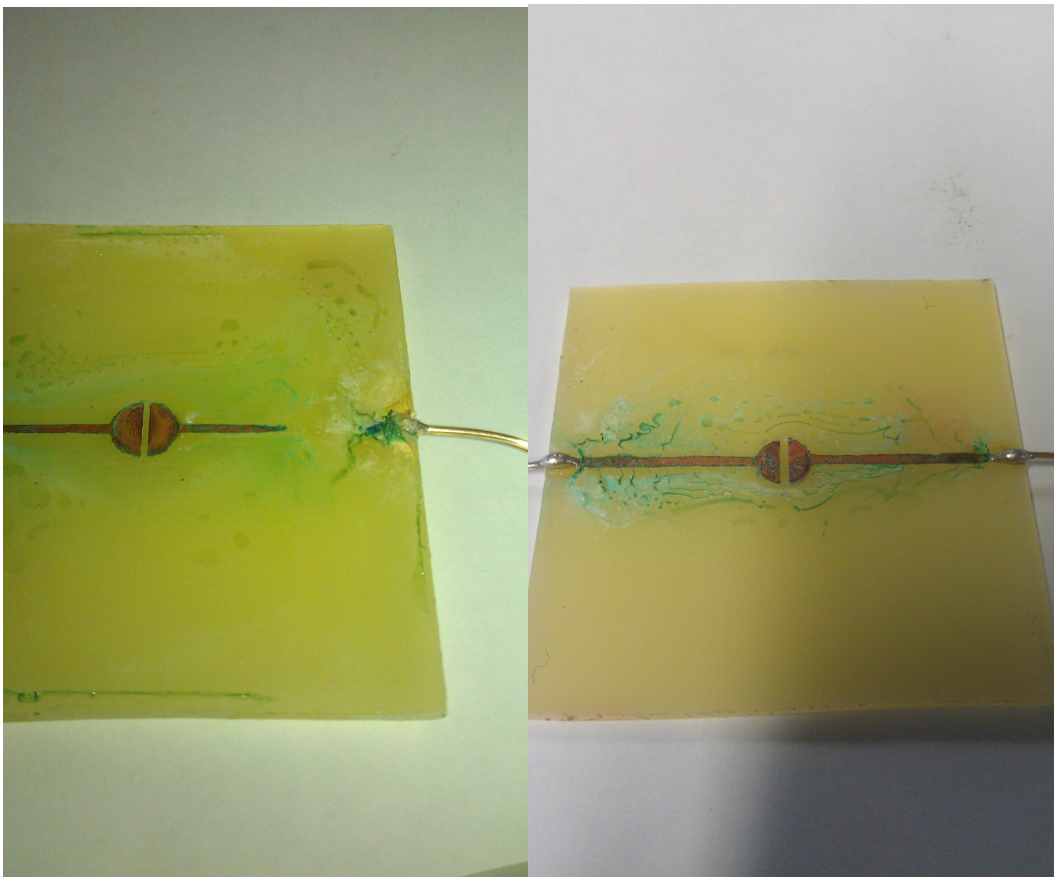

Figure 3.32: Damage to co-planar test assembly caused by prolonged exposure to sample and storage media.

As is visible on the left in **figure 3.32** the corrosion reached such a level that it caused the thin copper to come away from the PCB base substrate itself, breaking the connection.

There was also a much greater problem with noise which occurred as a result of this new design. Though the spread of the data collected was reduced compared to that collected with the planar assembly, the noise level incurred in the data was much higher. This is an effect of dislocation and the co-planar arrangement of the capacitor plates.

3.4 FT-IR Results

In-order to understand the changes that happened within the GIC's as they set a FT-IR spectra was collected from the cement in various states, both before mixing and post mixing at different times throughout the setting period.

3.4.1 FT-IR of Powder

FT-IR spectra for the different powder components which were used throughout the investigation are shown in **figure 3.33**.

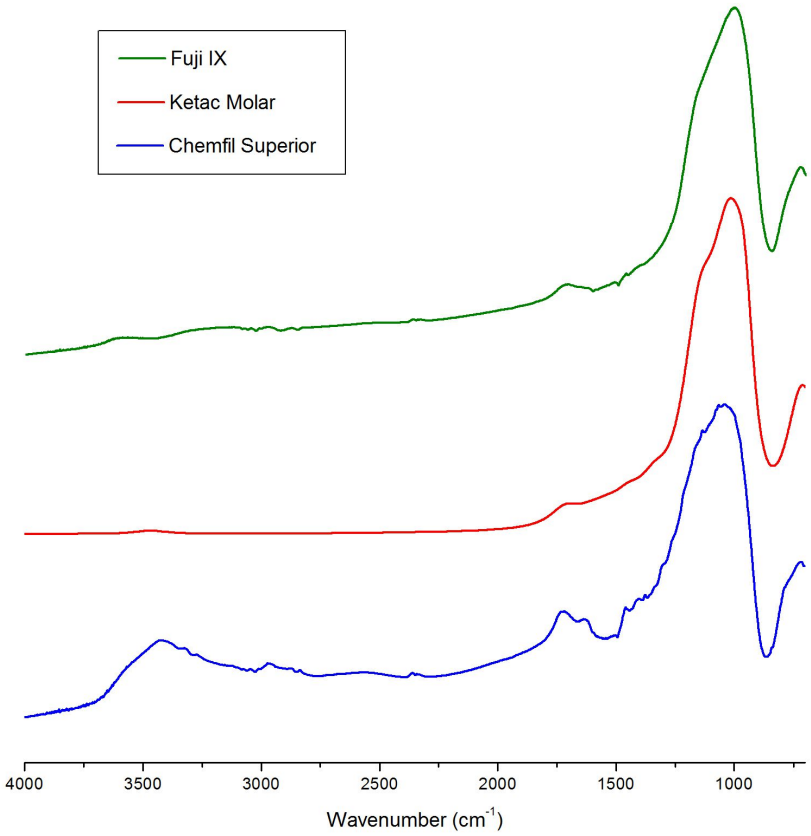

Figure 3.33: The gathered spectra of Fuji IX (green), Ketac Fil Plus (red) and Chemfil Superior (blue) vertically offset and shown against each other.

This graphs shows the difference between the chemical make up of the cements both the Fuji IX and Ketac Fil Plus have a similar spectra, however the Chemfil demonstrates other peaks in its spectra as a result of the inclusion of the PAA into its powder component (thus allowing the cement to be mixed using only water). The deconvolution process was performed using OMNIC FT-IR software's peak resolving "Gaussian/Lorentzian" analysis routine.

3.4.2 Deconvolution of Fuji IX

Further deconvolution of the spectra for the Fuji IX and Ketac Fil Plus gave a greater indication of the composition of the powder component through the various peaks present.

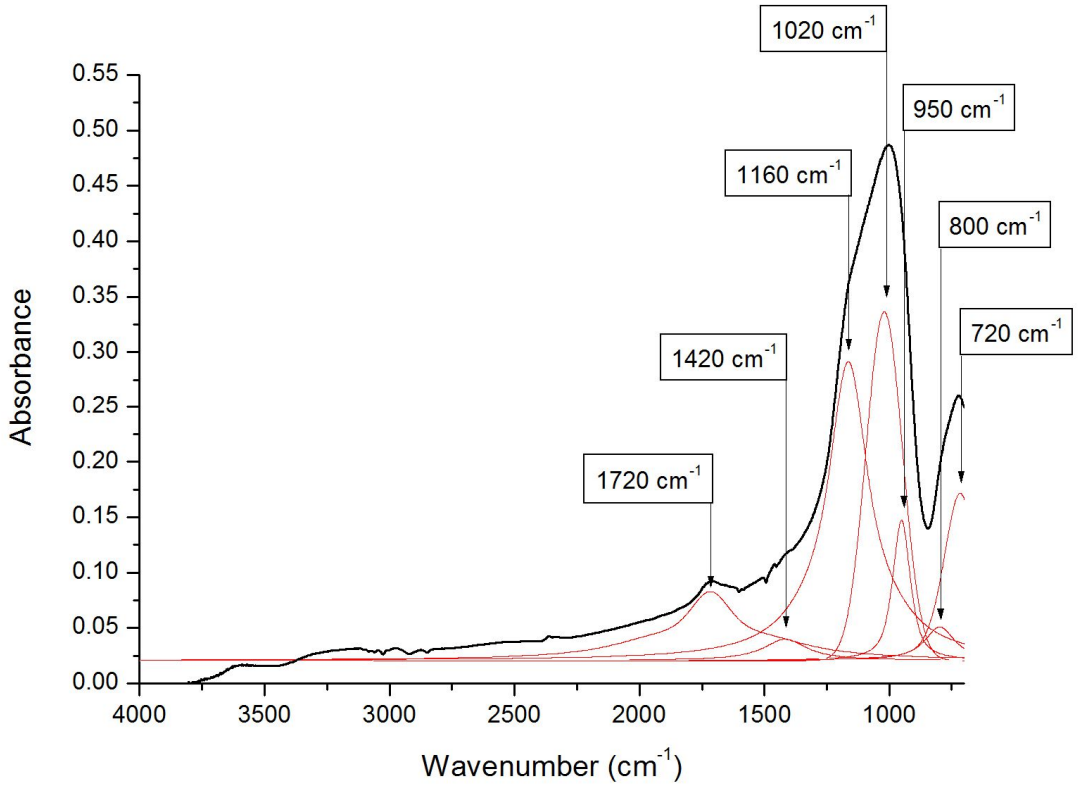

Figure 3.34: Deconvoluted spectra of Fuji IX, indicating key peaks observed.

The spectra shown in **figure 3.34** shows the deconvolved spectra of Fuji IX. The peak found at 1720cm^{-1}, is potentially indicative of the C=O stretching vibration found in PAA, which suggest that there is at least a small quantity of powdered PAA premixed into the glass powder component [40]. The peak identified at 950cm^{-1} is most likely from that of Si-OH stretching vibration glass and not visible fully at this point. The peak identified at 1420cm^{-1} represents the symmetrical stretching vibration of the COO- bonds in polyacrylate salts [41]. The peak at 720cm^{-1} is an indicator of the symmetrical stretching between Si-O-Si tetrahedral of the glass component [42]. The lowest peak identified at 800cm^{-1} is from the Si-O-Si bending mode of the glass [14]. The peak at 1160cm^{-1} is likely that from Si-O-Si asymmetric stretching vibration normally found between 950cm^{-1} to 1200cm^{-1} [14]. The main peak at 1020cm^{-1} is the C=O stretching and SI-O asymmetric vibration modes which overlap at this point, and ranges from 1000-1300cm^{-1} [14, 41]. These peaks are outlines in **table 3.1**.

Wavenumber (cm^{-1})	Assignment	Compound	Reference
1720	C=O stretching vibration	PAA	[40]
1420	COO- symmetrical stretching vibration	Polyacrylate salts	[12, 41, 43]
1160	Si-O-Si asymmetric stretching vibration	Glass	[14, 41]
1020	C=O Stretching vibration Si-O asymmetric vibration	Glass	[14, 41]
950	Si-OH stretching vibration	Glass	[13, 40]
800	Si-O-Si bending mode	Glass	[13, 14]
720	Si-O-Si symmetric stretching tetrahedral	Glass	[42]

Table 3.1: Description and assignment of FT-IR peaks identified in Fuji IX

3.4.3 Deconvolution of Ketac Fil Plus

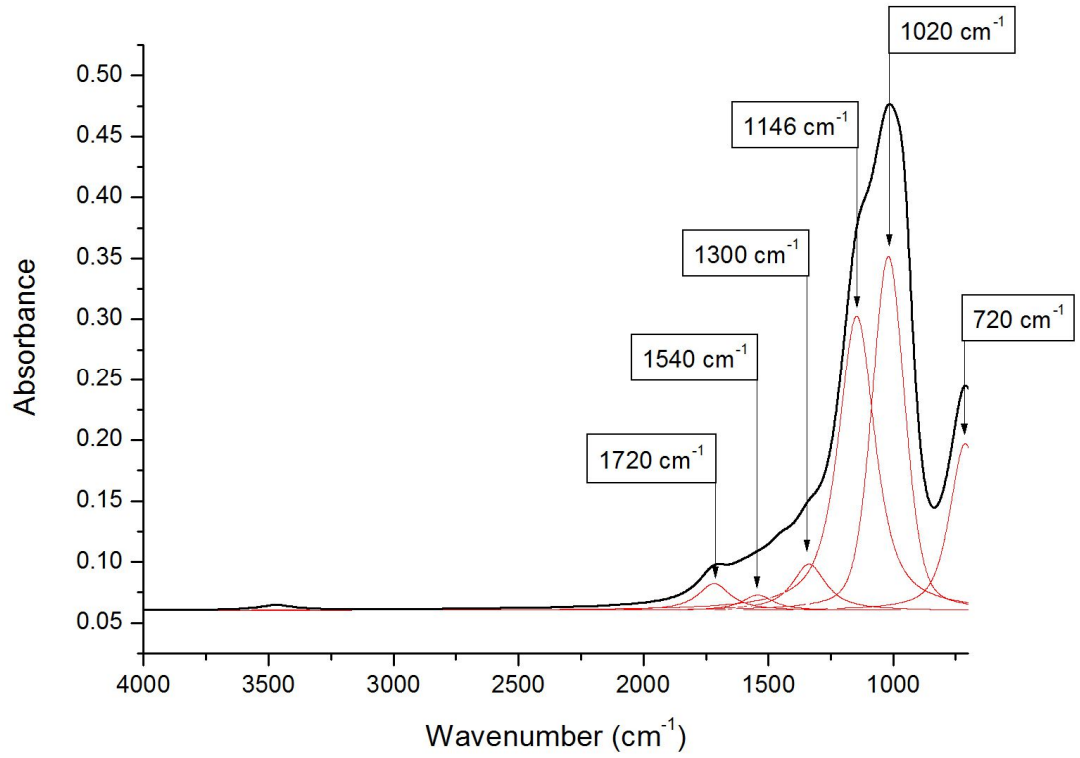

Figure 3.35: Deconvoluted spectra of Ketac Fil Plus, indicating key peaks observed.

The spectra shown in **figure 3.35** shows the deconvolved spectra of Ketac Fil Plus. Once again the peak found at 1720cm^{-1}, is potentially indicative of the C=O stretching vibration found in PAA, suggest there is a quantity of PAA premixed into the glass powder component [40]. The peak identified at 1560cm^{-1} represents the asymmetrical stretching vibration of the carboxyl group (COO-) bonds in polyacrylate salts [41]. The peak at 1300cm-1 is associated with C-O stretching vibration in monomers present in the powder, indicating further the inclusion of PAA in the powder [40]. The peak at 1146cm^{-1} is likely that from Si-O-Si asymmetric stretching

vibration normally found between 950cm^{-1} to 1200cm^{-1}[14]. AS with Fuji IX the main peak at 1020cm^{-} is the C=O stretching and SI-O asymmetric vibration modes which overlap at this point, and ranges from 1000-1300cm^{-1} [14, 41]. The peak at 720cm^{-1} is an indicator of the symmetrical stretching between Si-O-Si tetrahedral of the glass component [42]. These peaks are outlines in **table 3.2**.

Wavenumber (cm^{-1})	Assignment	Compound	Reference
1720	C=O stretching vibration	PAA	[40]
1540	COO- asymmetric vibration	Polyacrylate salts	[41]
1300	C-O stretching vibration	monomers	[40, 41]
1146	Si-O asymmetric vibration	Glass	[41]
1020	C=O stretching vibration Si-O asymmetric vibration	Glass	[14]
720	Si-O-SI symmetric stretching tetrahedral	Glass	[42]

Table 3.2: Description and assignment of FT-IR peaks identified in Ketac Molar

3.4.4 Deconvolution of Chemfil Superior

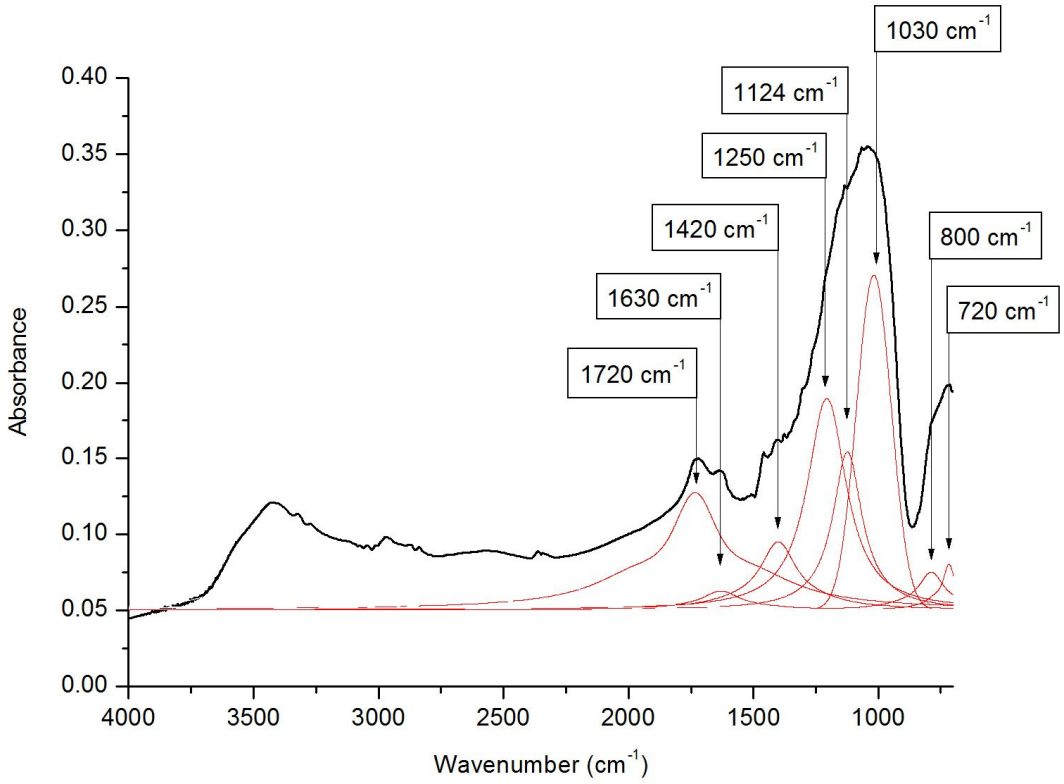

Figure 3.36: Deconvoluted spectra of Chemfil Superior, indicating key peaks observed.

The wide peak from 3500cm^{-1} to 2600cm^{-1} represents the –OH stretching vibration of both PAA and water [40]. The peak at 1720cm^{-1} represents the C=O stretching vibration of the PAA present in the powder [40], the peak intensity being much higher than in both Fuji IX and Ketac Fil Plus as all the PAA for the curing of the cement is incorporated into the powder [37]. The peak at 1630cm-1 represents the C=C stretch of PAA monomers within the powder [40]. The peak identified at 1420cm^{-1} represents the symmetrical stretching vibration of the carboxyl group COO- bonds in polyacrylate salts [41], and the peak identified at 1250cm^{-1} is associated with the C-O stretching vibration in PAA [14, 40, 41]. The main peak at 1030cm^{-1} is the C=O

stretching and SI-O asymmetric vibration modes which overlap at this point, and ranges from 1000-1300cm^{-1} [14, 41]. The peak at 1124cm-1 most likely represents the asymmetric vibration of Si-O-Si bonds in the glass [14]. The lowest peak identified at 800cm^{-1} is from the Si-O-Si bending mode of the glass [14].The peak at 720cm^{-1} is an indicator of the symmetrical stretching between Si-O-Si tetrahedral of the glass component [42]. These peaks are outlines in **table 3.3**.

Wavenumber (cm^{-1})	Assignment	Compound	Reference
3500 – 2600	-OH stretching vibration	Water, PAA, TA	[40]
1720	C=O stretching vibration	PAA	[40]
1630	C=C stretching vibration	PAA Monomers	[40]
1420	COO- symmetrical stretching vibration	Polyacrylate salts	[12, 41, 43]
1250	C-O stretching vibration	PAA	[14, 40, 41]
1124	Si-O-Si asymmetric vibration	Glass, TA	[14]
1030	Si-O-Si asymmetric stretching	Glass	[14, 42]
800	Si-O-Si asymmetric stretching	Glass	[13, 14]
720	Si-O-SI asymmetric stretching tetrahedral (between)	Glass	[42]

Table 3.3: Description and assignment of FT-IR peaks identified in Chemfil Superior

3.4.5 Deconvolution of PAA Polymer

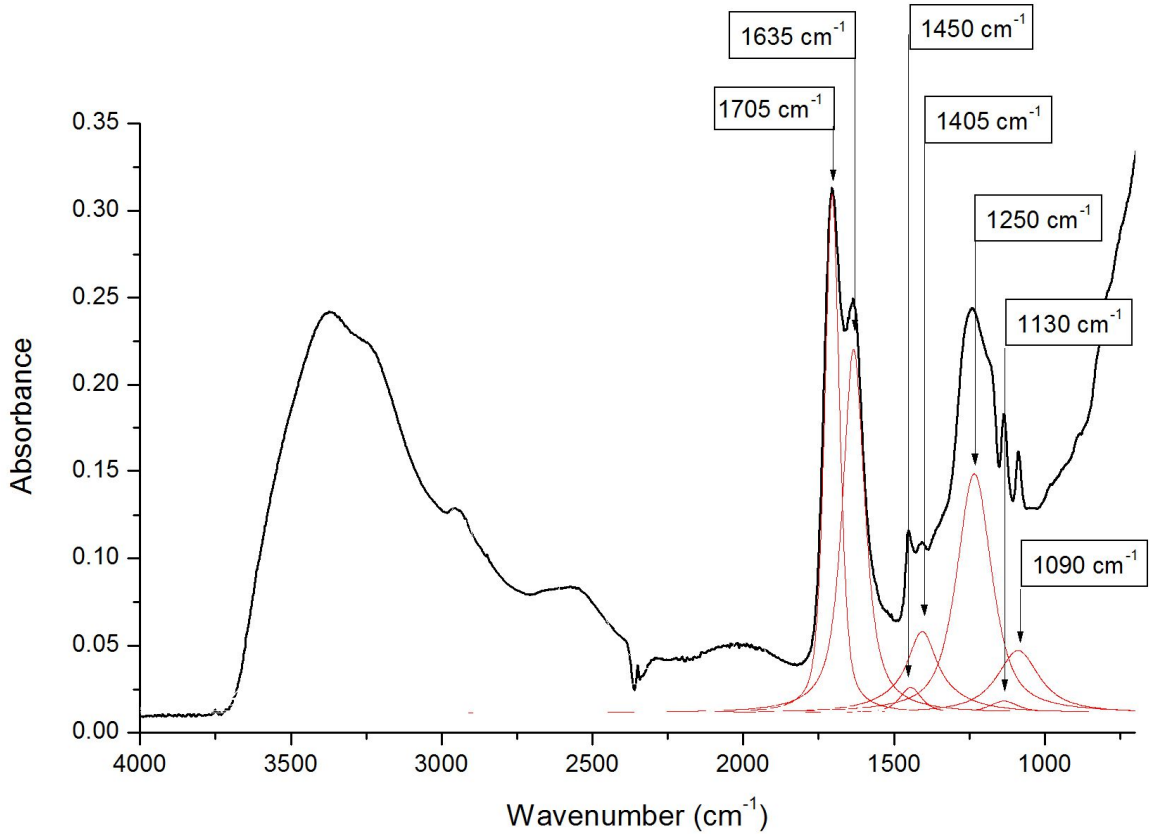

Figure 3.37: Deconvoluted spectra of Polymer, indicating key peaks observed.

The deconvolution of the liquid polymer provided with both the Ketac Fil Plus and the Fuji IX is shown in **figure 3.37**. The wide peak for –OH stretching vibration in PAA and water is seen between 3600 and 2700cm^{-1} and has a large intensity as a result of the high fluid content of the sample. The most defined peaks present were at 1705cm-1 and 1635cm-1 which represent the C=O and O-H stretching vibration of PAA and monomers, respectively, in the polymer [40]. The next peak of significance is that at 1250cm^{-1} representing C-O stretching in the PAA [40]. At 1450cm^{-1} there is the indication of C-H scissor mode from PAA and monomers within the polymer [40].

The peak at 1405cm^{-1} falls into the band from 1470cm^{-1} to 1400cm^{-1} which could indicate COO- symmetrical stretching in the polymer[40]. The peaks at 1130cm^{-1} and 1090cm^{-1} indicate the presence of Tartaric acid within the polymer solution [40]. These peak assignments are shown in **table 3.4**.

Wavenumber (cm^{-1})	Assignment	Compound	Reference
3500 – 2600	-OH stretching vibration	Water, PAA, TA	[40]
1705	C=O stretching vibration	PAA, TA	[40, 41]
1635	O-H stretching vibration	PAA	[40]
1450	C-H scissor vibration	PAA and monomers	[40, 41]
1405	COO- symmetric stretching vibration	PAA	[12, 43]
1250	C-O stretching vibration	PAA	[14, 40, 41]
1130	C-OH stretching vibration	TA	[13, 40, 41]
1090	C-OH stretching vibration	TA	[13, 40, 41]

Table 3.4: Description and assignment of FT-IR peaks identified in Fuji IX over 24hrs post mixing

3.4.6 FT-IR of Fuji IX During curing

Once the Fuji IX was prepared and placed onto the FT-IR for monitoring, the interaction of the glass particles with the PAA as the setting reaction began caused a change in the prevalence of certain peaks. The majority of these changes occurred over the first hour after the mixing of the cement, shown in **figure 3.38**, immediately after mixing the peak at 1720cm^{-1} associated with the C=O stretching vibration of uncross linked PAA as identified from the polymer component shifted to 1705cm^{-1}, began to reduce in intensity as the availability of uncross linked polymer dropped as more an more cross linking occurred. This particular peak reduction can be tied to the gradual increase of a peak at 1550cm^{-1} which most likely corresponds to the COO- asymmetric stretching vibration of acid neutralisation within the polysalt mixture. This indicates that the ionic bonding of the polymer has started and as such is slowly using up the free ions released by the initial mixing of the cement where the glass was hydrolysed. The peak at 945cm^{-1} in most likely from the Si-OH stretching vibration of the as yet un-hydrolysed glass particles within the polysalt matrix [12, 14]. This Si-OH is the result of the inclusion of pre-reacted glass particle within the powder component of the system, which is common in commercial cement systems. Over the first hour this also shows a decrease in intensity and can be paired with the appearance and increase in intensity of the peak at 1042cm^{-1} which first appears as a prominent shoulder at 5min (**figure 3.38, b)**) before progressing to a full independent peak after the hour. This particular peak corresponds to the Si-OH stretching vibration of the hydrolysed glass particles in the cured gel-sol matrix [14]. This represents the leeching of cations from the glass as the PAA acts on the particles.

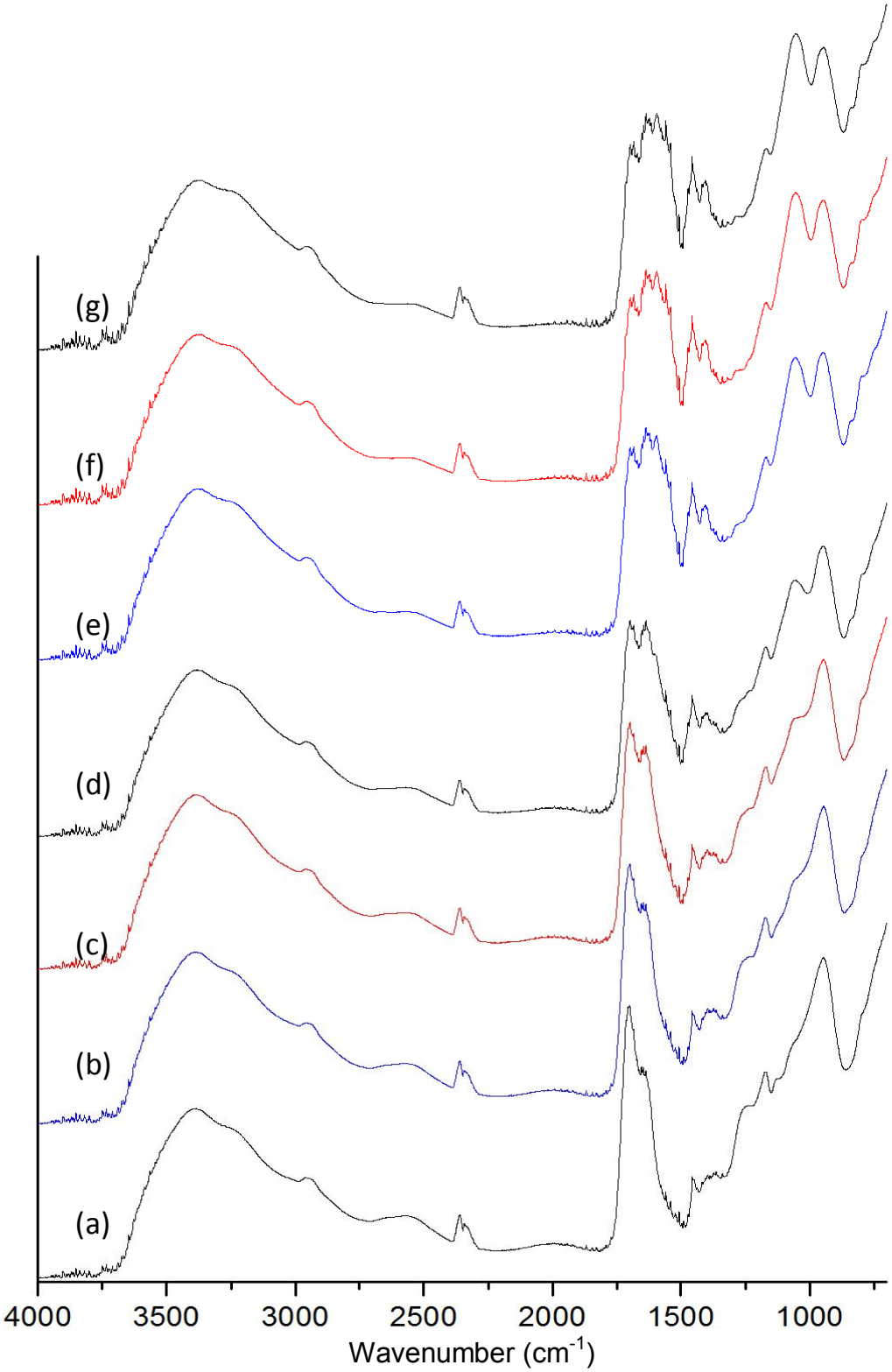

Figure 3.38: Stacked FT-IR spectra for Fuji IX over the course of an hour at; a) 0min, b) 5min, c) 10min, d) 15min, e) 30min, f) 45min, g) 60min

The change in the peaks at 1705cm^{-1} and 1550cm^{-1} represents the neutralisation of the PAA within the gel-sol matrix. The peak at 1705cm^{-1} represents the C=O bond stretching vibration within PAA prior to its neutralisation by the free ions. The peak gradually decreases in intensity over the 24hrs measured (**figure 3.39**), representing the change in uncross linked polymer within the matrix. Simultaneously the peak at 1550cm^{-1}, which is indicative of the COO- in neutralised PAA, increases in intensity over the same period, as the cross linking of the polymer progresses. However beyond the first hour mixing the intensity of the peak a 1550cm^{-1} does not increase particularly significantly, though the peak at 1705cm^{-1} does continue to recede when compared to the other. As with the peaks at 1705cm^{-1} and 1550cm^{-1}, the change in intensity continues over the full 24hrs, with the peak corresponding to un-hydrolysed glass particles at 945cm^{-1} decreasing further and intensity of the peak for hydrolysed and encapsulated glass at 1042cm^{-1} continuing to rise, gently plateauing after the 24hrs (**figure 3.39**). This represents the free acid and salt formation which occurs during the setting reaction. The peaks identified and their possible corresponding bond interactions, from the setting reaction of Fuji IX, are detailed in table **3.5**.

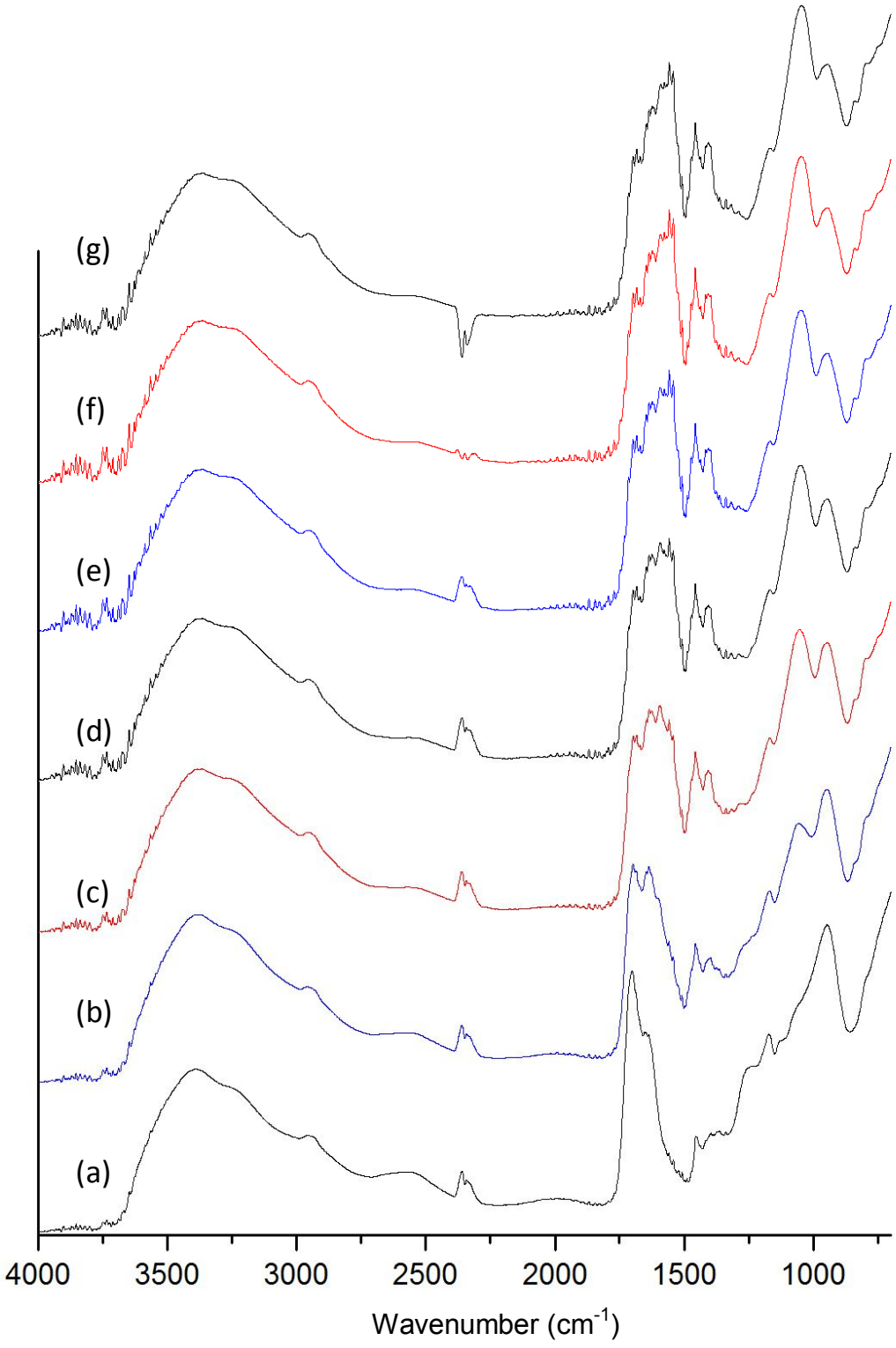

Figure 3.39: Stacked FT-IR spectra for Fuji IX over the course of a 24hour period at ; a) 0min, b) 15min, c) 1hr, d) 3hrs, e) 6hrs, f) 12hrs, g) 24hrs

Wavenumber (cm^{-1})	Assignment	Compound	Reference
3200 – 2600	-OH stretching vibration	Water, PAA, TA	[40]
1705	C=O stretching vibration	PAA, TA	[40, 41]
1635	C=O stretching vibration	PAA, TA	[40]
1550	COO- asymmetric stretching vibration	PAA	[40]
1450	C-H scissor vibration	Al PAA	[40, 41]
1405	C-O symmetric and asymmetric stretching vibration	Al-Tartrate	[12, 43]
1250	C-O, Si-CH_3 stretching vibration	PAA	[14, 40, 41]
1170	Si-O asymmetric stretching vibration	Glass	[41]
1042	Si-OH stretching vibration	Glass	[13, 14]
960	Si-OH stretching vibration	Glass	[13, 40]

Table 3.5: Description and assignment of FT-IR peaks identified in Fuji IX over 24hrs post mixing

3.4.7 FT-IR of Ketac Fil Plus During Curing

As with the Fuji IX the Ketac Fil Plus was prepared and placed onto the FT-IR for monitoring, and the interaction of the glass particles with the PAA as the setting reaction began caused a change in the prevalence of certain peaks, with the majority of these changes occurring over the first hour after the mixing of the cement, shown in **figure 3.40**. As with the Fuji IX the peak at 1720cm^{-1} associated with the C=O stretching vibration of uncross linked PAA shifted to a new position of 1707cm^{-1}. Over the course of the first hour the reduction in the intensity of this peak was much more rapid than in the Fuji IX, indicating a more rapid cross linking of the polymer. The corresponding increase of a peak at 1552cm^{-1} related to the C-O asymmetric stretching vibration of forming Ca-PAA within the polysalt mixture is also present and after the first hour is equally pronounced. The presence of a peak at 950cm^{-1} again represents the Si-OH stretching vibration of un-hydrolysed glass particles within the polysalt matrix [12, 14]. Over the first hour this also shows a decrease in intensity and can be paired with the appearance and increase in intensity of the peak at 1042cm^{-1} however unlike Fuji IX this shoulder becomes apparent at 15min (**figure 3.40, d)**) before progressing to a full independent peak after the hour. This particular peak corresponds to the Si-OH stretching vibration of the hydrolysed glass particles in the cured gel-sol matrix [14].

These changes in the sample continue over the course of the 24hrs (**figure 3.41**), and the rate of change in the peaks decreases as time continues and the cement could be considered to be fully set. The peaks identified and their possible corresponding bond interactions in the Ketac Fil Plus are detailed in **table 3.6**.

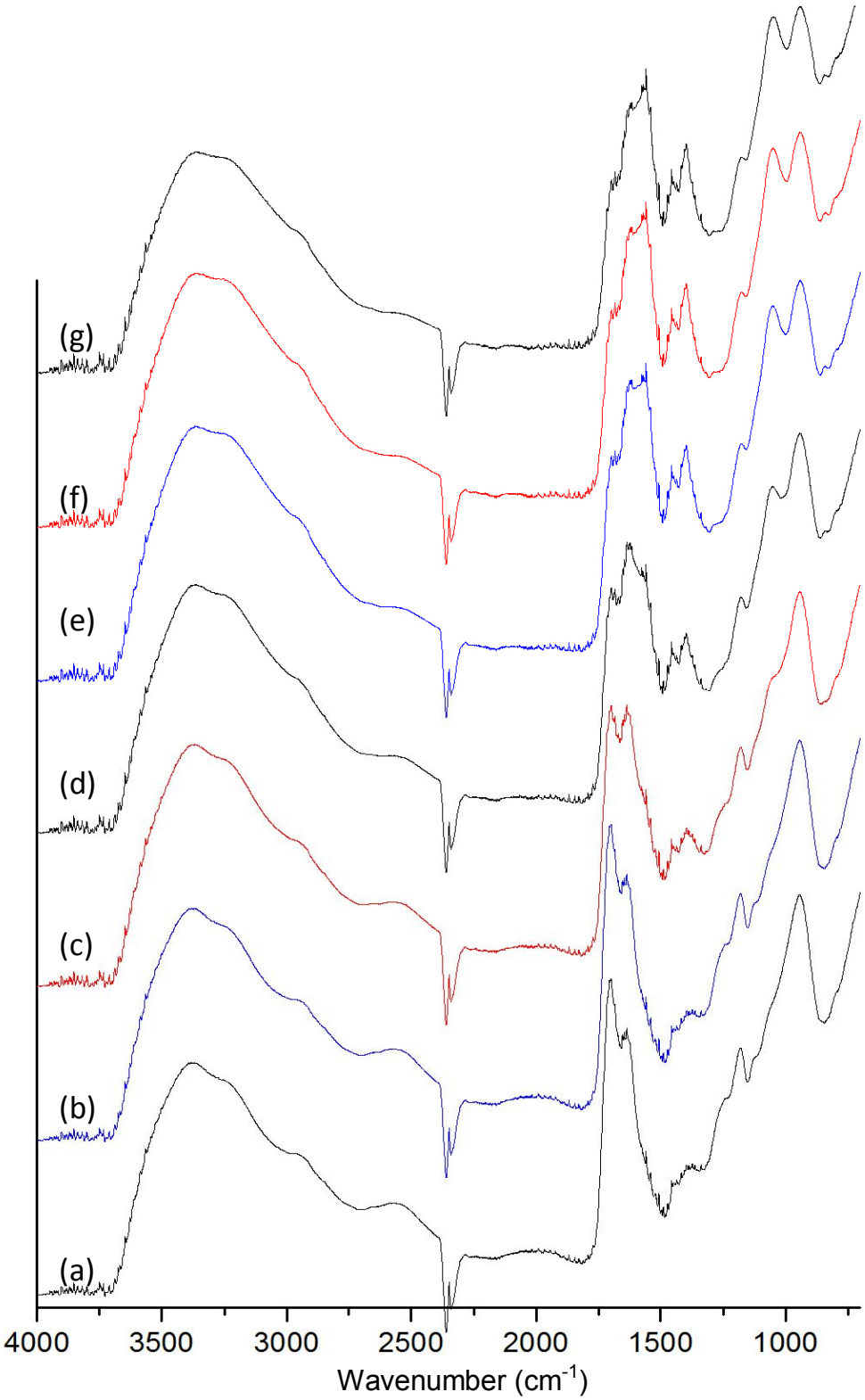

Figure 3.40: Stacked FT-IR spectra for Ketac Fil Plus over the course of an hour at ; a) 0min, b) 5min, c) 10min, d) 15min, e) 30min, f) 45min, g) 60min

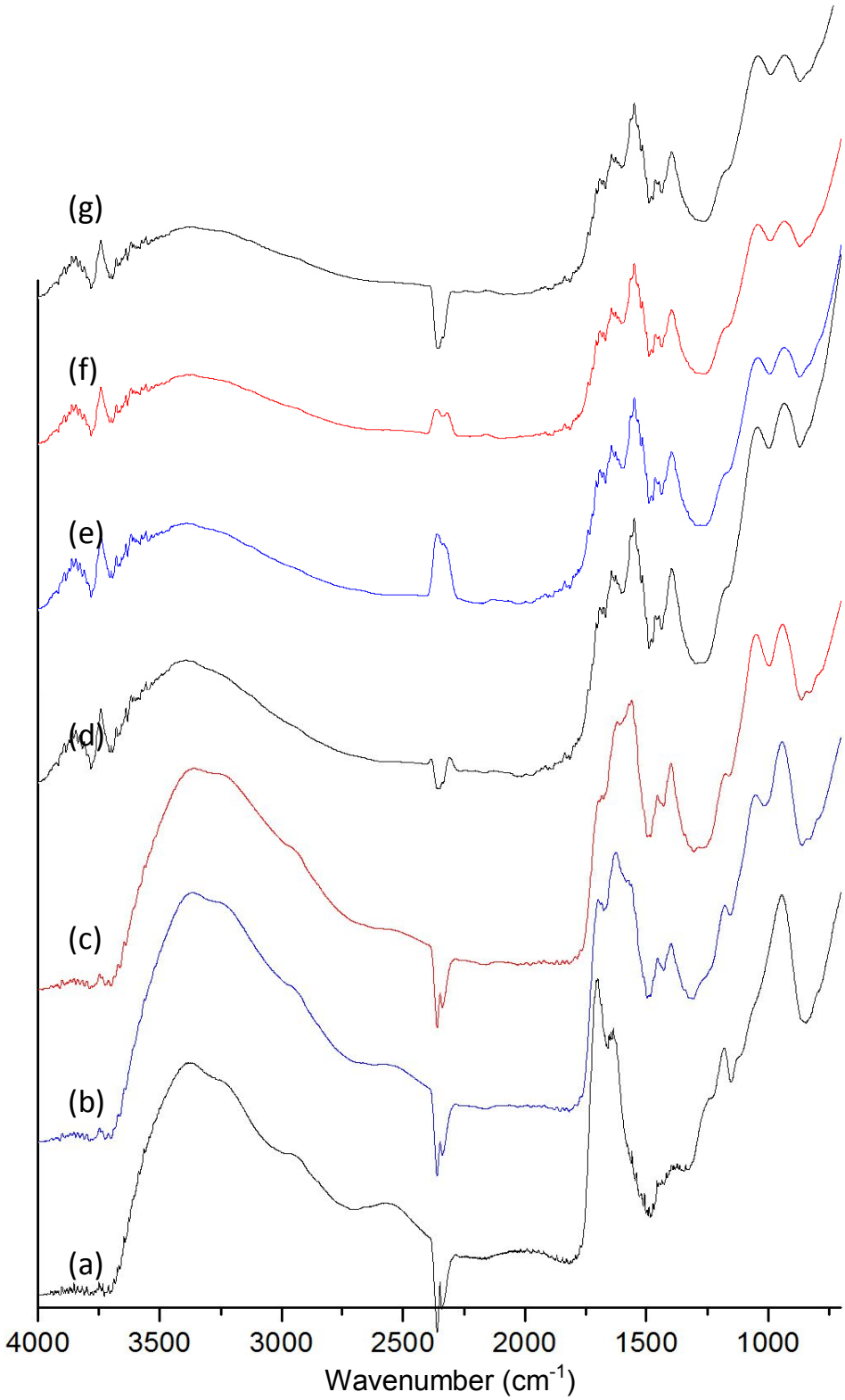

Figure 3.41: Stacked FT-IR spectra for Ketac Fil Plus over the course of a day at; a) 0min, b) 15min, c) 1hr, d) 3hrs, e) 6hrs, f) 12hrs, g) 24hrs

Wavenumber (cm^{-1})	Assignment	Compound	Reference
3200 – 2600	-OH stretching vibration	Water, PAA, TA	[40]
1707	C=O stretching vibration	PAA, TA	[40, 41]
1635	C=O stretching vibration	PAA, TA	[40]
1552	C-O asymmetric stretching vibration	Ca-PAA	[40]
1450	C-H scissor vibration	Al PAA	[40, 41]
1405	C-O symmetric and asymmetric stretching vibration	Al-Tartrate, Ca-PAA	[40, 41]
1250	C-O, Si-CH_3 stretching vibration	PAA	[14, 40, 41]
1170	Si-O asymmetric stretching vibration	Glass	[41]
1040	Si-OH stretching vibration	Glass	[13, 14]
960	Si-OH stretching vibration	Glass	[13, 40]

Table 3.6: Description and assignment of FT-IR peaks identified in Ketac Molar over 24hrs post mixing

An issue with the data collected with the Ketac Fil Plus was that the background subtraction for CO_2, represented as a trough at 2300 rather than the peak that is expected. It is important to note that this did not affect the results collected as the over subtraction was localised to the CO_2 and likely a result of an overly CO_2 rich atmosphere at the time of the background spectra was collected.

3.4.8 FT-IR of Chemfil Superior During curing

As with the other GIC's the interaction of the glass particles with the PAA as the setting reaction began caused a change in the peaks present, with the majority of these changes occurring over the first hour after the mixing of the cement, **figure 3.42**. As with the Fuji IX the peak at 1720cm^{-1} associated with the C=O stretching vibration of uncross linked PAA shifted to 1705cm^{-1}. Over the course of the first hour the reduction in the intensity of this peak was much more rapid than in the Fuji IX more akin to that of the Ketac Fil Plus. The corresponding increase of a peak at 1552cm^{-1} related to the C-O asymmetric stretching vibration of the Sr-PAA (Salt-PAA) is equally pronounced. The peak at 950cm^{-1} representing the Si-OH stretching vibration of un-hydrolysed glass particles within the polysalt matrix [12, 14], is also much wider. Over the first hour this also shows a rapid decrease in intensity and can be paired with the appearance and increase in intensity of the peak at 1042cm^{-1} which becomes apparent after 5min (**figure 3.42, b)**) and continues to increase in intensity over the hour. This particular peak corresponds to the Si-OH stretching vibration of the hydrolysed glass particles in the cured gel-sol matrix [14]. In addition to these the peaks at 1450cm^{-1} and 1405cm^{-1} representing the C-H Scissor vibration of AL-PAA and the C-O symmetric and asymmetric stretching vibration of Al-TA and

Sr-PAA (Salt-PAA) becomes much more pronounced in this particular cement as it sets.

These changes in the continue over the course of the 24hrs, **figure 3.43**, and the rate of change in the peaks does decrease as time continues and the cement could be considered to be fully set. The peaks identified and their possible corresponding bond interactions in the Ketac Fil Plus are detailed in **table 3.7**.

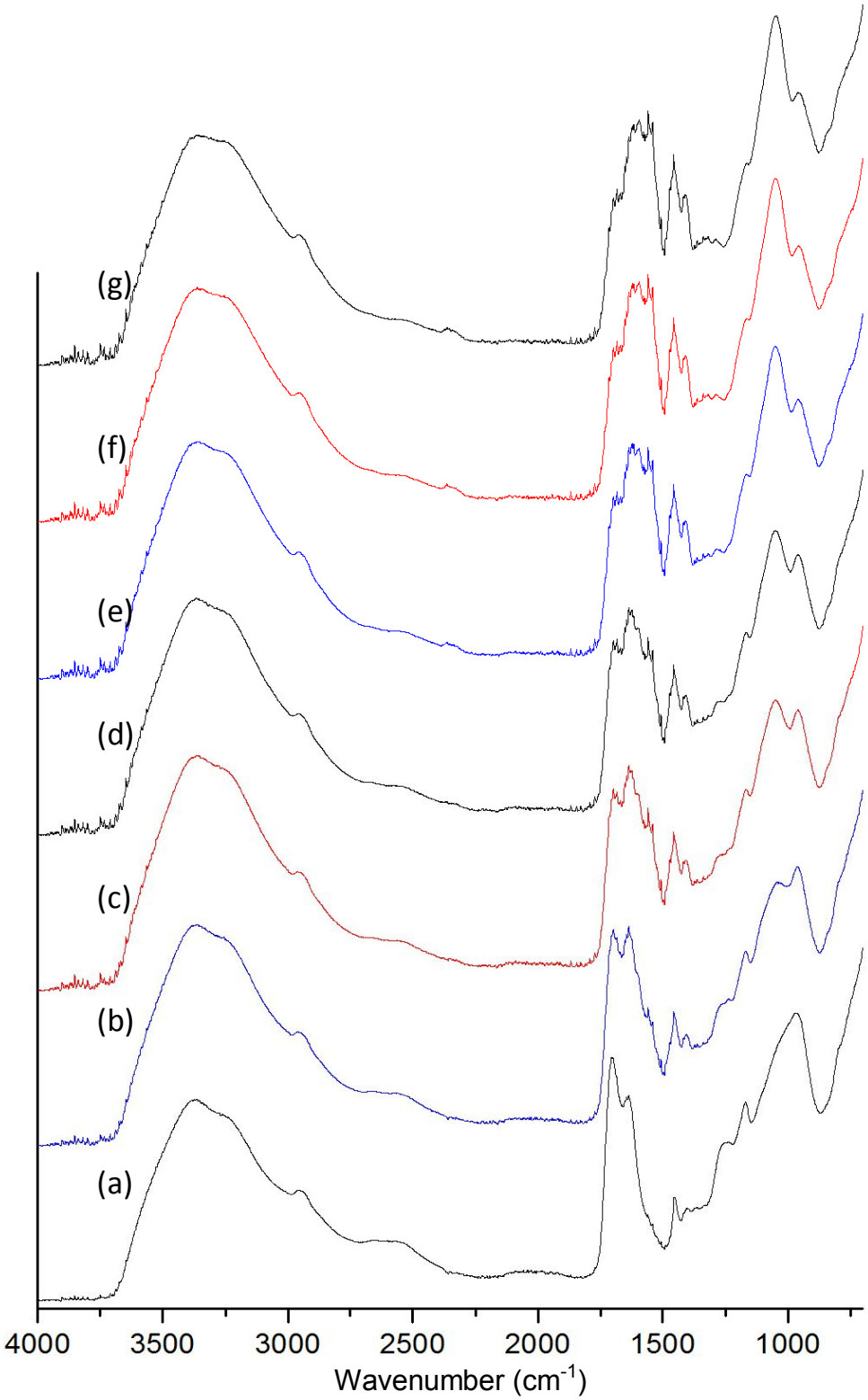

Figure 3.42: Stacked FT-IR spectra for Chemfil Superior over the course of an hour at ; a) 0min, b) 5min, c) 10min, d) 15min, e) 30min, f) 45min, g) 60min

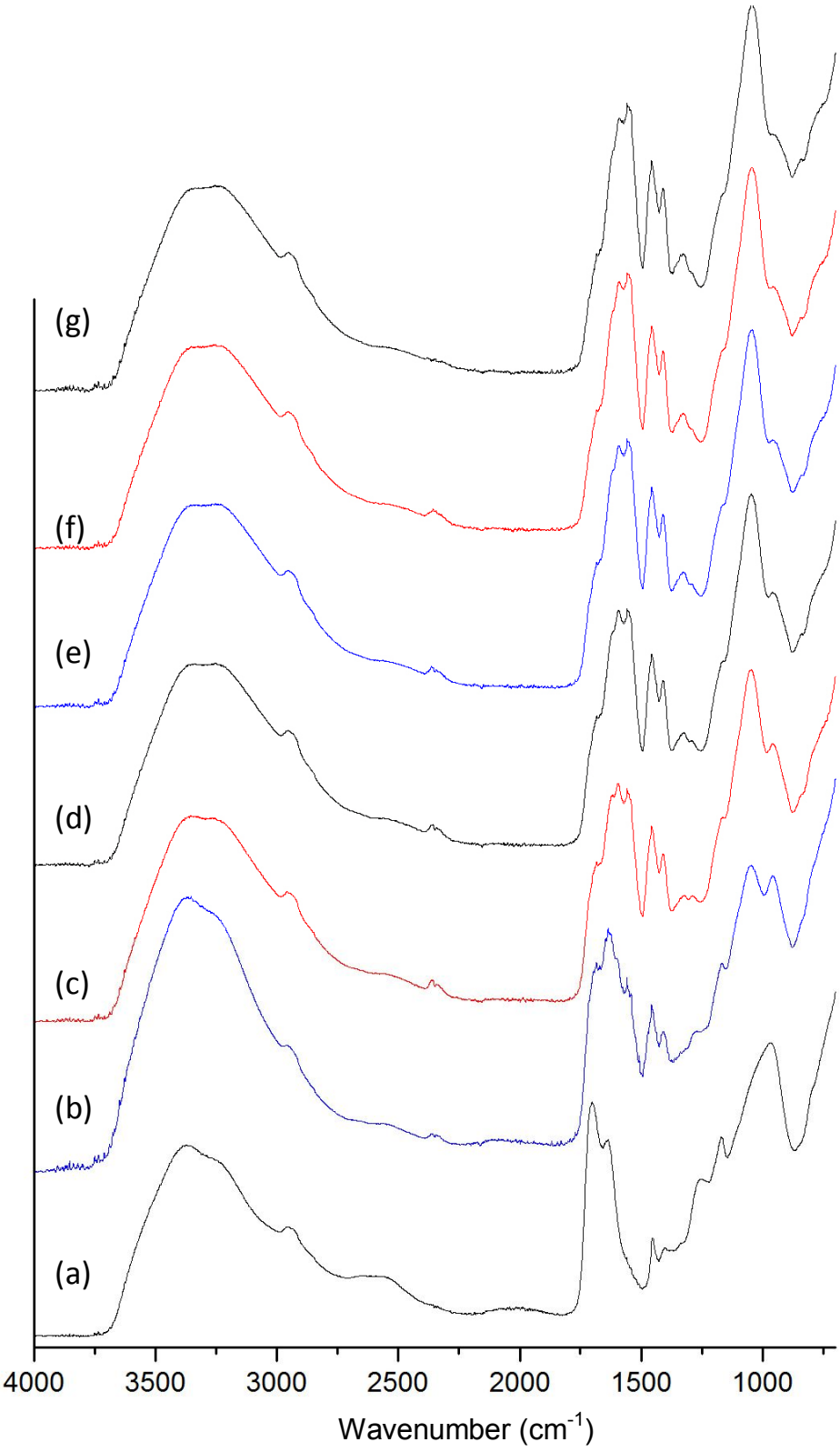

Figure 3.43: Stacked FT-IR spectra for Chemfil Superior over the course of an hour at ; a) 0min, b) 15min, c) 1hr, d) 3hrs, e) 6hrs, f) 12hrs, g) 24hrs

Wavenumber (cm^{-1})	Assignment	Compound	Reference
3200 – 2600	-OH stretching vibration	Water, PAA, TA	[40]
1705	C=O stretching vibration	PAA, TA	[40, 41]
1635	C=O stretching vibration	PAA, TA	[40]
1552	C-O asymmetric stretching vibration	Sr-PAA, Salt-PAA	[40]
1450	C-H scissor vibration	Al PAA	[40, 41]
1405	C-O symmetric and asymmetric stretching vibration	Al-Tartrate, Sr-PAA, Salt-PAA	[40, 41]
1250	C-O, Si-CH_3 stretching vibration	PAA	[14, 40, 41]
1170	Si-O asymmetric stretching vibration	Glass	[41]
1040	Si-OH stretching vibration	Glass	[13, 14]
960	Si-OH stretching vibration	Glass	[13, 40]

Table 3.7: Description and assignment of FT-IR peaks identified in Chemfil Superior over 24hrs post mixing

3.5 FT-IR in Comparison with Impedance

Given the change in the ionic mobility and availability within the setting cements there is a correspondence with the progression of the setting reaction as measured by FT-IR spectroscopy and the measuring of the change in impedance through the use of the impedance bridge and test assembly.

By taking the change in the ratio change between the intensity, and therefore the prevalence of a particular bond, it is possible to infer the ionic freedom within the cement and thus give an indication of the 'locking in' or free ions in the system. By looking at the change between the peak at 945cm^{-1} representing the un-hydrolysed glass particles within the system and that of the peak at 1042-1046cm^{-1} which represents the hydrolysed glass particles in the sol gel matrix, it is possible to see the level to which the glass particles have been hydrolysed and thus the amount of ions that have been released into the system. Equally the change between the peaks at 1705cm^{-1} representing the un-polymerised PAA within the system compared to that of the peak at 1552cm^{-1} which represents the polymerised PAA, indicates the degree to which the PAA has been polymerised by the free ions within the system.

This change in these ratios within Fuji IX is shown in **figure 3.44**.

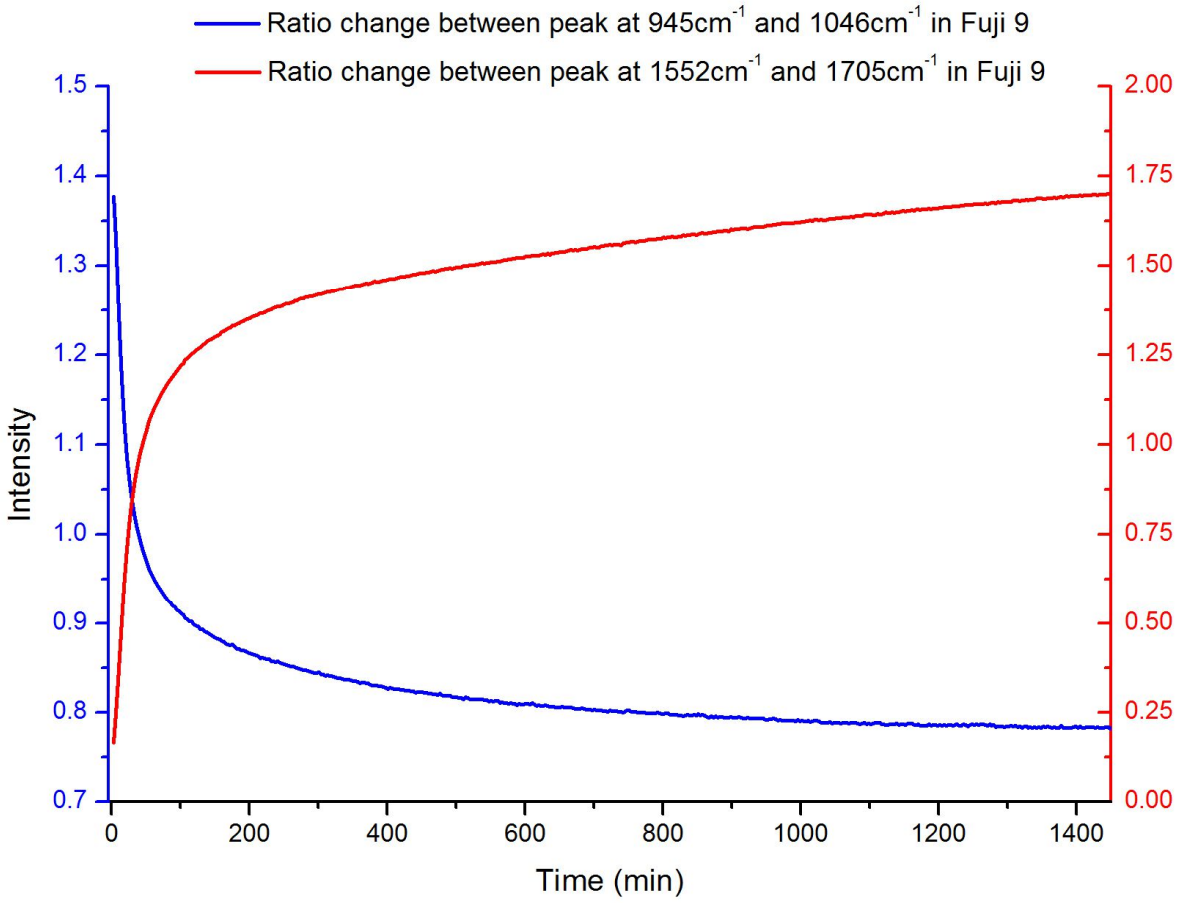

Figure 3.44: Ratio change between the peaks for Ca-PAA (1552cm^{-1}) and PAA (1705cm^{-1}) representing the degree of polymerisation of the polymer, and the ratio change between representing the un-hydrolysed glass particles (945cm^{-1}) and the hydrolysed glass particles (1042-1046cm^{-1}).

What this graph shows is that during the curing of the cement the majority of the polymerisation of PAA and hydrolysing of the glass particles within the cement occurs in the first 2 hours of the setting. This is concurrent with the current understanding of the setting process of glass ionomer cements and is to be expected. Over the full 24hrs the rate of cure slowly levels off but never completely stops as the cement continues to cure beyond the measured time [12, 13]. At this

time period its setting reaction is completed to the order of 90%, and further measurement would be beyond this time frame is not particularly useful for the investigation of the setting reaction. However, an implanted sensor would be capable of measurements weeks, months and years into the lifespan of the restoration, monitoring both ionic changes in the composition (as with the setting reaction) and also detecting defect formation.

If this change is compared to the change in measured impedance of the cement then it is possible to see if there is a correlation between the two sets of results for curing progression. This comparison is shown in **figure 3.45**.

Both curves follow and increase in their respective measured value, as the PAA polymerises to Ca-PAA reducing the availability of Ca^{2+} ions within the system. As the availability of free ions decrease, so the impedance of the material increases. There is a difference in the rate of increase in resistance and the increasing scarcity of Ca^{2+} ion's within the system, due to a number of factors. Firstly the ratio change represented here is only for that of PAA to Ca-PAA and given that this only covers the polymerisation with Ca^{2+} ions the other ion's present in the polymerisation must be considered i.e. $PO4^{3-}$, F^{-}, Al^{3+} ions. As the impedance given is the sum of all of these ion's availability, a more accurate curve should be used which incorporates all of these ion's availability in the cement during curing. In addition to this, free ions within the system which are not ionically bonded to the cured PAA will have an effect on the impedance, such as is the case with fluorine uptake and release within a cement.

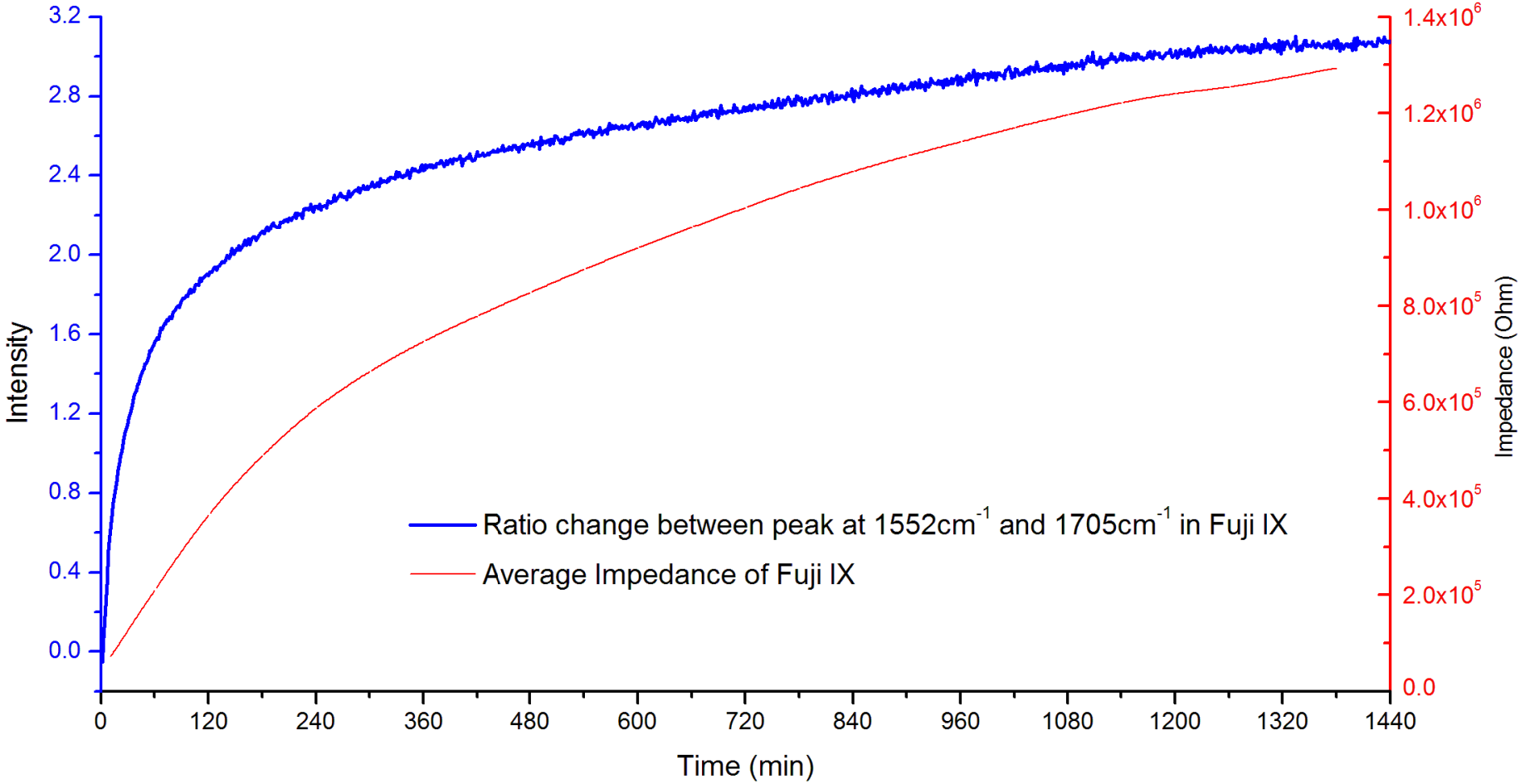

Figure 3.45: Comparison of both change in impedance and ratio of the intensity of peaks as given by FT-IR data, for Ca-PAA and PAA, over a 24 hour period within Fuji IX.

The difference in area measured also has a significant effect. FT-IR spectroscopy is a measurement technique which measures the interactions within the cements bulk not just the immediate surface in contact with the scanning cell. The measurement of impedance is also a bulk measurement technique and returns data for the whole of the cement, giving an understanding to the progression to the reactions which occur within the heart of the material, however the measurement of impedance using co-planar plates may pose an issue as the route taken by the current through the cement is complex, and as a result the condition of the cement in the immediate area around the sensor is of a greater significance to the total measured impedance.

Despite this difference in the rate of curing as recorded by the different methods it is possible to observe the gradual levelling out of the cements ionic availability over the 24hrs with that of the impedance over the same time as they both follow a similar trend increase initially slowing as curing progresses (**figure 3.45**).

The change in capacitance within the cement suggest that the cement has changed phase from a highly ionic, polar environment to one which is less ionic and ostensibly non polar [1, 2, 7, 8] which ties into the change in cement as it cures. During the setting the initial hydrolysation would give rise to this highly polar environment caused by the acid release of H+ ions, which as the curing progresses would reduce as the acid etching of un-etched particle reduces and the availability of the free ions is reduced. This change in the composition is matched by that measured by FT-IR interrogation.

The setting reaction as monitored by the co-planar test assembly also indicates that the cement is a less than ideal capacitor, and as with the results measured by the planar assembly it is possibly a form of lossy capacitor. This means that the equivalent electric circuit could be considered to be both a capacitor and resistor in series with each other. This circuit is detailed in **figure 3.46**.

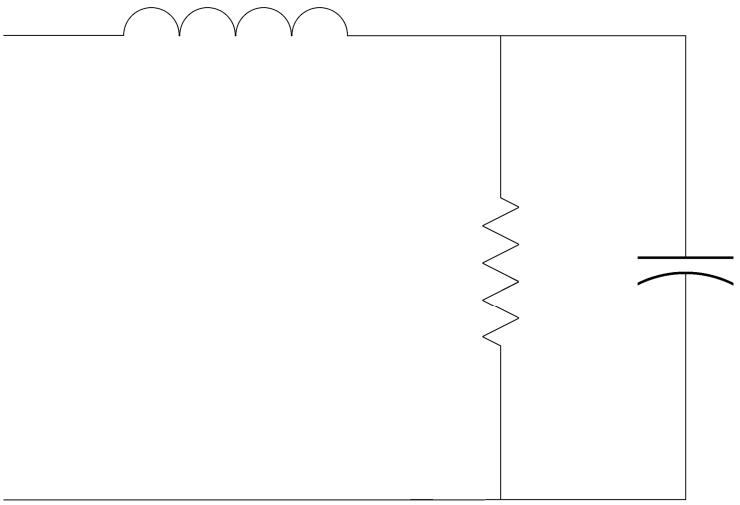

Figure 3.46: Lossy capacitor circuit of a capacitor in series with a resistor.

An ideal capacitor does not allow the passing of current through via a restive pathway; the capacitor merely reacts to an applied current. However, all real materials will possess some effective resistive pathways, and a material with a low enough resistance is called a lossy capacitor. This type of material is a less than an ideal capacitor as it allows for the passing through of current via resistive pathways, so in terms of the relative electrical circuit, then the capacitor component could be considered to be in parallel with a resistor [20].

Chapter 4

4 Conclusions

What can be seen from the results is that the use of the relatively simple co-planar capacitor test assembly is capable of providing usable data on the dielectric properties of setting cement.

The FT-IR data collected shows the changes in the prevalence of various chemical bonds associated with the setting of GIC's. The changes in the prevalence of various peaks which can be associated with different compounds both from the pre-mixed constituents to the setting cement. This indication of the chemical changes within the cement gives and indication as to the rate of setting of the GIC.

The dielectric data collected from the co-planar assembly also showed a change in the recorded value for the impedance over the course of the setting of the cement. Over time the value for impedance within the measured GIC increases, with the rate of increase gradually decreasing as time progresses. The measured change in impedance is by at-least a factor of 10 over the course of the 24hrs. This change in the dielectric properties is sufficiently large that it is possible to measure the change in the materials condition both on a macro and potentially micro scale.

When compared to one and other the FT-IR data and dielectric data show that there is direct correlation between the changes in the FT-IR spectra and the change in

dielectric properties. Immediately after mixing the hydrolysation of the glass by the PAA causes the release of a large number of ions into the mixture of glass and liquid components. This increase in Ion motility would account for the initially low value for impedance. Over the 24hrs as the GIC sets, the availability of free ions within the gel-sol mixture of the cement results in the recorded increase in impedance of the cement. The change in the FT-IR intensity of these bonds over the 24 hour period parallels the change in dielectric properties of the cement, indicating the correlation between the changes in the FT-IR spectra and the change in dielectric properties. This shows that the use of dielectric measurement as a method of monitoring the setting reaction of glass ionomer cements would be very useful in indicating the materials condition once implanted.

The wired dielectric data showed a change in capacitance which is large enough to potentially be used to measure the change in the materials condition on a MEMs scale. This data can be used to develop a working MEM sensors design which can be used within the cement to monitor its condition, as it shows that despite a number of issues with the design that was used for the monitoring of the cement, the use of direct contact monitoring of impedance with a co-planar test assembly is a very real possibility for the development of a MEM sensor.

Chapter 5

5 Future work

Before the information and experience that has been collected over the course of this investigation can be implemented into the design of a fully functional MEM sensor for possible commercial implementation there are still a number of areas that need to be explored further. Due to the novel nature of the research, the time taken to develop and test the macro scale sensor was longer than originally anticipated. Possible avenues of further work that could be pursued to continue this research and lead into the miniaturisation of the sensor are:

1. The investigation of changes in dielectric properties due to damage to the GIC would be a key factor in the suitability of the design for dental applications. The creation of micro cracks within the cement, through the use of thermal shock, and then measuring the impedance of the cement would allow the testing of the sensors ability to detect such phenomena in the cements structure. Indications of this as a possibility were detected during the investigation, through miss mixes of the cement, however were never subject to systematic investigation. The creation of porosities and other physical defects would also allow for further testing of the sensors sensitivity.

2. An investigation into the effect of polarisation and the Maxwell-Wagner effect on the sample should also be performed. The nature of GIC systems is highly

conducive to Maxwell-Wagner effects, as the gel-sol matrix of polymer and glass particles. It is possible that the Maxwell-Wagner effect could occur at the cathode surface or within the GIC at the glass particles, and thus be significant to the recorded dielectric properties.

3. Further comparison between the impedance and the curing cements chemical bonds should be conducted. The use of MAS-NMR spectroscopy would provide a more quantitative analysis of the changes within the cement and would allow for greater clarity on the bond present within the cement.

4. The effect of scaling the sensor down would also need to be considered as it would change the recorded dielectric properties of the cement, which could potentially have further effects on the interrogation of the cement. This would have to be tested to see whether this negatively affects this particular assembly's ability to monitor the changing dielectric properties.

5. The actual mechanical effect of sensor itself within the greater structure of the cement itself would also be a key property to be investigated. Mechanical testing, such as compression testing, would have to be performed to assess the effect of the inclusion of the MEMs sensor on the mechanical properties of the cement. The ideal would be no effect, however this is unlikely and the possible viability of use in any biomedical application would be dependant of the MEMs not completely negating the physical attributes of the cements.

6. For the full completion of the ideal design for implantation the sensor would have to be remotely interrogated through wireless transmission. One possible method of interrogation would be the inclusion of an induction loop, like that detailed in **figures 5.1** and **5.2**.

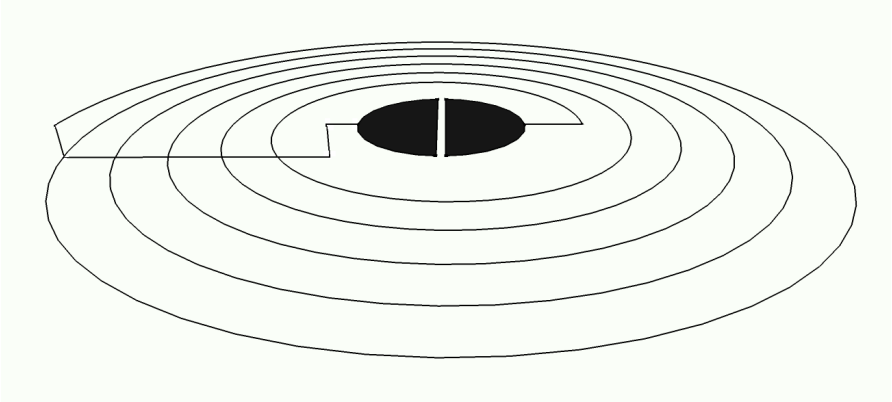

Figure 5.1: Co-planar assembly connected to flat induction loop

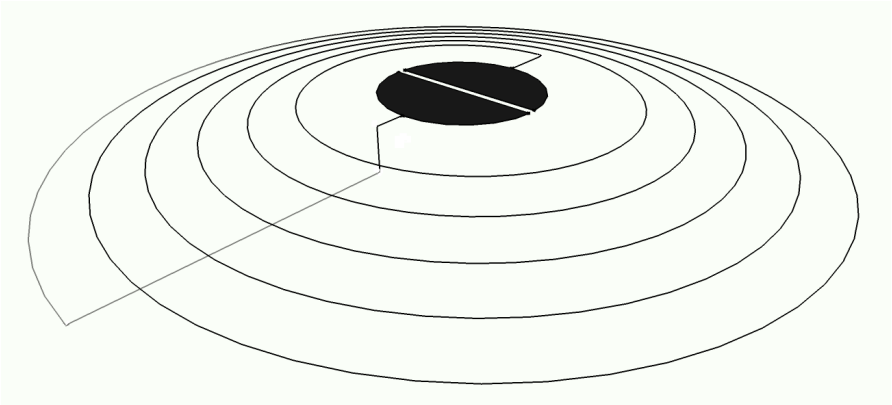

Figure 5.2: Co-planar assembly connected to a raised spiral induction loop

This design is relatively easy to produce with current techniques however the interrogation such a set up may be prohibitively difficult, however this is not the only possible set-up.

7. The materials used in the design are also an area that should be further investigated. Though the copper PCB board was a perfect material for the macro assembly there are a number of issues with this choice. As detailed previously the copper reacted poorly with both the cement and the storage medium. Prolonged exposure to the copper caused staining and contamination of the cement, possibly affecting the values for the impedance which were collected. The difference in material will change the way in which the sensor functions and the results collected, however as copper is not biocompatible this change is necessary purely to make implantation a possibility.

8. The total encasing of the MEMs sensor in the cement would also need to be investigated. Ideally this would eliminate the effect of dislocation of the cement from the test assembly, which proved to be an issue with prolonged monitoring of the sensor beyond the initial 24hrs. Hopefully this would also reduce the noise that is detected as a result of a disconnect developing.

9. With improved connectivity it would be possible to detect the changes in the dielectric properties over an extended period of time. Cement samples containing the sensor would be stored in distilled water for prolonged periods of time (testing after 24hrs, 1 week, 4 weeks, 3 months, 6 months, 12 months), whereupon they are removed at various times and any changes in the dielectric properties, or the ability to measure these properties measured and assessed. This same procedure could be carried out using foetal calf serum,

to replicate some of the conditions in the saliva, in substitution for the distilled water; thereby giving a more accurate view of how the aging of the cement affects the dielectric properties in a patient.

6 References

1. **Braden, M. and R.L. Clarke, *Dielectric properties of zinc oxide-eugenol type cements.* Journal of Dental Research, 1974. 53(5): p. 1263-1267.**
2. **Tay, W.M. and M. Braden, *Dielectric properties of glass ionomer cements--further studies.* Journal of Dental Research, 1984. 63(1): p. 74-75.**
3. **Hurrell-Gillingham, K., et al, *In vitro biocompatibility of a novel Fe2O3 based glass ionomer cement.* Journal of Dentistry, 2006. 34(8): p. 533-538.**
4. **Hatton, P.V., K. Hurrell-Gillingham, and I.M. Brook, *Biocompatibility of glass-ionomer bone cements.* Journal of Dentistry, 2006. 34(8): p. 598-601.**
5. **Nicholson, J. and E.A. Wasson, *Effect of Operator Skill in Determining the Physical Properties of Glass-Ionomer Cements.* Clinical Materials, 1994. 15: p. 169-172.**
6. **Fleming, G.J.P., A.A. Farooq, and J.E. Barralet, *Influence of powder/liquid mixing ratio on the performance of a restorative glass-ionomer dental cement.* Biomaterials, 2003. 24: p. 4173-4179.**
7. **Braden, M. and R.L. Clarke, *Dielectric properties of polycarboxylate cements.* Journal of Dental Research, 1975. 54(1): p. 7-9.**
8. **Tay, W.M. and M. Braden, *Dielectric properties of glass ionomer cements.* Journal of Dental Research, 1981. 60(7): p. 1311-1314.**
9. **Chung, D.D.L., *Damage in cement-based materials, studied by electrical resistance measurement.* Materials Science & Engineering Reports, 2003. 42(1): p. 1-40.**
10. **Stamboulis, A., *Glass Ionomer Cements.* Metallurgy and Materials: p. 62.**
11. **Stamboulis, A., R.V. Law, and R.G. Hill, *Characterisation of commercial ionomer glasses using magic angle nuclear magnetic resonance (MAS-NMR).* Biomaterials, 2004. 25(17): p. 3907-3913.**
12. **Nicholson, J., *Chemistry of glass-ionomer cements: A review.* Biomaterials, 1998. 19: p. 485-494.**
13. **Maeyer, E.A.P.D., R.M.H. Verbeeck, and C.W.J. Vercruyssee, *Infrared Spectrometric Study of Acid-degradable Glasses.* Journal of Dental Research, 2002. 81: p. 552-555.**
14. **Kim, M.T., *Deposition behavior of hexamethydisiloxane films based on the FTIR analysis of S-O-Si and Si-CH_3 bonds.* Thin Solid Films, 1997. 311: p. 157-163.**
15. **Hattab, F.N. and W.M. Amin, *Fluoride release from glass ionomer restorative materials and the effects of surface coating.* Biomaterials, 2001. 22: p. 1449-1458.**
16. **Stamboulis, A., et al., *MAS-NMR spectroscopy studies in the setting reaction of glass ionomer cements.* Journal of Dentistry, 2006. 34(8): p. 574-581.**
17. **Wilson, A.D., T.I. Barry, and D.J. Clinton, *The Structure of a glass-ionomer cement and its relationship to the setting process.* Journal of Dental Research, 1979. 58: p. 1072-1079.**
18. **Wang, Y. and B.W. Darvell, *Failure behavior of glass ionomer cement under Hertzian indentation.* Dental Materials, 2008. 24(9): p. 1223-1229.**
19. **Zhao, J., Y.M. Weng, and D. Xie, *In vitro wear and fracture toughness of an experimental light-cured glass-ionomer cement.* Dental Materials, 2009. 25(4): p. 526-534.**

20. Johnson, D.G.L., *Lossy Capacitors*. Solid State Tesla Coil. Vol. Chapter 3. 2001, Manhattan, Kansas. 26-49.
21. Nassr, A.A., W.H. Ahmed, and W.W. El-Dakhakhni, *Coplanar capacitance sensors for detecting water intrusion in composite structures.* Measurement Science and Technology, 2008. 19: p. 1-8.
22. Cabeza, M., et al., *Impedance spectroscopy study of hardened Portland cement paste.* Cementand Concrete Research, 2002. 32: p. 881-891.
23. Pradelle-Plasse, N., et al., *Evaluation of microleakage of composite resin restorations by an electrochemical technique: the impedance methodology.* Dental Materials, 2004. 20: p. 425-434.
24. Watts, D.C., *Analysis of reactions in glass-polyalkenoate/resin systems by dielectric impedance spectroscopy.* Biomaterials, 1998. 19: p. 551-557.
25. Cryril Villat, V.X.T., Nelly Pradelle-Plasse, Pierre Ponthiaux, Francois Wenger, Brigitte Grosgogeat, Pierre Colon, *Impedance Methodology: A new way to characterize the setting reaction of dental cements.* Dental Materials, 2010. 26: p. 1127-1132.
26. Sánchez, a., et al., *Microstructural modifications in Portland cement concrete due to forced ionic*
***migration tests. Study by impedance spectroscopy.* Cement and Concrete Research, 2008. 38: p. 1015-1025.**
27. Hashimoto, M., et al., *Crystal growth by fluoridated adhesive resins.* Dental Materials, 2008. 24(4): p. 457-46.
28. Zainuddin, N., et al., *A long-term study on the setting reaction of glass ionomer cements by Al-27 MAS-NMR spectroscopy.* Dental Materials, 2009. 25(3): p. 290-295.
29. Stappert, C.F.J., et al., *Effect of mouth-motion fatigue and thermal cycling on the marginal accuracy of partial coverage restorations made of various dental materials.* Dental Materials, 2008. 24(9): p. 1248-1257.
30. Collard, D., S. Takeuchi, and H. Fujita, *MEMS technology for nanobio research.* Drug Discovery Today, 2008. 13(21-22): p. 989-996.
31. Felnhofer, D., et al., *Device physics of capacitive MEMS.* Microelectronic Engineering, 2007. 84(9-10): p. 2158-2164.
32. Romig, A.D., M.T. Dugger, and P.J. McWhorter, *Materials issues in microelectromechanical devices: science, engineering, manufacturability and reliability.* Acta Materialia, 2003. 51(19): p. 5837-5866.
33. Tsai, N.C. and C.Y. Sue, *Review of MEMS-based drug delivery and dosing systems.* Sensors and Actuators a-Physical, 2007. 134(2): p. 555-564.
34. Spratley, J.P.F., et al., *Flexible SU-8 microstructures for neural implant design.* Sensors and Actuators a-Physical, 2008. 147(1): p. 324-331.
35. GC, *GC Fuji IX $_{GP}$ Radiopaque Posterior Glass Ionomer Restorative Cement*. GC Corportation. 1991, Tokyo, Japan.
36. ESPE, M., *KetacTM Fil Plus AplicapTM, Glass Ionomer Filling Material, Instructions for Use*. 3M ESPE. 2011, Neuss, Germany.
37. DENTSPLY, *Directions for Use, Chemfil® Superior, Fast Setting Glass-Ionomer Restorative Material*. DENTSPLY Limited. 2005, Konstanz, Germany.
38. GC, *Fuji IX 1-1PKG.jpg*.
39. *Glass Ionomer Mixing*.

40. **Young, A.M., S.A. Rafeeka, and J.A. Howlett, *FTIR investigation of monomer polymerization and polyacid neutralization kinetics and mechanisms in various aesthetic dental restorative materials.* Biomaterials, 2004. 25: p. 823-833.**
41. **Young, A.M., *FTIR investigation of polymerisation and polyacid neutralisation kinetics in resin-modified glass-ionomer dental cements.* Biomaterials, 2002. 23: p. 3289-3295.**
42. **Bertolini, M.J., et al., *Preparation of new glass systems by the polymeric precursor method for dental applications.* Journal of Non-Crystalline Solids, 2004. 344: p. 170-175.**
43. **Nicholson, J., et al., *Fourier transform infrared spectroscopic study of the role of tartaric acid in glass-ionomer dental cements.* Journal of Dental Research, 1988. 67: p. 1451-1454.**